FUNDAMENTAL ASPECTS OF CHEMICAL-LOOPING

WITH OXYGEN UNCOUPLING USING COPPER

OXIDE-BASED OXYGEN CARRIERS

by

Christopher K. Clayton

A dissertation submitted to the faculty of
The University of Utah
in partial fulfillment of the requirements for the degree of

Doctor of Philosophy

Department of Chemical Engineering

The University of Utah

May 2016

The University of Utah Graduate School

STATEMENT OF DISSERTATION APPROVAL

The dissertation of   Christopher K. Clayton

has been approved by the following supervisory committee members:

Kevin J. Whitty	, Chair	3/18/2016
		Date Approved
JoAnn S. Lighty	, Member	8/12/2015
		Date Approved
Swomitra K. Mohanty	, Member	2/26/2016
		Date Approved
Terry A. Ring	, Member	8/12/2015
		Date Approved
Hong Y. Sohn	, Member	8/12/2015
		Date Approved

and by   Milind D. Deo   , Chair of

the Department of

Chemical Engineering

and by David B. Kieda, Dean of The Graduate School.

ABSTRACT

        The chemical-looping technology is quickly becoming an attractive alternative for

the combustion of fossil fuels in energy production. With the rapid growth in the

anthropogenic production of carbon dioxide (CO_2) due, in large part, to the combustion

of fossil fuels, it is becoming increasingly important to identify technologies that are

capable of producing energy, at the same rate as traditional fossil-fuels units, while

serving in a secondary capacity of managing emissions.

        Among the materials suggested for use in chemical-looping, copper-oxide has

emerged as a front runner. Materials such as copper oxide allow the direct combustion of

solid fuels, without an intermediary gasification step, by spontaneously decomposing

from cupric oxide (CuO) to cuprous oxide (Cu_2O), liberating free oxygen in the process.

The rate at which these particles decompose can be as much as 50 times faster than the

rates of gasification.

        This work provides the academic community with results geared toward the

production and implementation of copper-based oxygen carriers by:

1.   Developing novel oxygen carrier materials and,

2. Developing models describing both the oxidation and decomposition of copper

    oxide-based materials.

        It has been determined that the decomposition of copper-oxide is well described

by a global reaction rate for a wide range of copper oxide-based oxygen carrier materials.

This global reaction rate suggests that the activation energy of decomposition that best predicts reaction rates of the different CuO-based materials is 62 kJ/mol and that the rate law has a zero order dependence on the concentration of the solid carrier.

The modeled oxidation kinetics of Cu_2O to CuO for two different oxygen carrier materials is presented. Unlike the simple case of decomposition of CuO, the oxidation of Cu_2O is highly dependent on the solid concentration. During oxidation, the volume change of the solid is about a 5% increase. This causes a pore-blocking effect which is observed at low temperatures (below 700°C). However, at higher temperatures (above 800°C), this effect is not apparent. These two regimes are best described by two different kinetic models: pore-blocking kinetics is used for the lower temperature regime while nucleation/growth kinetics, given by Avrami-Erofeev, is used to model the higher temperature regimes.

I would like to dedicate this work to my beautiful wife and loving children.

Without your support this does not exist. My love, always.

Anybody who has been seriously engaged in scientific work of any kind realizes that over the entrance to the gates of the temple of science are written the words: "Ye must have faith." It is a quality which the scientist cannot dispense with.

~Max Planck: Where is Science Going? (1932)

TABLE OF CONTENTS

LIST OF TABLES

Tables

ACKNOWLEDGEMENTS

I would like to thank my wife and kids for the love and support they have given throughout the course of this work.

I would also like to thank my parents for their support – thank you for instilling within me from such a young age the desire to achieve greatness.

To my siblings and in-laws, there have been many a night that you have helped to inspire and support me.

Thanks go to Crystal Allen, Blake Wilde, Gabor Konya, Sean Peterson and Edward Eyring for assisting with all the experimental work.

To my committee, thank you for your time and your thoughts without which I would have been lost.

To my advisor, Kevin, thank you for being patient with and pushing me when I didn't want to be pushed.

CHAPTER 1

INTRODUCTION

According to the U.S. Department of Energy (DOE), of the world's total carbon

dioxide (CO_2) emissions, the United States is responsible for more than 18%, producing

nearly 5.5 million metric tons in 2010 – second only to China. The greatest source for

production of CO_2 is the combustion of fossil fuels. From study of Figure 1, it may be

understood that the United States is heavily dependent on fossil fuels. Table 1 tabulates

the amount of electricity produced from different sources. Nearly 70% of electricity

produced in the U.S. in 2010 was created from fossil fuel sources.

This reliance on the combustion of fossil fuels has led to a near 2 ppm/year

increase of CO_2 globally according to the National Oceanic and Atmospheric

Administration (NOAA) [1]. According to the United States Environmental Protection

Agency (EPA) CO_2 is the largest of the reported greenhouse gases emitted in 2011 at

nearly 84% of the total reported greenhouse gases emitted [2]. The emission of

greenhouse gases, specifically CO_2, into the atmosphere along with the allegedly induced

effects has been the subject of numerous studies. These studies have sparked a growing

concern on the effects of these gases on the environment. This concern has, in turn,

driven researchers to develop technologies directed toward the mitigation of these effects.

These technologies are generally aimed at reducing emissions at the source as opposed to
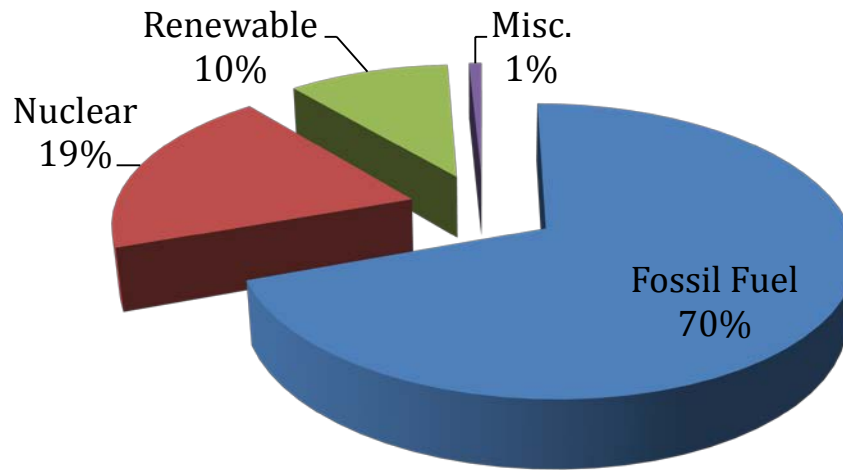
Figure 1: United States electricity production by source in 2010. Adapted from U.S. EIA 2011.

Table 1: United States electricity production by source. Adapted from U.S. EIA, 2011.

Year	Fossil Fuels	Nuclear	Renewable	Misc.	Total
2011	2790.3	790.2	520.1	-	-
2010	2883.4	807.0	427.4	33.3	4151.0
Proportion 2010	69.5%	19.4%	10.3%	0.8%	100.0%
2009	2726.5	798.9	417.7	41.4	3984.4
2008	2926.7	806.2	380.9	38.3	4152.2

environmental cleanup post emission.

1.1 CO_2 Capture Technologies

Current CO_2 capture techniques are expensive and require large pieces of equipment. The removal of CO_2 gas from a gaseous stream of mixed gaseous species can be performed either precombustion, postcombustion or in-situ. Although there are other greenhouse gases being emitted, due to the vast difference between emission rates (84% of GHG emissions are CO_2), it seems prudent to focus a large portion of our resources toward the carbon emission mitigating technologies.

The U.S. Department of Energy via the National Energy and Technology Laboratories (NETL) has selected various technologies in each of the categories while assigning priority to the research of these technologies for carbon capture and storage (CCS). For postcombustion solutions, they have listed various solvents, solid sorbents, and membranes. For precombustion solutions, they have identified physical solvents, solid sorbents, and membranes, including H_2/CO_2 and water-gas-shift membranes, as potentially suitable CCS technologies. For the oxy-combustion approach (also sometimes referred to as in-situ), the list of likely suitable candidate technologies includes oxy-fuel combustion and chemical-looping [3].

Although many challenges still exist in the development of the chemical-looping combustion technology, the payoff seems to be well worth it. In the same report, the NETL reported the results of their study to determine the cost reduction benefits versus an expected demonstration ready unit time frame. These results have been reproduced in Figure 2. Chemical-looping technology has been identified as having the greatest
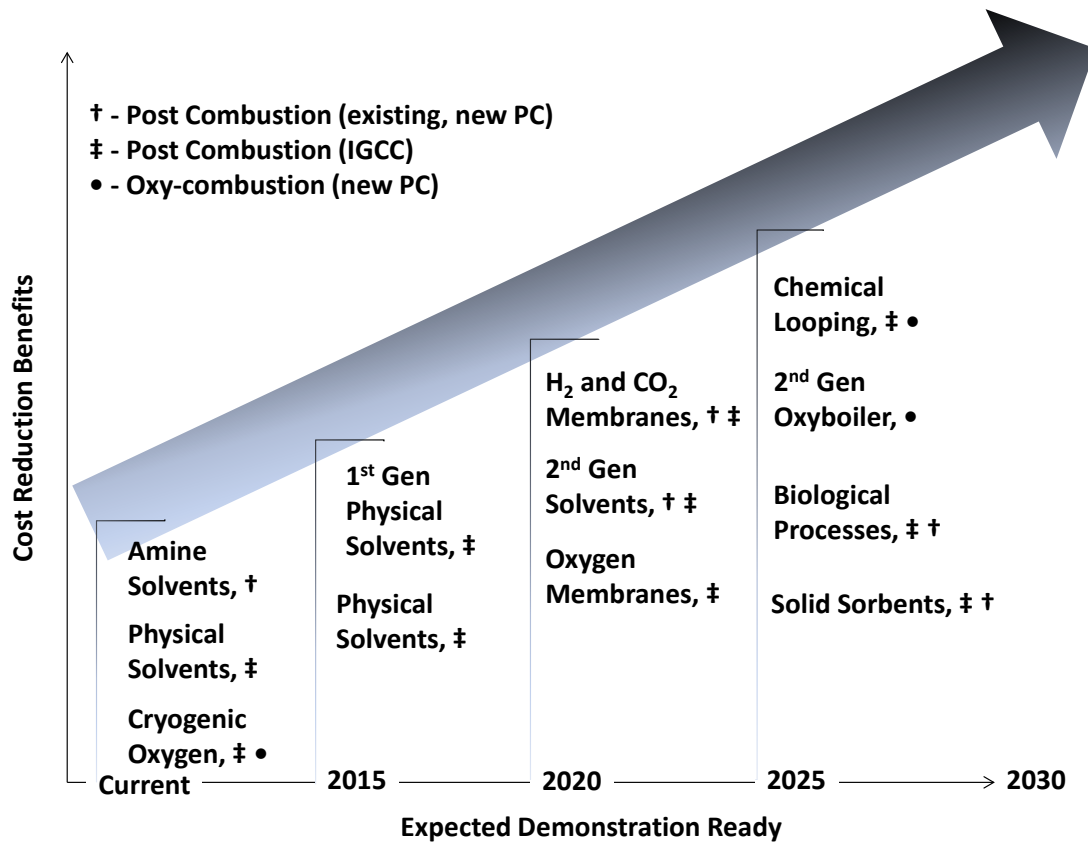
Figure 2: Expected CCS technologies demonstration date compared by cost reduction benefits according to the U.S. Department of Energy.

expected cost reduction benefit while also indicating the many challenges still existing in its development by assigning the demonstration ready time for some time after 2025 [4, 5].

1.2 Traditional Chemical-looping Combustion (CLC)

The name Chemical-looping combustion was first coined in 1987 by Ishida, Zheng and Akehata in their exergy analysis of a chemical-looping combustor [6]. From there, the Japanese group seemed to take the forefront of CLC studies and reported work completed from several other studies in the 1990s [7-11]. Mattisson [12] reports that by the new millennium, there were just a handful of institutions producing the bulk of the studies into chemical-looping, namely: Chalmers University of Technology in Sweden [13, 14, 27,16] , ICB-CSIC Spain [7, 15 , 22, 25], the Technical University of Vienna [16, 17, 18] and the Korea Institute of Energy Research [19, 22-25] with a few other institutions beginning studies [26, 27]. From then, several institutions have investigated various transition metals and their oxides for suitability as oxygen carriers (OC) in a few different reactor designs, including transport reactors, bubbling-fluidized-beds, and moving- and fixed-bed reactors. This technology has become increasingly popular among researchers as given by the number of literature sources reporting chemical-looping studies increasing, seemingly exponentially, over the past few years. Mattisson references over 130 sources in his latest review of the technology while focusing mainly on sources presenting results for the nontraditional CLC called Chemical-looping with Oxygen Uncoupling (CLOU) [12].

CLC takes advantage of a the redox characteristics of a material, called the

oxygen carrier (OC), which is typically a transition metal, by oxidizing the material at high-temperatures using an oxygen rich stream, typically air, in one reactor (the Air Reactor – AR) and reducing that material in a second reactor (Fuel Reactor – FR) using a fluid fuel [3, 20, 21, 22, 27]. The basic idea behind CLC may be visualized in Figure 3.

The air for oxidation is introduced in a reactor separate from the fuel; in so doing, the product CO_2 from combustion is inherently separated and may be purified further by condensing the product water from the effluent stream. This inherent separation of CO_2 is what makes the CLC technology so attractive.

The drawback of CLC lies in the challenge of utilizing solid fuels. For a traditional CLC oxygen carrier, the fuel directly reduces the carrier; therefore, a fluid fuel is necessary as the reaction rates of a solid-solid system are highly unfavorable. Therefore, in order to utilize a chemical-looping combustion system with solid fuels, the fuel must first be gasified.
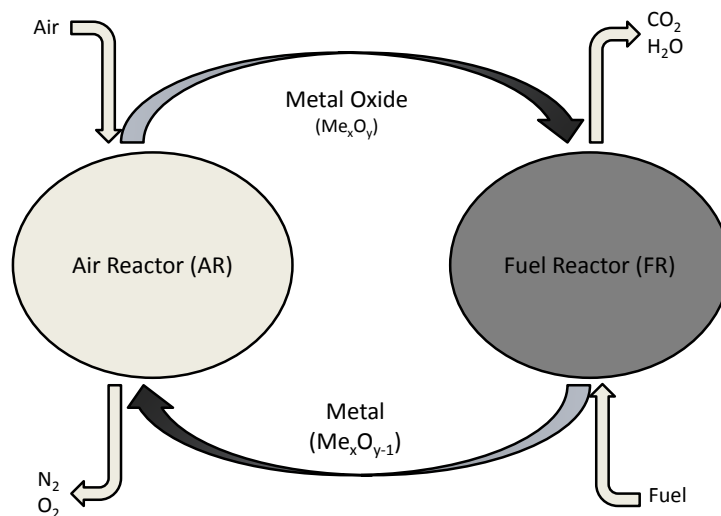
Figure 3: Basic schematic of CLC technology.

1.3 Chemical-looping with Oxygen Uncoupling (CLOU)

The use of traditional CLC materials has been successfully performed and reported in a multitude of studies. Moreover, these oxygen carriers have been tested with solid fuels and syngas mixtures. In an attempt to bypass the necessary gasification step, Mattisson et al. from Chalmers University of Sweden uncovered a technology they coined "Chemical-looping with Oxygen Uncoupling." They discovered that with certain materials, there exists a thermodynamic regime within which these materials may be oxidized in an oxygen rich atmosphere and may be reduced by subjecting the oxidized metal to an oxygen-depleted atmosphere [22]. This spontaneous reduction of the metal oxide may be more clearly understood when termed "decomposition" as opposed to "reduction."

The mechanism for this reaction is altered from traditional CLC only within the FR. Although traditional CLC relies on direct reduction of the OC from the fuel, CLOU first decomposes liberating gaseous oxygen which is then available for combustion. This oxygen then reacts with the fuel, once again depleting the atmosphere of oxygen driving the decomposition. The generalized reactions occurring within the fuel reactor for both CLC and CLOU are given in equations (1) - (3). Equation (2) defines the decomposition of the metal oxide and equation (3) gives the combustion of the fuel using the oxygen liberated by reaction (2). It may be readily shown that the sum of equations (2) and (3) is equation (1).

Although the name CLOU was not coined until 2009, this technology was actually tested and reported more than 50 years prior by Lewis, Gilliland and Sweeney [23]. Their results suggested that combustion of the solid fuel was roughly 50 times

faster, using the oxygen liberated from CuO decomposition, than the rate of gasification [24].

CLC

$$(2n + m)Me_xO_y + C_nH_{2m} \rightarrow (2n + m)Me_xO_{y-1} + nCO_2 + mH_2O \qquad (1)$$

CLOU

$$2Me_xO_y \rightarrow 2Me_xO_{y-1} + O_2 \qquad (2)$$

$$C_nH_{2m} + \left(n + \frac{m}{2}\right)O_2 \rightarrow nCO_2 + mH_2O \qquad (3)$$
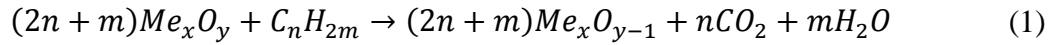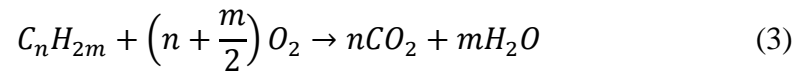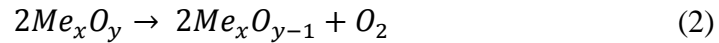
The determination of a suitable oxygen carrier is pivotal to the success of CLC/CLOU research and implementation. These materials must exhibit suitable physical and chemical reactivity characteristics. Typically, oxygen carrier materials are put upon a supporting substrate to improve both physical durability and internal surface area of the particles. The metal/substrate combination must retain high reactivity rates. In order to reduce the total amount of solids circulating between the reactors, it is important to optimize the loading of the metal on the substrate, thereby maximizing the oxygen carrying capacity of the solids.

1.4 Selection of Material for Oxygen Carriers

A few materials have been identified as having CLOU capabilities, including: CuO, Mn_2O_3, Co_3O_2 and the bimetallic compound $(Mn_{0.8}Fe_{0.2})_2O_3$ [22, 25]. These metal oxides all undergo a change in the equilibrium partial pressure of oxygen between the oxidized and reduced states at elevated temperatures. These elevated temperatures are in the range of a typical chemical-looping system, which, for long chain hydrocarbons such as solid fuels or oils, is above 700 °C according to Fan [26]. Fan also gives an upper limit on the temperature by referencing the Boudouard reaction given in equation (4). The Boudouard reaction is favored at higher temperatures and will decrease the degree of fuel conversion if not fully considered. Also, when deciding on a temperature ceiling for chemical-looping, it is important to consider the melting point and softening point temperatures of the materials being considered.

$$C + CO_2 \rightarrow 2CO \qquad\qquad (4)$$

The melting point of copper is relatively low compared to other CLOU carriers such as manganese and cobalt. The melting points of these metals along with some of the associated oxides are given in Table 2. Although the melting point of copper is considerably lower than the melting points of the other base metals, a comparison of the melting points of the relevant oxides associated with each base metal reveals the copper-based oxides have the highest melting points. This consideration of these melting points is critically important for the determination of a suitable carrier in a chemical-looping system for both traditional CLC and CLOU technologies – especially when applying the generally accepted concept of an interconnected dual fluidized-bed system for chemical-

Table 2: The melting points of different CLOU capable species.

Species	Melting Point (°C)
Cu	1,084
Cu_2O	1,232
CuO	1,201
Mn	1,246
Mn_2O_3	940
Mn_3O_4	1,567
Co	1,495
Co_3O_4	895
CoO	1,933

looping given by Lyngfelt et al. in 2001 [27]. Although the melting points of these species are known, a more difficult measure to quantify is the softening point of these species at which point these species begin to agglomerate and eventually sinter.

Agglomeration and sintering of fluidized-bed materials can prove catastrophic for operation and must be avoided. Along with other benefits, including additional internal surface area and improved structural durability, supporting substrates have been and are continually investigated to mitigate the risk of agglomeration within a fluidized-bed by raising the agglomeration temperature.

Typical supports either being investigated or having been reported on include: TiO2, ZrO2, Al2O3, Ilmenite, Sand, MgAl2O4, ZrO2/MgO and others. These supports are reported as having varying degrees of success in chemical-looping environments, and are continually investigated as to their effectiveness. Mattisson compiled a list of literature sources reporting investigations of CLOU using many different carriers at various temperatures [12].

Selection of materials for use in a CLOU system may be performed based upon reaction rates, carrying capacity, relevant reaction temperature regime, cost of the material (both for the initial charge and replacement of fragmented or deactivated material) and auto-thermal capabilities. The oxidation reaction of the relevant species in CLOU is always exothermic while the reverse reaction, decomposition, is always endothermic [28]. The endothermic nature of the decomposition reaction may present a challenge from the necessary additional heat needed to drive the reaction. For the reactions with lower heats of reaction, given in Table 3, the heat release from fuel combustion may overcome the endothermic nature of the oxygen carrier decompositions giving overall exothermic reactions in both the AR and FR. Of the four listed below, only the cobalt-based material has a heat of reaction too large to be overcome by the heat release from fuel combustion. Cobalt, therefore, creates challenges that almost certainly remove it from the list of suitable oxygen carriers for a chemical-looping system [22].

Further selection of a proper base for the oxygen carrier requires a closer thermodynamic analysis. Cao and Pan (2006) investigated the selection of both the proper carrier and reactor for a chemical-looping system. Their investigation revealed that manganese oxide-based carriers were not suitable for a chemical-looping reactor for a couple of different reasons. The lower oxidation state pair (Mn_3O_4/MnO) did not favor full conversion of the fuel to CO_2. They also mentioned that for the higher oxidation state pair (Mn_3O_4/Mn_2O_3), the oxygen carrying capacity is too low to be economical [29]. Additionally, the equilibrium partial pressure versus temperature plot, reference Figure 4, identifies the higher temperature capabilities of copper versus manganese and cobalt.

Copper-based oxygen carriers have been determined as having a high likelihood

Table 3: List of CLOU reactions and the resultant heats of reaction.

Species Reaction	Heat of Reaction	
$4CuO \leftrightarrow 2Cu_2O + O_2$	$\Delta H_{850} = 263.2 \; {}^{kJ}/_{mol \; O_2}$	(5)
$6Mn_2O_3 \leftrightarrow 4Mn_3O_4 + O_2$	$\Delta H_{850} = 193.9 \; {}^{kJ}/_{mol \; O_2}$	(6)
$2Co_3O_4 \leftrightarrow 6CoO + O_2$	$\Delta H_{850} = 408.2 \; {}^{kJ}/_{mol \; O_2}$	(7)
$(Mn_{0.8}Fe_{0.2})_2 \leftrightarrow (Mn_{0.8}Fe_{0.2})_3O_4 + O_2$	$\Delta H_{850} = 254 \; {}^{kJ}/_{mol \; O_2}$	(8)

of success for a CLOU-operated system. Although there are more expensive alternatives to copper, there are also more economical ones. Copper is an expensive substance which happens to have a relatively low melting point. Therefore, it is critically important to create an oxygen carrier material with a suitable support and production method. These two factors will determine whether a suitable copper-based carrier may or may not be found.

One challenge that exists for the production of a suitable carrier is to homogeneously disperse the copper (oxide) throughout the particle. This will maximize structural support from the substrate, decrease the risk of agglomeration by minimizing copper-copper contact between particles and increase internal surface area, thereby diffusing possible internal mass transfer limitations to redox rates.

1.5 Objectives of This Work

Given the myriad of information available in the field of chemical-looping, it is essential to the further development of this technology that the fundamental kinetic
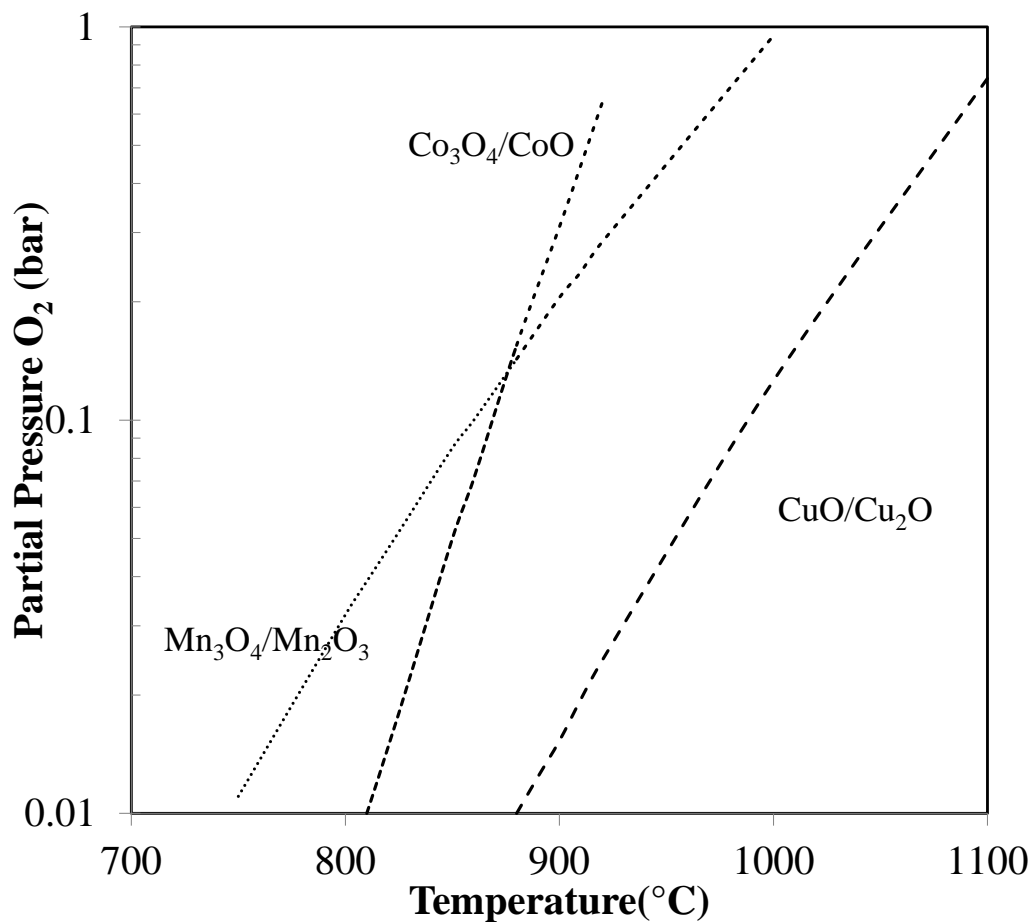
Figure 4: Equilibrium partial pressure of oxygen for three different metal oxide pairs.

modeling of the suggested oxygen carrier materials be understood. In the case of copper

oxide, the kinetics of decomposition and, more particularly, oxidation are not adequately

understood. For the industrial and commercial implementation of this technology and

these materials, the fundamental kinetics must be understood for proper modeling.

Additionally, the development of novel carriers and production methods is

important to the industrialization of this technology. The development of materials that

are optimally suited for solid fuels combustion in a fluidized-bed environment requires

further investigation.

Although gaining popularity among researchers, the investigation of directly injected solid fuels combusted using copper oxide-based oxygen carriers still needs additional attention. The effects fuel type, fuel particle size and temperature must be understood for successful design and operation of commercial/industrial-scale CLOU reactors. Hence, it is the purpose of this work to:

1. Improve understanding of and develop kinetic models for the oxidation and decomposition of copper oxide-based oxygen carriers,

2. Evaluate performance of promising novel carriers, and

3. Investigate conversion of solid fuels with regard to fuel type, particle size and temperature.

<u>1.6 References</u>

[1]   U.S. NOAA. The NOAA Annual Greenhouse Gas Index (AGGI). Boulder, CO. Web 18 June 2013.

[2]   United States Environmental Protection Agency. Inventory of U.S. Greenhouse Gas Emissions and Sinks: 1990 – 2011. EPA 430-R-13-001. Washington D.C.   Web 13 June 2013.

[3]   United States Department of Energy. DOE/NETL Carbon Dioxide Capture and Storage RD&D Roadmap. Web 17 June 2013.

[4]   Ekström, C., Schwendig, F., Biede, O., Franco, F., Haupt, G., De Koeijer, G., Papapavlou, C., Røkke, P.E., Techno-Economic Evaluations and Benchmarking of Precombustion CO2 Capture and Oxy-fuel Processes Developed in the European ENCAP Project. Energy Procedia 2009; 1 (1): 4233–4240.

[5]   Marion, J., Mohn, N., Liljedahl, G.N., Nsakala, N., Morin, J-X., Henriksen, P.-P., Technology options for controlling CO_2 emissions from fossil-fueled power plants, Third Annual Conference on Carbon Capture and Sequestration, 3-6 May 2004, Alexandria, VA; 2004.

[6]   Ishida, M., Zheng, D., Akehata, T. Evaluation of a chemical-looping combustion power-generation system by graphic exergy analysis. Energy. 1987, 12 (2): 147-154.

[7]   Ishida, M., Jin, H. A new advanced power-generation system using chemical-looping combustion. Energy. 1994, 19 (4): 415-422.

[8]   Ishida, M., Jin, H. A novel chemical-looping combustor without NOx formation. Ind Eng Chem Res. 1996, 35 (7): 2469-2472.

[9]   Ishida, M., Jin, H. CO2 recovery in a power plant with chmical looping combustion. Energ Conv Mange. 1997, 38 (1): 2469-2472.

[10]   Ishida, M., Jin, H., Okamoto, T. A fundamental study of a new kind of medium material for chemical-looping combustion. Energ Fuel. 1996, 10 (4): 958-963.

[11]   Ishida, M., Jin, H., Okamoto, T. Kinetic behavior of solid particle in chemical-looping combustion: suppressing carbon deposition in reduction. Energ Fuel. 1998, 12 (2): 223-229

[12]   Mattisson, T. Materials for chemical-looping with oxygen uncoupling. ISRN Chem. Eng. 2013. http://dx.doi.org/10.1155/2013/526375.

[13]   Johansson, E., Lyngfelt, A., Mattisson, T., Johnsson, F. Gas leakage measurements in a cold model of an interconnected fluidized-bed for chemical-looping combustion. Powd. Tech. 2003, 134 (3): 210-217.

[14] Mattisson, T., Lyngfelt, A., Cho, P. The use of iron oxide as an oxygen carrier in chemical-looping combustion. Energ Fuel. 2003, 17 (3): 643-651.

[15] Garcia-Labiano, F., de Diego, L., Adanez, J., Abad, A., Gayan, P. Temperature variations in the oxygen carrier particles during their reduction and oxidation in a chemical-looping combustion system. Chem Eng Sci. 2005, 60 (3): 851-862.

[16] Kronberger, B., Johansson, E., Loffer, G., Mattisson, T., Lyngfelt, A., Hofbauer, H. A two-compartment fluidized-bed reactor for CO2 capture by chemical-looping combustion. Chem Eng Tech. 2004, 27 (12): 1318-1326.

[17] Kronberger, B., Loffler, G., Hofbauer, H. Simulation of mass and energy balances of a chemical-looping system. Int J Energ Clean Env. 2005, 6 (1): 1-14.

[18] Kronberger, B., Lyngfelt, A., Loffler, G., Hofbauer, H. Design and fluid dynamic analysis of a bench-scale combustion system with CO2 separatoin-chemical-looping combustion. Ind Eng Chem Res. 2005, 44: 546-556.

[19] Ryu, H., Bai, D., Jin, G. Carbon deposition characteristics of NiO based oxygen carrier particles for chemical-looping combustor. Proceedings of the 6th International Conference on Greenhouse Gas Control Technologies, J. Gale and Y. Kaya, Eds., pp. 175-180, Elsevier, Oxford, UK, 2002.

[20] Ishida, M., Jin, H. A Novel Combustor based on chemical-looping reactions and its reaction kinetics. J Chem Eng. 1994, 3: 296-301.

[21] Lyon, R. K., Cole, J. A. Unmixed combustion: an alternative to fire. Combust Flame. 2000, 121 (1-2): 249-261.

[22] Mattisson, T., Lyngfelt, A., Leion, H. Chemical-looping with oxygen uncoupling for combustion of solid fuels. Int J Greenh Gas Con. 2009, 3 (1): 11-19.

[23] Lewis, W.K., Gilliland, E.R., Sweeney, M.P. Gasification of carbon: metal oxides in a fluidized powder bed. Chem Eng Pro. 1951, 47: 251-256.

[24] Eyring, E., Konya, G., Lighty, J., Sahir, A., Sarofim, A., Whitty, K. Chemical looping with copper oxide as carrier and coal as fuel. Oil Gas Sci Tech. 2011, 66: 209-221

[25] Azimi, G., Rydén, M., Leion, H., Mattisson, T., Lyngfelt, A. (MnzFe1-z)yOx combined oxides as oxygen carrier for Chemical-Looping with Oxygen Uncoupling (CLOU). AIChE J. 2013, 59: 582-588.

[26] Fan, L. Chemical-looping systems for fossil energy conversion. John Wiley and Sons, Hoboken, NJ, USA, 2010.

[27] Lyngfelt, A., Leckner, B., Mattisson, T. A fluidized-bed combustion process with inherent CO2 separation; application of chemical-looping combustion. Chem Eng

Sci. 2001, 56 (10): 3101-3113.

[28] Jerndal, E., Mattisson, T., Lyngfelt, A. Thermal analysis of chemical-looping combustion. Chem Eng Res Des. 2006, 9: 795-806.

[29] Cao, Y., Pan, W.P. Investigation of chemical looping combustion by solid fuels. 1. process analysis. Energ. Fuel. 2006, 20: 1836-1844.

CHAPTER 2

REVIEW OF LITERATURE

The term chemical-looping was first introduced into the literature in 1987 by

Ishida et al. [1], but Lewis and Gilliland studied a copper-based chemical-looping system

in the 1940s and 50s [1, 2]. About 30 years later, Richter and Knoche [3] proposed that

combustion efficiency be improved through a CLC process in 1983.

By 2008, there were nearly 100 published articles reporting CLC testing with

different materials as potential oxygen carriers [4]. Among those tested up to that point,

the most common materials tested were NiO and Fe_2O_3, although there were also a few

studies involving other materials such as CuO, CoO and MnO. Only six of those articles

reported using solid fuels as the reductant (i.e., coal, petroleum coke and lignite char).

The remaining sources all reported results of CLC testing using gaseous fuels. It should

be noted that a significant number of those reports discussed the use of syngas as a

reductant, which may also be included as solid fuels testing due to syngas being the main

product of gasification reactions [4].

2.1 CLC

Traditional CLC carriers refer to those unable to spontaneously uncouple from

scavenged oxygen such as Ni-, Fe- and Ca-based materials. Fang et al. reported that

nickel-oxide-based carriers were believed to be the most promising oxygen carrier candidates [5]. Jin and Ishida [6] established that unsupported NiO lost reactivity over extended cycling times and attributed it to the agglomeration of NiO particles. Due to the low melting points of most transition metals, especially those most suitable for CLC, agglomeration becomes a significant design challenge and is generally circumvented by the use of an inert support material. These inert supports range from those commonly used in other applications such as Al_2O_3, bentonite, SiO_2 and TiO_2 to some less common supports such as ZrO_2/MgO, $MgAl_2O_4$, YSZ and $NiAl_2O_4$.

Judging from reactivity studies of different oxygen carriers with natural gas, NiO and CuO show the most intriguing rates [7-10]. The disadvantages of Ni include its toxicity and thermodynamic limitations in conversion of fuels. However, Ni remains attractive due to its higher melting point than Cu [11]. Mattisson et al. presented results of using NiO/NiAl2O4 in TGA, lab-scale fluidized-bed (FB) and a 10 kW continuous CLC reactor at temperatures from 750 °C to 900 °C. They concluded that the FB displayed faster reaction rates than those observed in TGA which translated to a solids inventory of 9-24 kg/MW assuming a strictly plug-flow model (for the gas) in the FB. This assumption proved insufficient for estimating scale-up parameters for the 10 kW system where an incomplete gas yield was observed [11].

Fe-based carriers are very attractive due to their low cost, availability and high strength, according to Lyngfelt et al. [4]. Fan et al. have done extensive work on Fe-based systems, including H_2 production, coal and biomass studies [26,12]. Among the Fe-based carriers, iron-ores have received some attention due to the very low cost. An attractive iron-ore, ilmenite (generally accepted as $FeTiO_2$), has been described as an

attractive material as an oxygen carrier [13, 14]. Leion et al. (2008) tested the reactivity and effectiveness of ilmenite as an oxygen carrier in a lab-scale fluidized-bed [14]. They concluded that ilmenite showed no decrease in reactivity when exposed to alternating oxidizing/reducing cycles over 37 cycles. They stated also that the reduction of ilmenite is endothermic, but less so than both NiO/Ni and Fe_2O_3/Fe_3O_4 on a per mole basis.

Adanez et al. reported a study of manganese oxide on 5 different support materials in 2004 [15]. They reported testing on Al_2O_3, sepiolite, SiO_2, TiO_2 and ZrO_2. Of these supports, ZrO_2 was found to be the only material suitable for CLC based on mechanical strength and reactivity. Further exploration by Mattisson et al. [16] and Cho et al. [8] suggested that Mn supported by Al_2O_3 was unsuitable as an oxygen carrier due to particles sintering. Johansson et al. then investigated ZrO_2-supported manganese-based carriers [17]. In all, four different carriers were prepared and tested which include: pure ZrO_2, and then ZrO_2 stabilized by CaO, MgO and CeO_2. They reported that the carrier supported by ZrO_2 stabilized by MgO displayed the highest reactivity.

Although the advantages and disadvantages of oxygen carriers developed using single-metal oxides have been established repeatedly, some institutions thought it wise to develop an oxygen carrier that takes the advantages of different single-metal oxygen carriers and combine the metals in an effort to utilize the desirable characteristics of each while overcoming the undesirable characteristics [5]. Jin et al. suggested that the hybrid Ni-Co/YSZ carrier outperformed the single-metal counterparts (Ni/YSZ and Co/YSZ) [18]. While nickel normally performs well as a carbon deposition catalyst (which is undesirable in CLC), Adanez et al. [19] reported that when used in a mixed Ni-Cu-based oxygen carrier, 100% conversion of CH_4 to CO_2 and H_2O was observed with no carbon

deposition. Additionally, due to the higher melting point of nickel, the low melting point agglomeration effects of copper were not observed. Johansson et al. discovered that a combination of 3% nickel oxides in 97% iron oxides nearly doubled the CO_2 output per unit time when compared to the sum of the CO_2 output by the two individual metals separately [9].

Adánez et al. recently presented a review of oxygen carriers proposed for CLC using gaseous fuels. They reviewed carriers based on copper, nickel, manganese, iron and cobalt. Through thermodynamic analysis, the report shows the 6 forms of copper-based oxygen carriers as among the most favorable toward full conversion of the fuel to CO_2 and H_2O [20].

2.2 CLOU

Lewis, Gilliland and Sweeney first reported the CLOU capabilities of copper in 1951 [2]. They were using the Cu/CuO loop as a means to generate CO_2. Their findings showed that the rate of decomposition of CuO to Cu_2O is many times faster than the rates of coal gasification. By utilizing the spontaneous reduction tendencies of CuO, they determined it was possible to bypass the gasification step altogether and directly combust the fuel using the oxygen given off during CLOU. Mattisson et al. demonstrated the CLOU process using both CuO/Cu and Mn_2O_3/Mn_3O_4 as oxygen carriers. They demonstrated that the reaction rate of petroleum coke could be increased by a factor of 50 when using a CLOU process compared to an iron-based carrier under the same conditions, but operating under a CLC process [21].

Copper oxide has exhibited the fastest reaction rates of the possible metal oxides

for CLC [22]. In addition to fast reaction rates, the typically overall endothermic nature

of the FR in a CLC system is exothermic for CuO. Copper oxide displays the following

positive characteristics: (1) lower solids inventory and circulation due to high reactivity

and high oxygen carrying capacity [23]; (2) Cu/CuO exhibit an overall exothermic

reaction system in both the AR and FR, eliminating the need to heat the FR [24]; (3)

thermodynamically speaking, CuO is favored to completely convert gaseous

hydrocarbons to CO_2 and H_2O [22].

Early testing indicated the need for an inert support because copper has a very low

melting point and agglomerates readily when used in a CLC reactor. The reaction rate of

CuO decreased very quickly with increasing cycle number according to de Diego et al.

[25]. They also reported upon further investigation that any mass loading of CuO on and

inert support material below 10 wt% would never agglomerate while anything over 20

wt% would always agglomerate. Furthermore, they recommended that impregnation

methods may be the only effective method for carrier preparation. However, Chuang et

al. in 2008 rejected the preparation methods of mechanical mixing as well as wet-

impregnation and displayed positive results for carriers prepared using co-precipitated

techniques [26]. These carriers did not show any signs of agglomeration and maintained

high reactivity over the 18 test cycles.

2.3 Kinetics of CLOU

Although previous studies have addressed many issues regarding the performance

of a multitude of potential carriers, there is still much to be understood. One important

gap in the understanding is the fundamental kinetics of the oxygen carriers. Although

Adánez-Rubio et al. began to discuss the specific kinetic parameters of copper-based oxygen carriers in 2012 [20], the level of scientific work is, as of yet, incomplete. These parameters include reaction rate as a function of: temperature, pressure, oxygen loading, support material, particle size, oxygen partial pressure and coal type.

The oxidation kinetics of copper oxide, particularly, has yet to be adequately described within the literature. As temperature is increased, the reaction rates for oxidation begin to slow, thereby making the Arrhenius plot reverse direction and thereby generate a negative apparent activation energy. This is mainly due to a decrease in oxidation rate at high temperature which has been reported as a reversal of activation energy at elevated temperatures. Adánez-Rubio et al. ascribe the reversing activation energy strictly due to the decrease in the oxygen partial-pressure driving force as a function of temperature [20]. Wilkins and Rideal [27] suggested that the decreasing oxidation rate with increasing temperature was governed by the rate of diffusion of oxygen through the film of oxide. Although conflicting ideas are proposed here, it is possible that more than 1 of these mechanisms play a role in this phenomenon. What is certain is that for larger-scale copper oxide-based CLOU plants, a better understanding of these kinetics are necessary for design and scale-up.

Mattisson provided a generalized reaction rate as follows:

$$r_d = k_r \left(\frac{p_{O_2,eq} - p_{O_2}}{p_{O_2,eq}} \right) \qquad (9)$$

where $p_{O_2,eq}$ is the equilibrium partial pressure of oxygen, an exponential function of temperature and k_r is a reaction rate constant. The rate of decomposition is challenging to

determine. Adánez-Rubio et al. reported an apparent decrese in the decomposition rate with an increase in the oxygen partial pressure by supplying different concentrations of oxygen during decomposition [29]. Because the rate of decomposition is a function of the local oxygen partial pressure, inversely related, it is necessary to either estimate the partial pressure at the particle surface or to design experiments to deplete the local partial pressure of oxygen enough to remove any influence generated. This may be accomplished in a few ways, all of which have their own challenges.

In order to deplete the oxygen partial pressure at the surface of the particle, a sweeping diluent may be added in sufficient quantity as to remove the oxygen molecules quickly enough to mitigate any influence created. Alternatively, a fuel may be added in order to immediately react with the liberated oxygen. This second approach presents the challenge of fuel selection. Most fuels with directly reduce the oxygen carrier, which commonly has faster reaction rates than the rates of CuO decomposition. This direct reduction likely occurs with most gaseous reactants. Likewise, due to the thermal breakdown of solid fuels (devolatilization), the liberated volatile compounds will also directly reduce the oxygen carrier particles. For this method to be successfully performed, it is necessary to use a char produced at a temperature above the targeted operating temperature and at high heating rates in order to prevent the release of any volatile species after introduction to the fuel reactor.

In an effort to decrease the local partial pressure of oxygen without directly reducing the oxygen carrier, Arjmand et al. [28] introduced an excess of devolatilized wood char to a bed of freeze-granulated $CuO/MgAl_2O_4$. The goal of this approach was to have the released oxygen consumed by the char as close to the instant of release as

possible. In order for this to be successful, the char must be completely devolatilized or the released volatiles may react directly with the oxygen carrier, thereby reducing the oxygen carrier in a path other than spontaneous decomposition and skewing the decomposition rate data. The tests were performed in the range of 850-900 °C and the decomposition reaction was modeled using the Avrami-Erofeev mechanism. The resulting Arrhenius expression produced an apparent activation energy of 139.3 kJ/mole. In a similar manner, Adańez-Rubio et al. [29] obtained a decomposition rate of 2.3×10-3 kgO_2/kg carrier. Sahir et al. reported an activation energy of 281 kJ/mole [30], which was somewhat smaller to the work produced by Chadda et al. [31] where an activation energy of 313 kJ/mole was determined. The work by Eyring et al. [32] produced an activation energy very similar to Chadda et al. of 327 kJ/mole.

Although only a small range of models and methods exist for the description of the kinetics of decomposition of CuO, there are relatively fewer descriptions for the oxidation of Cu_2O to CuO. This particular reaction is challenging to adequately describe while developing a simple enough model to be used in large-scale modeling projects.

It has been reported in several sources that the rate of oxidation reaches a maximum at elevated temperatures and then begins to decrease with increasing temperature [26, 32 -34]. This is due at least in part to a decrease in the difference between the equilibrium O_2 partial pressure and air's partial pressure of 0.21 atm, at sea level. In addition to the change in the driving force of oxidation, the molar volume of CuO is 5% larger than that of Cu_2O; therefore, during oxidation, the solid must "grow" in order to accommodate the added molar volume [35, 36]. This "growth" of the solid particle may cause collapsing of the smaller pores within the particle [37]. The

collapsing of these smaller pores may "block" access to the remaining unreacted solid. This effect may be recognized by a distinct change in the reaction rate, creating two different regions of the conversion vs. time curve: the first region shows high reaction rates, whereas the second shows a distinct change in the rate at a considerably slower value [38, 39, 40]. The mechanism used to describe this phenomenon is labeled "pore-blocking kinetics" and uses a logarithmic rate law which includes an empirically determined pore-blocking constant. This pore-blocking constant may be a function of temperature [39, 40] as well as number of redox cycles.

Therefore, if the pore-blocking constant is a function of temperature, then the full kinetic expression includes three terms, all dependent on temperature (activation energy, $p_{O_2,eq}$ and the pore-blocking constant). This triple dependency on temperature makes it difficult to ascertain the truly inherent activation energy of this reaction, and has thus given rise to the very limited amount of literature on the subject. The most applicable source on this matter was produced by Zhu et al. [36], where they describe a logarithmic rate law to which they were able to adequately fit their data. They report two activation energies, one at low temperatures and one at the higher temperatures where the oxidation rates begin to slow. This work is not directly applicable due to the experimental differences. For chemical-looping, the generally accepted design is an interconnected fluidized-bed of porous particles. The experimental approach of Zhu et al. utilized the oxidation/decomposition of pure copper rods. The effects seen and described by Zhu et al. are almost certainly influenced by mass-transfer resistances due to the sample size and nonporous nature and are, therefore, inadequate for the description of CuO-based particles in a chemical-looping process.

2.4 Combustion of Solid Fuels

The first demonstration of the CLOU concept by Mattisson et al. was performed in a batch fluidized-bed reactor by the oxidation of 0.1 g of petroleum coke at 985 °C using two different cupric oxide-based materials: CuO/Al_2O_3 and CuO/ZrO_2. Their results showed that the rate of CuO decomposition was faster than the oxidation rate of the petcoke observed by a nonzero value of the O_2 volume fraction during fuel combustion [22]. The individual reaction regimes for this test (1) OC oxidation, (2) CLOU decomposition, (3) fuel oxidation and (4) OC regeneration are all clearly identified by the changes in temperature. It is clear that during the reduction cycle, even though the decomposition reaction is endothermic, the combustion of the fuel is exothermic enough to overcome the temperature drop. Burnout of the petcoke is completed within 30 seconds, and the rate of conversion observed within the reaction is roughly a 45 fold increase to that observed using an iron-based carrier [12].

The conversion of 0.1 g of petcoke during the decomposition of a CuO-based oxygen carrier with a zirconia support may be seen in Figure 5. Three obvious regimes may be seen. The figure shows the end of the oxidation cycle with the oxygen volume fraction around 0.21. The air is turned off and the nitrogen purge is cycled on, leading to the oxygen fraction decrease seen around 30 seconds. The remaining excess oxygen is purged from the reactor before the fuel is introduced into the reactor. The petcoke is then combusted as evidenced by the spikes of the carbonaceous species. Upon fuel burnout, the oxygen volume fraction once again increases toward the equilibrium partial pressure. When the fuel is first introduced, a small methane peak may be seen,   which represents devolatilization of the fuel.
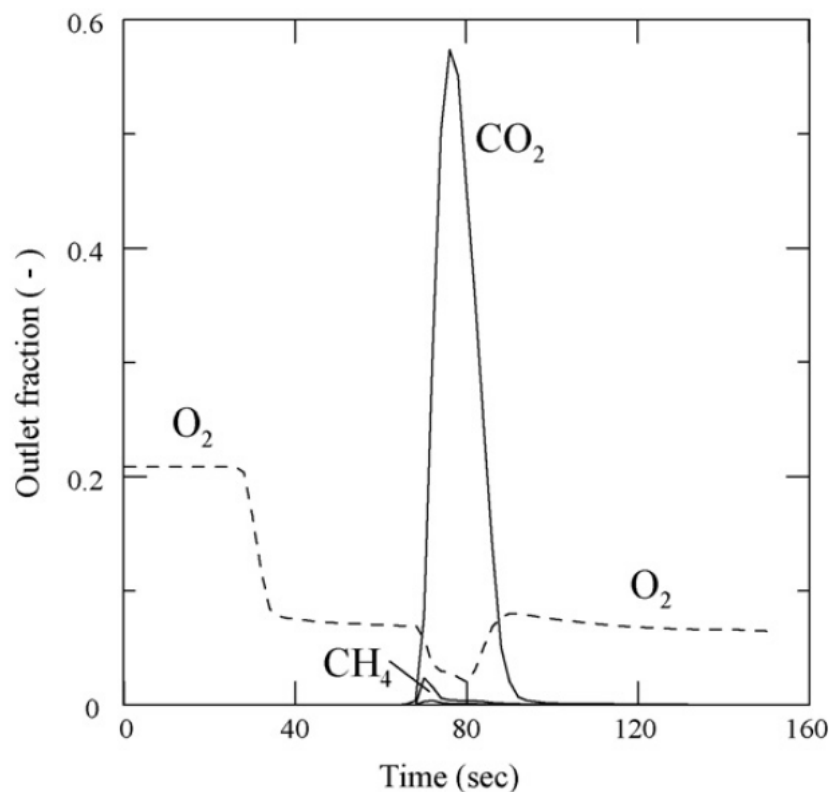
Figure 5: Concentration profile during the conversion of 0.1 g of petroleum coke with 15 g CuO/ZrO2. The temperature was measured to 985 °C in the bed of material at the start of the experiment. The fluidizing gas is pure nitrogen. From Mattisson et al., Chemical-looping with oxygen uncoupling for combustion of solid fuels, Int J Green H Gas Con, 2009, 3: 11-19.

Leion et al. performed a set of CLOU experiments in the range of 850 – 985 °C using 6 different solid fuels while testing the performance of a CuO/ZrO_2 material. This set of experiments helped to solidify the advantage CLOU has in solid fuel conversion over traditional CLC. This advantage was especially realized in the low volatile fuels.

Gayán et al. performed a set of experiments covering 27 different fuels and several different oxygen carriers [33]. Through a set of three different campaigns, the most promising materials tested were spray dried CuO/ZrO_2 and $CuO/MgAl_2O_4$. They were able to obtain complete combustion using a solid inventory in the FR of 235

kg/MWth [33, 41, 42].

A large number of sources report the use of solid fuels for combustion in both CLC and CLOU. The fuels ranged from lignite [14, 42, 43], to petcoke [21, 22, 44-48], to biomass chars [44, 49, 50] to coals [29, 44, 46, 51].

2.5 References

[1] Lewis, W. K., & Gilliland, E. R. Patent No. 2,665,972. United States of America. 1954.

[2] Lewis, W. K., Gilliland, E. R., & Sweeney, W. P. Gasification of carbon: metal oxides in a fluidized powder bed. Chem Eng Prog. 1951, 251-256.

[3] Richter, H., & Knoche, K. Reversibility of combustion processes. ACS Symposium Series. 1983, 235: 415-422.

[4] Lyngfelt, A., Johansson, M., & Mattisson, T. Chemical-looping combustion - status of development. 9th International Conference on Circulating Fluidized-beds. Hamburg. 2009.

[5] Fang, H., Haibin, L., & Zengli, Z. Advancements in developmnet of chemical-looping combustion: a review. Int J Chem Eng. 2009, 16.

[6] Jin, H., & Ishida, M. A new type of coal gas fueled chemical-looping combustion. Fuel. 2004, (83), 2411-2417.

[7] Adanez, J., Adanez, J., de Diego, L. F., Garcia-Labiano, F., Gayan, P., Abad, A. Selection of oxygen carriers for chemical-looping combustion. Energ Fuel. 2004, 18 (2), 371-377.

[8] Cho, P., Mattisson, T., & Lyngfelt, A. Comparison of iron-, nickel-, copper- and manganese-based oxygen carriers for chemical-looping combustion. Fuel. 2004, 83 (9), 1215-1225.

[9] Johansson, M., Mattisson, T., & Lyngfelt, A. Comparison of oxygen carriers for chemical-looping combustion. Therm Sci. 2006 (10), 93-107.

[10] Johansson, M., Mattisson, T., & Lyngfelt, A. Comparison of oxygen carriers for chemical-looping combustion of methane rich fuels. 19th International Conference on Fluidized-bed Combustion. Vienna. 2006.

[11] Mattisson, T., Jerndal, E., Linderholm, C., & Lyngfelt, A. Reactivity of a spray-dried $NiO/NiAl_2O_4$ oxygen carrier for chemical-looping combustion. Chem Eng Sci. 2011, 66 (20): 4636-4644.

[12] Fan, L. S., & Li, F. Ind Eng Chem Res. 2010, (49): 10200-10211.

[13] Bergurand, N., & Lyngfelt, A. Chemical-Looping Combustion of Petroleum Coke Using Ilmenite in a 10 kWth. Energ. Fuel. 2009: 5257-5268.

[14] Leion, H., Lyngfelt, A., Johansson, M., Jerndal, E., & Mattisson, T. The use of ilmenite as an oxygen carrier in chemical-looping combustion. Chem Eng Res Des. 2008, (86): 1017-1026.

[15] Adanez, J., Adanez, J., de Diego, L. F., Garcia-Labiano, F., Gayan, P., Abad, A. Selection of Oxygen Carriers for Chemical-Looping Combustion. Energ Fuel. 2004, 18 (2): 371-377.

[16] Mattisson, T., Jardnas, A., & Lyngfelt, A. Reactivity of some metal oxides supported on alumina with alternating methane and oxygen - application for chemical-looping combustion. Fuel. 2003, 17 (3): 1749-1757.

[17] Johansson, M., Mattisson, T., Lyngfelt, A. Investigation of Mn3O4 with stabilized ZrO2 for chemical-looping combustion. Chem Eng Res Des. 2006, 84 (9): 807-818.

[18] Jin, H., Okamoto, T., & Ishida, M. Development of a novelchemical-looping combustion: synthesis of a lopping material with a double metal oxide of CoO-NiO. Energ Fuel. 1998, 12 (6): 1272-1277.

[19] Adanez, J., Garcia-Labiano, F., de Diego, L. F., Gayan, P., Celaya, J., & Abad, A. Nickel-copper oxygen carrier to reach zero CO and H2 emissions in chemical-looping combustion. Ind Eng Chem Res. 2006, 45 (8): 2617-2625.

[20] Adanez, J., Abad, A., Garcia-Labiano, F., Gayan, P., & de Diego, L. F. Progress in Chemical-Looping Combustion and Reforming technologies. Prog Energ Comb. 2012, (38): 215-282.

[21] Mattisson, T., Leion, H., & Lyngfelt, A. Chemical-looping with oxygen uncoupling for combustion of solid fuels. Int J Greenh Gas Cont. 2009, 3 (1): 11-19.

[22] Garcia-Labiano, F., de Diego, L. F., Adanez, J., Abad, A., & Gayan, P. Reduction and oxidation kinetics of a copper-based oxygen carrier prepared by impregnation for chemical-looping combustion. Ind Eng Chem Res. 2004, 43 (26): 8168-8177.

[23] Abad, A., Adanez, J., Garcia-Labiano, F., de Diego, L. F., Gayan, P., & Celaya, J. Mapping of the range of operational conditions for Cu-, Fe-, and Ni-based oxygen carriers in chemical-looping combustion. Chem Eng Sci. 2007, 62 (1-2), 533-549.

[24] de Diego, L. F., Garcia-Labiano, F., Gayan, P., Celaya, J., Palacios, J. M., & Adanez, J. Operation of a 10 kWth chemical-looping combustor during 200 h with a CuO-Al2O3 oxygen carrier. Fuel. 2007, 86: 1036-1045.

[25] de Diego, L. F., Garcia-Labiano, F., & Adanez, J. Development of cu-based oxygen carriers for chemical-looping combustion. Fuel. 2004, 83 (13): 643-651.

[26] Chuang, S. Y., Dennis, J. S., Hayhurst, A. N., & Scott, S. A. Development and performance of Cu-based oxygen carriers for chemical-looping combustion. Comb Flame. 2009, 154 (1-2): 109-121.

[27] Wilkins, F. J., & Rideal, E. K. The kinetics of the oxidation of copper. Part I. The initial Oxidation of Copper at Low Pressures. The Royal Society. 1980, 128: 394-406.

[28] Arjmand, M., Keller, M., Leion, H., Mattisson, T., Lyngfelt, A. Oxygen release and oxidation rates of MnAl2O4-supported CuO oxygen carrier for chemical-looping with oxygen uncoupling (CLOU). Energ Fuel. 2012, 26: 6528-6539.

[29] Adańez-Rubio, I., Abad, A., Gayan, P., de Diego, F., Garcia-Labiano, F., Adanez, J. Identification of operational regions in the chemical-looping with oxygen uncoupling (CLOU) process with a cu-based oxygen carrier. Fuel. 2012, 102: 634-645.

[30] Sahir, A., Sohn, H., Leion, H., Lighty, J. Rate analysis of chemical-looping with oxygen uncoupling (CLOU) for solid fuels. Energ Fuel. 2012, 26: 4395-4404.

[31] Chadda, D., Ford, J., Fahim, M. Chemical energy storage by the reaction cycle of CuO/Cu2O. Int J Energ Res. 1989, 13 (1): 63-73.

[32] Eyring, E., Konya, G., Lighty, J., Sahir, A., Sarofim, A., Whitty, K. Chemical looping with copper oxide as carrier and coal as fuel. Oil Gas Sci. Tech. 2011, 66: 209-221.

[33] Gayan P, Adánez-Rubio I, Abad, A, de Diego LF, García-Labiano F, Adánez J. Development of Cu-based oxygen carriers for chemical-looping with oxygen uncoupling (CLOU) process. Fuel. 2012, 96:226-238.

[34] Brandt B, Gruene P, Rosowski F, Farrauto RJ, Castaldi MJ. Oxygen uptake and release kinetics of Cu/Cu2O/CuO on Al2O3 and ZrO2-SiO2 as materials for chemical looping combustion, AIChE Annual Meeting. Minneapolis, MN, USA; 2011.

[35] Prisedsky V, Vinogradov V. Fragmentation of diffusion zone in high-temperature oxidation of copper. J Solid State Chem 2004; 177: 4258-4268.

[36] Zhu Y, Mimura K, Isshiki M. Oxidation mechanism of Cu2O to CuO at 600-1050 °C. Oxid Met. 2004, 62 (3): 207-222.

[37] Evans, U.R. The Corrosion and Oxidation of Metals: Scientific Principles and Practical Applications. Edward Arnold Ltd.: London, 1960.

[38] Sohn, H.Y., Byung, S.K. A novel cyclic reaction system involving CaS and CaSO2 for converting sulfur dioxide to elemental sulfur without generating secondary pollutants. 2. Kinetics of the reduction of sulfur dioxide by calcium sulfide powder. Ind Eng Chem Res. 2002, 41: 3087-3091

[39] A novel reaction system involving BaS and BaSOR for converting SO2 to elemental sulfur without generating pollutants: Part I. Feasibility and kinetics of SO2 reduction with BaS. Chem Eng Sci. 2006, 61: 5088-5093.

[40] Won, S., Sohn, H.Y. Kinetics of the Reaction between Hydrogen Sulfide and Lime Particles. Metall Trans B. 1985, 16 (B): 163-168.

[41] Abad, A., Adánez-Rubio, I., Gayán, P., García-Labiano, F., de Diego, L. F., Adánez, J. Demonstration of chemical-looping with oxygen uncoupling (CLOU) process in a 1.5 kWth continuously operating units using a Cu-baed oxygen-carrier. Int J Greenh Gas Con. 2012, 6: 189-200.

[42] Adanez-Rubio, I., Gayan, P., Abad, A., Garcia-Labiano, F., de Diego, L., Adanez, J. CO2 capture in coal combustion by chemical-looping with oxygen uncoupling (CLOU) with a cu-based oxygen carrier. Proceedings of the 5th International Conference on Clean Coal Technologies (CCT '11), Zaragoza, Spain, 2011.

[43] Adanez-Rubio, I., Abad, A., Gayan, P., de Diego, L., Garcia-Labiano, F., Adanez, J. Performance of CLOU process in the combustion of different types of coal with CO2 capture. Int J Greenh Gas Con. 2013, 12: 430-440.

[44] Leion, H., Mattisson, T., Lyngfelt, A. Using chemical-looping with oxygen uncoupling (CLOU) for combustion of six different solid fuels. Energ Proc. 2009, 1: 447-453.

[45] Leion, H., Larring, Y., Bakken, E., Bredesen, R., Mattisson, T., Lyngfelt, A. Use of CaMn0.875Ti0.125O3 as oxygen carrier in chemical-looping with oxygen uncoupling. Energ. Fuel. 2009, 23: 5276-5283.

[46] Azimi, G., Leion, M., Ryden, M., Mattisson, T., Lyngfelt, A. Investigation of different Mn-Fe oxides as oxygen carrier for chemical-looping with oxygen uncoupling (CLOU). Energ Fuel. 2013, 27: 367-377.

[47] Arjmand, M., Leion, H., Lyngfelt, A., Mattisson, T. Use of manganese ore in chemical-looping combustion (CLC) – Effect on steam gasification. Int J Greenh Gas Con. 2012, 8: 56-60.

[48] Arjmand, M., Leion, H., Mattisson, M., Lyngfelt, A. Evaluation of different manganese ores as oxygen carrier in chemical-looping combustion (CLC) for solid fuels. In Proceedings of the 2nd International Conference on Chemical Looping, Darmstadt, Germany, 2012.

[49] Arjmand, M., Hedayati, A., Azad, A. M. Leion, H., Ryden, M., Mattisson, T. CaxLa1-yMyO3-σ (M = Fe, Ti, Mg, Cu) as oxygen carriers for chemical-looping with oxygen uncoupling (CLOU). Energ Fuel. 2013.

[50] Azimi, G., Ryden, M., Leion, H., Mattisson, T., Lyngfelt, A. (MnzFe1-z)yOx combined oxides as oxygen carrier for chemical-looping with oxygen uncoupling (CLOU). AIChE J. 2013, 59: 582-588.

[51] Abad, A., Adanez-Rubio, I., Gayan, P., Garcia-Labiano, F., de Diego, L.F., Adanez, J. Demonstration of chemical-looping with oxygen uncoupling (CLOU) process in a 1.5 kWth continuously operating unit using a Cu-based oxygen-carrier. Int J Greenh Gas Con. 2012, 6: 189-200

CHAPTER 3

EXPERIMENTAL APPROACH AND DATA ANALYSIS

3.1 Oxygen Carrier Selection

For the selection of oxygen carriers, there are several factors needing

consideration: (1) oxygen carrying capacity, (2) reactivity, (3) chemical durability

(deactivation resistance), (4) physical durability (attrition resistance) and (5) total cost

(base materials, production and replacement). Each of these attributes plays a significant

role in OC selection and the pros and cons of each must be weighed for a proper selection

to be made. For example, if a material has very low attrition resistance, but has a very

low cost associated with procurement, then, it may be less expensive, both in money and

time, to use it as opposed to a high-cost/low-attrition manufactured material.

Alternatively, if the reactivity and oxygen carrying capacity are low, then the required

solids inventory within the reactor at any given time will be larger, thereby requiring a

higher capital investment.

An additional consideration to be understood is the suitability for combusting, or

oxidizing, the particular fuel in question. For example, while iron oxides are relatively

inexpensive and perform well in chemical-looping systems involving gaseous reactants,

they are ultimately inferior to the CLOU-type materials of Cu or Mn in the combustion of

solid fuels [1]. In their study of the use of copper oxide to produce CO_2, Lewis, Gilliland

and Sweeney were able to show reaction rates roughly 50 times faster than that of gasification of solid fuel [2]. For solid fuel combustion, using an iron-based OC gasification is necessary to avoid the very slow solid-solid reaction rates between the OC particles and the solid fuel.

Therefore, likely the first consideration to be made in the selection of an OC requires a decision to use a CLC material or a CLOU material. At the University of Utah's Institute for Clean and Secure Energy, the decision was made to investigate chemical-looping on the premise for combustion of solid fuels. Therefore, the CLOU materials were looked at very closely to understand the application of CLOU-based materials in the combustion of solid fuels in a chemical-looping system.

As outlined within the previous chapter, of the three main CLOU capable materials (Cu, Mn, Co), cobalt showed the least amount of promise [3] and was therefore discarded immediately. The choice between Mn and Cu came down to an understanding of the region. The University of Utah is nestled up against the Wasatch Mountain Range and overlooks the Salt Lake Valley. Across the valley, on a clear day, a smoke stack is visible. This smoke stack belongs to a smelter plant of Kennecott's Bingham Canyon Mine – one of the largest open pit copper mines in the world.

Along with the availability of copper, several studies had been performed where cu-based materials were reported as having very high potential as suitable OCs in a fluidized-bed CLOU system [4, 5, 6]. Therefore, several different copper-based materials were either acquired or produced and, subsequently, tested in an attempt to find a carrier suitable for large-scale testing. A list of these materials is provided in Table 4. The carrier name designations are assigned based upon, first, either CuO wt% loading or

Table 4: Copper-based materials tested at the University of Utah for suitability as oxygen carriers within a fluidized-bed based on CLOU.

Carrier	Source	Preparation Method	CuO Loading (wt%)
Non Cu-Based			
$FeTiO_2$ (Ilmenite)	Ilmen Mountains USA	NA	NA
Cu-Based			
3N Cu	Atlantic Engineers, USA	NA	99.9
12_Al2O3_IW	Sigma Aldrich, USA	Incipient Wetness	12
50_TiO2_MM	ICPC, Poland	Mechanical mixing	50
45_ZrO2_FG	Chalmers, Sweden	Freeze granulation	45
16_SiO2_IW	University of Utah	Incipient Wetness	16
64_SiO2_IW	University of Utah	Incipient Wetness	64
20_FeTiO2_IW	University of Utah	Incipient Wetness	20

purity (3N is 99.9%), second, support material, and, lastly, production method. As a base

case, a 3N (99.9%) pure copper powder was acquired from Atlantic Engineers and tested.

All additional materials were subsequently tested to find a more suitable candidate.

The substrates were selected based on a variety of reasons. There are a handful of

supporting materials which appear repeatedly within the literature such as: ZrO_2, Al_2O_3,

TiO_2, Sepiolite and SiO_2 [7]. The materials selected for this study were among the list of

the most common support used in the literature providing additional characteristics such

as durability, additional internal surface area and increased melting point.

Several production methods were used during this work. This was mostly out of a desire to understand variability of materials based upon production method. The methods of production used and discussed in the following sections are: freeze granulation, mechanical mixing and wet impregnation (also referred to as incipient wetness).

Freeze granulation is frequently used because of its ease of operation and ability to produce oxygen carrier particles with a favorable porosity and specific surface. In this method of production, chosen proportions of metal oxide, inert support and a dispersant are mixed with water and ball milled. A binder is added and then the slurry is pumped through a nozzle into liquid nitrogen. Moisture is removed from the spherical particles during the freeze drying process. The particles are then calcined at 950 and 1050 ^{o}C.

The mechanical mixing procedure uses a powdered mixture of metal oxide and inert combined in desired concentrations. A concentration of 10 wt. % graphite is included as a pore forming additive, increasing reactivity. Water is added to achieve a suitable viscosity and the resulting paste is extruded through a syringe. The material is allowed to soft dry at 80 ^{o}C overnight and then cut to a desired length. The particles are then sintered at various temperatures ranging from 950 to 1300 ^{o}C in a muffle oven. This method generally produces irregularly shaped particles compared to the sphericity of particles prepared by other methods.

Spray drying method begins with metal oxides and inert materials in a solution or slurry. The solution is atomized or sprayed through a nozzle, dispersing the liquid in a controlled drop size. The dispersed solution comes into contact with a cool gas (usually air or nitrogen) where it is rapidly hardened. This method generally provides the most

consistent particle size distribution.

Wet impregnation (or Incipient Wetness) is carried about by dropping an inert support particle into a saturated copper nitrate aqueous solution. The particles are then dried overnight and then calcined at 500 ^oC in order to decompose the copper nitrate to a copper oxide. This method provides a preferred particle porosity and surface.

For comparison, an iron-based material was selected to stand as a base material to be compared against with the copper-based materials. In the literature, the material ilmenite has received quite a bit of attention [8, 9]. Ilmenite is attractive due to its strong support material, TiO_2, and because it is a naturally occurring iron-ore, meaning it is unprocessed and therefore relatively inexpensive. Ilmenite is the largest source of titanium in the world, accounting for roughly 90% of the world's consumption of titanium materials [10]. Being both a naturally occurring ore and abundant, this material is an inexpensive alternative for CLC oxygen carriers.

<div align="center">3.2 Physical Characterization</div>

Certain physical characteristics are important considerations for a suitable oxygen carrier material in a chemical-looping system. These characteristics include:

1. Particle size distribution

2. Surface area

3. Mechanical strength

4. Particle shape (Sphericity)

Each of these characteristics was determined for each material tested at the University of Utah.

Particle size distribution may affect both the reaction rates and fluidizability of the selected material. If particles are too large, the material may exhibit mass transfer resistances during reaction. If the particle size distribution is too large, it is difficult to determine a proper gas velocity to maintain proper fluidization. According to Kunii and Levenspiel [11], the minimum fluidization velocity is a function of particle density, bed voidage and the sphericity of the particle along with the fluidizing fluid properties. Figure 6 gives a qualitative representation of fluidizability as a function of the solid material characteristics.

The physical characteristics of the oxygen carrier materials tested were ascertained by a few different methods.

To determine the particle size distribution of each of the powders, both a sieve method and a particle size analyzer were employed. The sieve trays were used to cut the powder to different size ranges. The ranges employed in this work were:

5. $D_p < 45$ μm – TGA Kinetic Studies

6. 45 μm $< D_p < 75$ μm – TGA Kinetic Studies

7. 75 μm $< D_p < 105$ μm – TGA/FzB (Fluidized-bed) Classification Studies

8. 105 μm $< D_p$ 150 μm – FzB Performance and Attrition Studies

9. 150 μm $< D_p$ 250 μm – FzB Attrition Studies

Surface area, particle morphology and attrition studies were determined using BET, SEM and a fines collector system. The BET employed is a Micromeritics Tristar II. SEM/EDS micrographs were used to understand particle sphericity as well as visual understanding of surface area and porosity. Particle attritted fines were collected in a dual fine filter apparatus designed at the University of Utah.
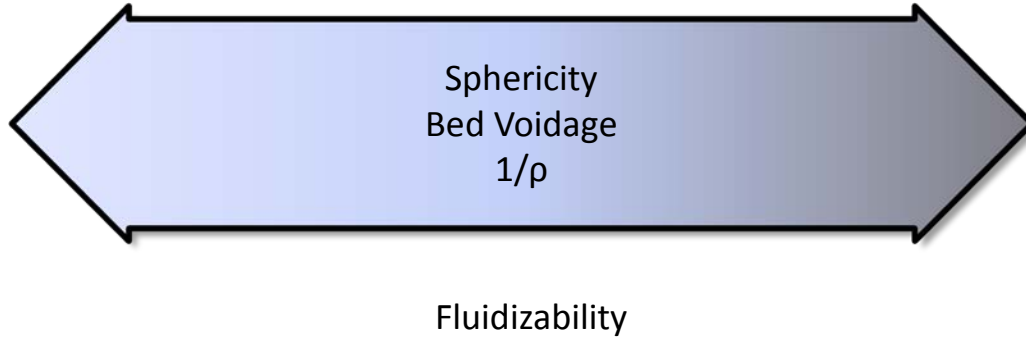
Figure 6: Qualitative representation of fluidizability as a function of sphericity, bed voidage and density.

The mechanical strength of the individual particles may serve as an indication of attrition resistance; therefore, the mechanical strength of the particles was determined using a Shimpo FGE-5X mounted on an aluminum frame for stability.

The influences of gas velocity, particle size, production method, operating temperature and support material on the rate of particle attrition were determined using a fluidized-bed. The attritted materials were collected using two in-line parallel PTFE (Teflon) filters. These filters were isolated from each other using ball valves at both the inlet and outlet of the filters. By so doing, the attritted materials were allowed to collect on the surface of one filter while the isolated filter could be removed and weighed to determine the amount of collected material. These collected materials were then viewed using SEM/EDS micrographs to determine surface morphology and to identify the elemental makeup of the fines collected.

3.3 Chemical Testing

The characteristics designated as "chemical" include oxygen carrying capacity, reactivity and deactivation resistance. These characteristics were determined using two different reactors – thermogravimetric analyzer (TGA) and a bubbling fluidized-bed reactor (FzB).   Typical reaction conditions are given for each apparatus in Table 5.

Each oxygen carrier material was analyzed by a TA Instruments Q500 thermogravimetric analyzer (TGA) to determine its reactivity without fuel in multicycle tests. The TGA experiments cannot predict oxygen carrier performance under CLOU conditions when fuel is present, but were used to observe complete oxidation and reduction reactions over multiple cycles. Reaction gases used during redox cycling ranged from pure nitrogen to 21% oxygen (Air) with the balance as N_2.

A schematic of the Q500 with EGA (Evolved Gas Analysis) furnace used in these tests is provided as Figure 7. The quartz liner of the EGA furnace decreases the internal volume to around 15mL. The sample is suspended from the balance into the center of the furnace chamber and reaction gases are fed to the sample perpendicular to the sample cup suspension. A small purge flow is provided to the balance chamber to reduce the temperatures observed there. This purge gas mixes with the exhaust gases and proceeds out of the reactor chamber. The reaction gas flow (80 – 100mL) is typically four to five times higher than the balance purge gas and therefore ensures that the reaction gas is not diluted prior to sample contact.

To analyze the TGA data, the conversion of the oxygen carriers for each oxidation and reduction reaction was determined using the equations (9) & (10). X_{ox} and X_{red} represent fractional conversion for the oxidation and reduction reactions, m_t is the sample

Table 5: Characteristic ranges used for the TGA and fluidized-bed reactors.

	Sample Size (g)	Particle Size (µm)	Temperature (°C)	Flow Rate (L/min)	Oxidation Time (min)	Decomp Time (min)
TGA Q500	0.010 – 0.050	< 45 – 105	650 – 1000	0.1 – 0.12	5-120	10-120
Fluidized-bed	10 – 50	75 – 250	650 – 1000	0.5 – 2	5 – 60	5 – 60

mass at a given time, m_{red} is the mass of fully reduced sample with all copper as Cu_2O, and m_{ox} is the mass of fully oxidized sample with all copper as CuO.

$$X_{ox} = \frac{m_t - m_{red}}{m_{ox} - m_{red}} \tag{10}$$

$$X_{red} = \frac{m_{ox} - m_t}{m_{ox} - m_{red}} \tag{11}$$

The rates of the reduction portions of the experiments were found by treating the conversion data with a linear model. The calculated regression slope of the line approximates the rate constant, dX_{red}/dt, in units of percent-conversion/second. The data were trimmed from 1% to 90% to capture the linear portion of the data.

Each rate constant was calculated by trimming the data so that initial reaction completion (X_i) was 5% and final reaction completion (X_f) was 100% to capture the portion of data that fit the pseudo first order model.

The FzB system (Figure 8) is very similar to that developed at Chalmers University. The reactor is made of quartz and is housed within a Carbolite VST 12/600
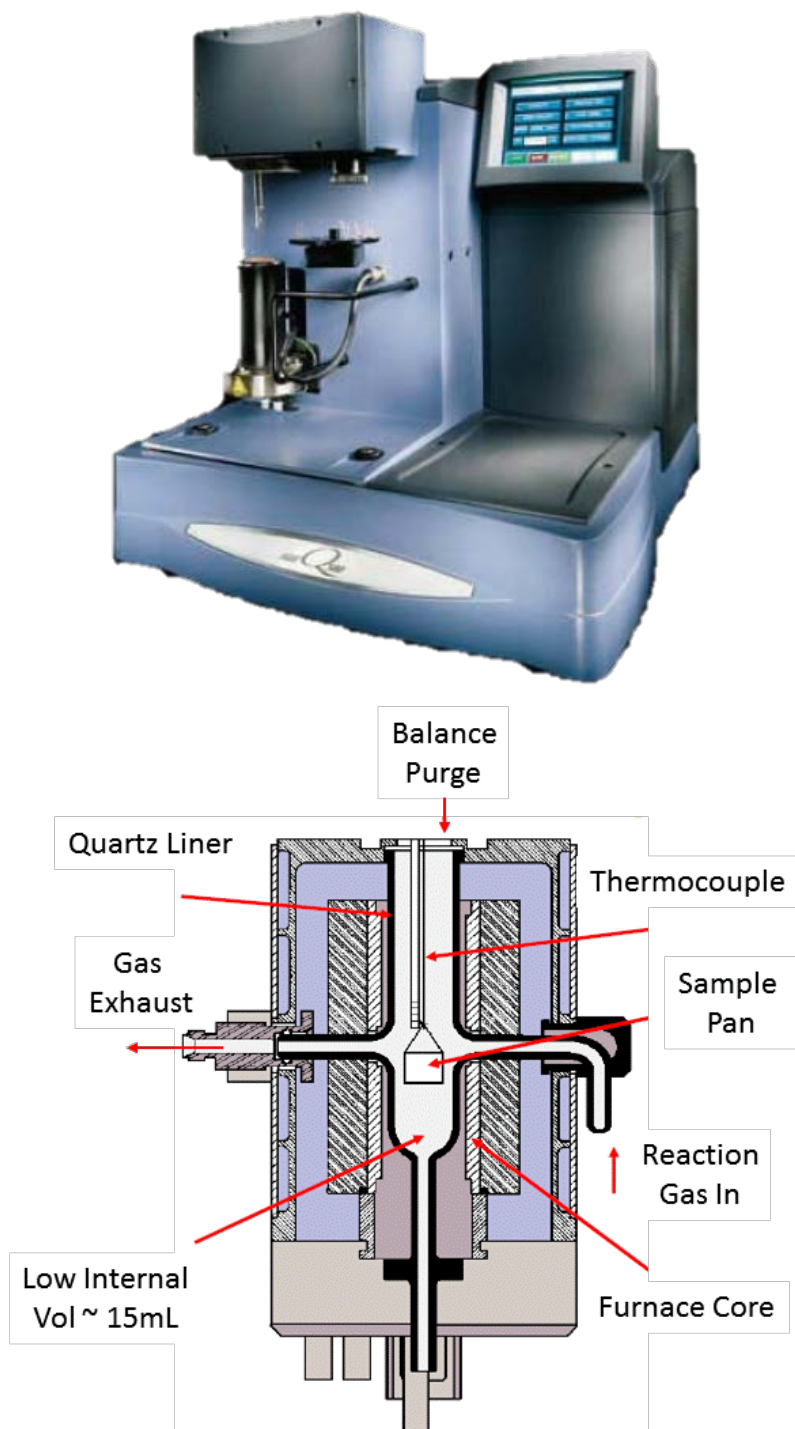
Figure 7: Picture of TGA Q500 with reactor schematic (bottom). The Q500 shown gives the EGA furnace which has quartz lining the furnace walls. Images courtesy of TA Instruments 2009, http://files.instrument.com.cn/bbs/upfile/200959204245.pdf.
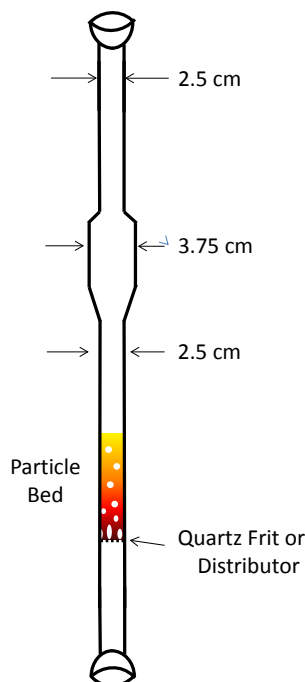
Figure 8: Schematic of quartz reactor used for fluidized-bed studies. The particle bed is held and the reactant gas is distributed by a sintered quartz frit. The particle bed is 2.5 cm in diameter.

Clamshell furnace (shown in Figure 9) with a maximum operating temperature of 1200°C. The reactor has four zones: (1) inlet, (2) sintered quartz distributor supporting the particle bed, (3) freeboard expansion zone and (4) outlet. Gas flow is controlled by a series of mass flow controllers and is introduced to the reactor housed within the furnace. The exit gas is filtered to remove fines and water is condensed from the gas before it is sent to a 4-channel California Analytical Instruments ZRE NDIR/fuel call analyzer. The analyzer measures the concentration of CO, CO_2, CH_4 and O_2 (see Figure 10).

The ID of the reaction tube is 2.5 cm. In order to maintain a well-fluidized system, the typical resting bed height was about 2.5 cm. Additionally, tests were conducted at about 5 cm and 1 cm bed height. In order to reduce the heating and cooling effects of the oxidation and reduction reactions, some samples were diluted with

Figure 9: Chemical-looping fluidized-bed reactor system at the University of Utah.

zirconium silicate beads with an approximate particle diameter of 100 µm.

Reactivity data are determined by the signals received from the gas analyzer. The gas analyzer data do not directly indicate what is going on within the reactor. The data are convoluted due to the reaction gas residence time distribution, gas dispersion in the gas lines after the reactor and analyzer time delay. To account for this convolution of the actual data, a deconvolution procedure was developed.

Several approaches for deconvolution of data are available. If the data set is a discrete set, then the set may be fit to a polynomial expression, which can then be subjected to a Laplace transform. The continuous Laplace transform method obeys the following relationship [11]:
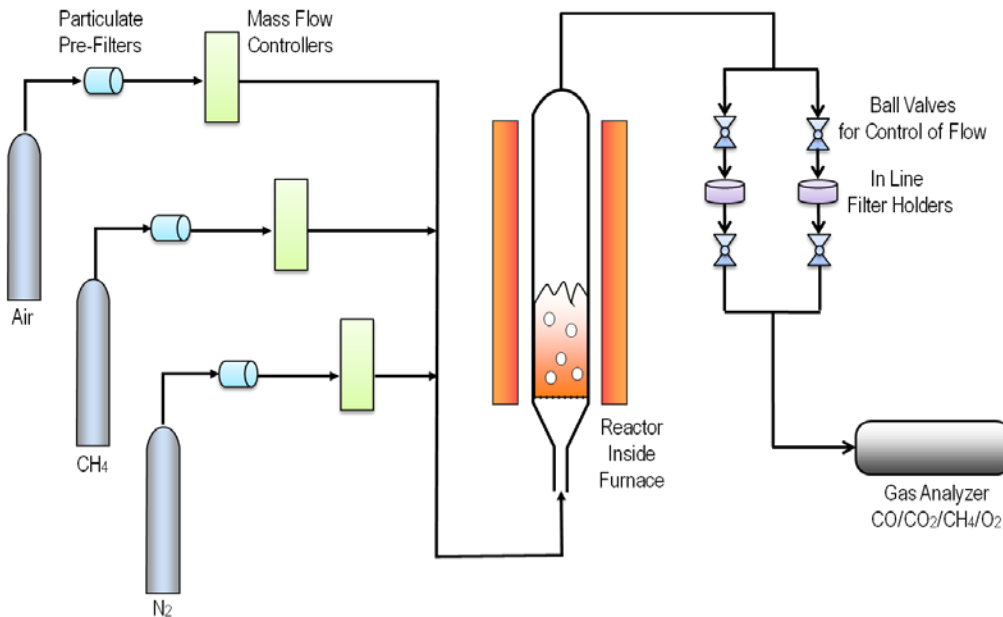
Figure 10: Fluidized-bed reactor system employed at the University of Utah for the testing of CLC/CLOU materials.

$$\mathcal{L}[F(t)] = \mathcal{L}[A(t)] \times \mathcal{L}[C(t)] = F(s) \qquad (12)$$

where F denotes the collected data, A denotes the actual data and C represents the convolution of the data. The function C may be determined from residence time distribution tests, with data then fit to a polynomial in similar fashion to the transformation of F from a discrete array to a continuous function. The resulting transformed equations may be rearranged as follows:

$$\frac{F(s)}{C(s)} = A(s) \qquad (13)$$

The inverse Laplace transform generates the final result of actual data as a function of time, or:

$$A(t) = \mathcal{L}^{-1}[A(s)] = \mathcal{L}^{-1}\left[\frac{F(s)}{C(s)}\right] \qquad (14)$$

This process has proven useful and may be utilized, but the accuracy depends on the accuracy of the polynomial fit.

Another method used to deconvolve a data set is much simpler and more quickly employed. In this method, the measured signal is subtracted from a second signal obtained by looping reaction gases over a bed of inert material (90 micron ceramic beads). The observed difference between the signal with inert material and a perfect step change represents the residence time distribution (RTD signal), or degree of data convolution. This method is displayed in Figure 11, which shows the result obtained when the measured signal is subtracted from the RTD signal.

The reasonableness of using this method was evaluated by comparing the results obtained in the fluidized-bed and deconvolved using this simple method against results obtained in a TGA using the same material.

Figure 12 shows a comparison between these methods. These tests were conducted at 800°C using air as the oxidizer and ilmenite as the oxygen carrier. While the signal lines do not line up exactly on top of each other, the two results agree very well. Due to the simplicity and reasonably good accuracy associated with this method, data analysis was conducted in this manner.
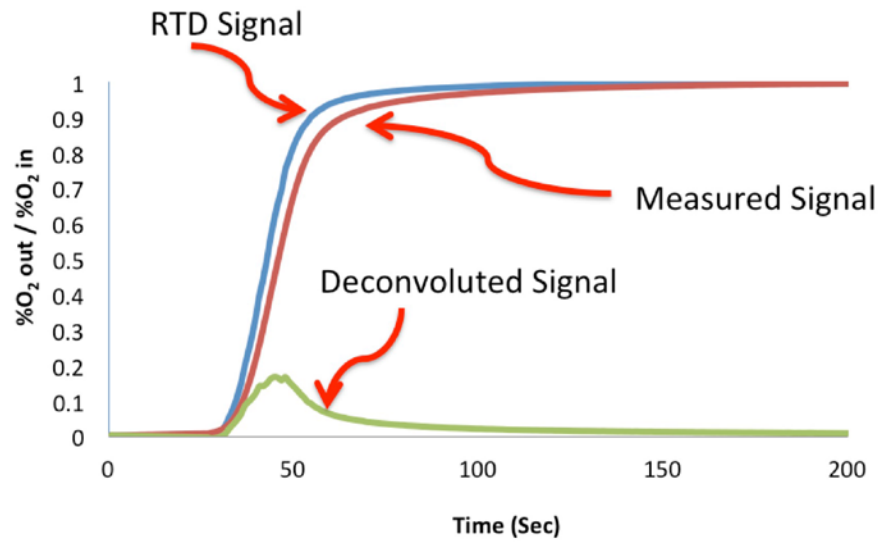
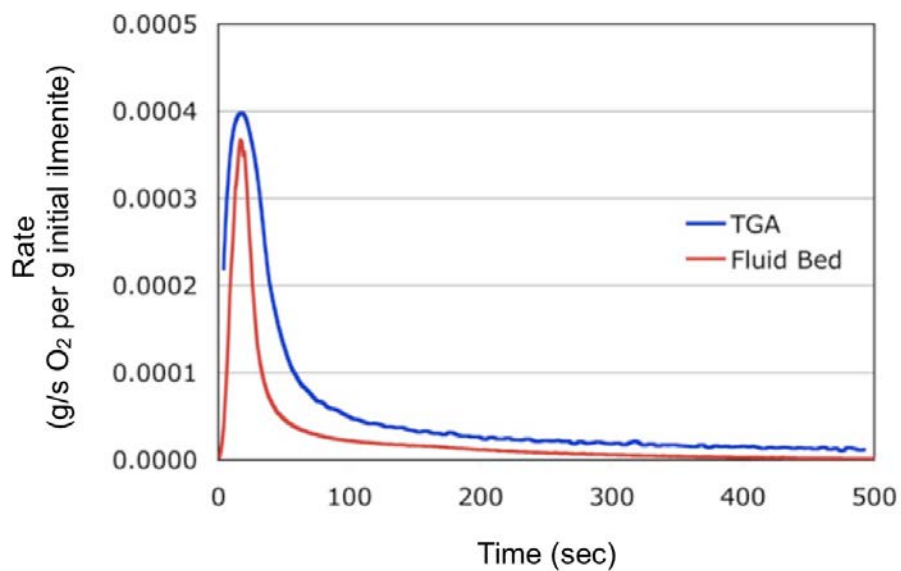Figure 11: Method of signal deconvolution used in this study.

Figure 12: Comparison between deconvolved rates obtained within a fluidized-bed and TGA. The error appears small enough that the method of deconvolution is justified.

3.4 Solid Fuels Testing

For the testing of solid fuels in a CLOU reactor, three fuels were chosen and were tested while using 3 different oxygen carriers. The fuels selected along the ultimate and proximate analyses are listed in Table 6. For further testing, the solid fuels listed were each used to produce a char resulting from the low heating rate release of volatile compounds at 900°C under nitrogen for 8 hours. Prior to testing, each of the fuels was heated to 110°C for 2 hours in an effort to remove accumulated moisture.

An additional unit was added to the quartz reactor scheme in order to provide a means of solid fuel delivery to the oxygen carrier particle bed. This additional unit was made of quartz as well and included a 0.3175 cm delivery port (Figure 13).

For testing with solid fuels, a brief purge cycle of N_2 at 1 L/min was used to clear the excess oxygen from the reactor to a level below the equilibrium partial pressure of oxygen. At this time, the purge gas was shut off to reduce blow-out of the fuel while it was added from the top of the reactor (Figure 13). After the addition of the solid fuels, the purge N_2 (1 SLPM) was once again switched on.

The volume percentages of CO_2, CO, CH_4 and O_2 were measured and recorded continuously during the combustion of the fuel. Figure 14 is a plot showing the evolution of these carbonaceous gases during the combustion of char made from Illinois#6 coal at 900°C. The oxygen carrier used to produce Figure 14 consisted of 30 wt% CuO loaded onto an ilmenite support. The oxygen trace quickly drops below 2 vol% before the fuel is added. Once the fuel is added, the oxygen volume percent drops to near zero, but is not completely consumed and the production of CO_2 dominates the evolved gases.

For the measured signals, the carbonaceous gases are very near real-time whereas

Table 6: Ultimate and proximate analyses of solid fuels used in this study.

Coal – Type	Illinois #6 Bituminous	Black Thunder (PRB) Sub-bituminous	Green Coke Petroleum Coke
Proximate Analysis			
Moisture (wt% as received fuel)	2.54	21.30	0.4
Ash (wt% Dry)	12.33	6.46	0.39
Volatile matter (wt% dry)	39.40	54.26	11.03
Fixed carbon (wt% dry)	48.28	39.28	88.01
Ultimate Analysis (wt% dry, ash-free)			
Carbon	78.91	74.73	89.21
Hydrogen	5.50	5.40	3.78
Nitrogen	1.38	1.00	1.73
Sulfur	4.00	0.51	5.82
Oxygen	10.09	18.27	4.41
Chlorine	0.11	0.08	-
Heating Value			
HHV, dry (Btu/lb)	12,233	12,815	15,622
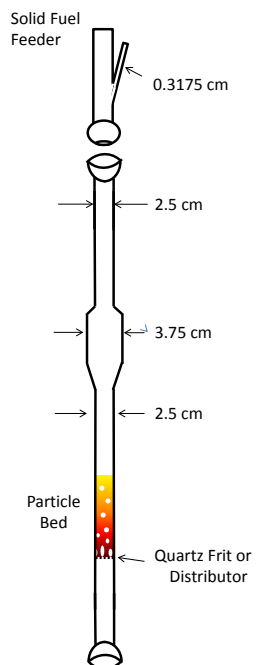
Figure 13: Quartz bubbling-fluidized-bed reactor showing additional solid fuel feeder.
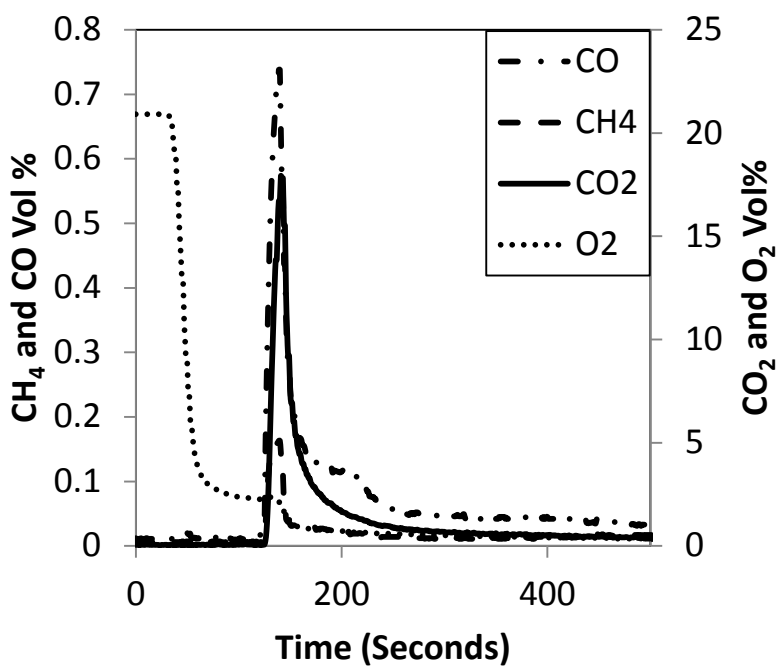
Figure 14: Evolution of gases during combustion of Illinois #6 Char at 900°C while using

in order to understand the true evolution of oxygen, the method of deconvolution previously discussed must be employed.

For the combustion of solid fuels, it is requisite to perform a carbon balance analysis to evaluate conversion of the fuel and to understand effective combustion rates. The carbon balance is performed using the flow rate of the purge gas as a baseline. It is assumed that the gases recorded by the analyzer, along with the inert purge, combine to make the majority of the gases evolved from fuel combustion. By assuming that any other species evolved from the combustion are in quantities small enough to have a negligible effect on the total flow rate of the effluent gases, the molar flow rate of the analyzed species may be determined.

The total volumetric flow rate may be determined by calculating the volume fraction of the inert purge gas (ϕ_{purge}) assuming that is the difference between one and the sum the volume fractions (ϕ_i) of CO_2, CO, CH_4 and O_2.

$$\phi_{purge} = 1 - \sum \phi_i ; \quad i = CO_2, CO, CH_4, O_2 \tag{15}$$

The volume fraction of the purge gas (N_2) is then used to calculate the total effluent volumetric flow rate of gases (Q_{tot}).

$$Q_{tot} = \frac{\phi_{N_2}}{Q_{N_2}} \tag{16}$$

The total volumetric flow rate multiplied by the individual specie volume fractions gives the volumetric flow rate of each of the individual gaseous species. The

ideal gas equation is then employed to determine the molar flow rate of each component.

$$Q_i = \phi_i \times Q_{tot}; \quad i = CO_2, CO, CH_4, O_2 \tag{17}$$

$$n_i = \frac{Q_i P}{RT} \tag{18}$$

The carbon balance is then performed by adding the total number of moles of carbonaceous gases and then multiplying by the molecular weight of carbon - 12 g/mole. The resulting mass of carbon is compared to the mass of the sample introduced to the reactor, generating a conversion profile based on the conversion of carbon.

<u>3.5 References</u>

[1] Eyring, E., Konya, G., Lighty, J., Sahir, A., Sarofim, A., Whitty, K. Chemical looping with copper oxide as carrier and coal as fuel. Oil Gas Sci. Tech. 2011, 66: 209-221.

[2] Lewis, W.K., Gilliland, E.R., Sweeney, M.P. Gasification of carbon: metal oxides in a fluidized powder bed. Chem Eng Pro. 1951, 47: 251-256.

[3] Mattisson, T., Lyngfelt, A., Leion, H. Chemical-looping with oxygen uncoupling for combustion of solid fuels. Int J Greenh Gas Con. 2009, 3 (1): 11-19.

[4] Mattisson, T., Lyngfelt, A., Leion, H. Chemical-looping with oxygen uncoupling for combustion of solid fuels. Int J Greenh Gas Con. 2009, 3 (1): 11-19.

[5] Lewis, W.K., Gilliland, E.R., Sweeney, M.P. Gasification of carbon: metal oxides in a fluidized powder bed. Chem Eng Pro. 1951, 47: 251-256.

[6] Adanez, J., Adanez, J., de Diego, L. F., Garcia-Labiano, F., Gayan, P., Abad, A. Selection of oxygen carriers for chemical-looping combustion. Energ Fuel. 2004, 18 (2), 371-377.

[7] Mattisson, T. Materials for Chemical-looping with oxygen uncoupling. ISRN Chem. Eng. 2013. http://dx.doi.org/10.1155/2013/526375.

[8] Leion, H., Lyngfelt, A., Johasson, M., Jerndal, E., Mattisson, T. The use of ilmenite as an oxygen carrier in chemical-looping combustion. Chem Eng Res. Des. 2008, 86 (9): 1017-1026.

[9] Berguerand, N., Lyngfelt, A. The use of petroleum coke as fuel in a 10 kWth chemical-looping combustor. Int J Greenh Gas Con. 2008, 2 (2): 169-179.

[10] U.S. Geological Survey. Mineral Commodity Summaries. Web: Minerals.usgs.gov/minerals/pubs/commodity/titanium/mcs-2012-timin.pdf

[11] Kunii, D., Levenspiel, O. Fluidization Engineering. Butterworth-Heinemann, Newton, MA, 1991.

[12] Blair, D. W.; Wendt, J. O.; Bartok, W. Evolution of nitrogen and other species during controlled pyrolysis of coal. International Symposium on Combustion (pp. 475-489). Elsevier 1977.

CHAPTER 4

RESULTS

4.1 Preliminary and CLOU Operation of Carriers

Several materials, listed in Table 7, were tested to determine their suitability as oxygen carriers. It was established early on during this work that copper was to be the material of choice for the reasons previously discussed. Because CuO is readily decomposed to Cu_2O at a rate greater than the rate of gasification of solid fuels, it was seen as the obvious choice for this work.
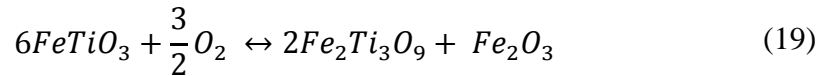

4.1.1 Ilmenite

While CuO was selected as the oxygen carrier of choice, it was necessary to test other materials in order to effectively compare the performance of the copper-based oxygen carriers. A commonly tested and inexpensive material was selected to serve as this comparison. Ilmenite is a naturally occurring iron-ore used most often in the manufacture of rutile and titanium metal.
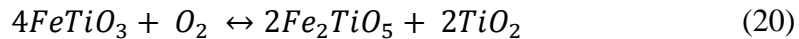
In its fully reduced state, ilmenite is comprised mostly of $FeTiO_3$, but admittedly, because it is a naturally occurring iron-ore, the composition of ilmenite has some variability. At temperatures below 800°C, not all of the ilmenite is oxidized obeying the following reaction:

Table 7: Materials tested for suitability as oxygen carriers in chemical-looping.

OC Name	CuO Wt%	Support	Production Method	Acquired from
Ilmenite FeTiO3	-	-	-	Atlantic Engineers, USA
Cu 99.999	100	-	-	Atlantic Engineers, USA
13_Al2O3_IW	13	Al_2O_3	IW	Sigma-Aldrich
50_TiO2_MM	50	TiO_2	MM	ICPC Poland
45_ZrO2_FG	45	ZrO_2/MgO	FG	Chalmers University Sweden
16_SIO2_IW	16	SiO_2	IW	University of Utah
42_SIO2_IW	42	SiO_2	IW	University of Utah
68_SIO2_IW	68	SiO_2	IW	University of Utah

$$6FeTiO_3 + \frac{3}{2}O_2 \leftrightarrow 2Fe_2Ti_3O_9 + Fe_2O_3 \tag{19}$$

At temperatures above 800°C, two reactions occur:

$$4FeTiO_3 + O_2 \leftrightarrow 2Fe_2TiO_5 + 2TiO_2 \tag{20}$$

$$Fe_2Ti_3O_9 \leftrightarrow Fe_2TiO_5 + 2TiO_2 \tag{21}$$
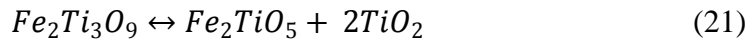
where TiO_2 is rutile and pseudobrookite (Fe_2TiO_5) is the most stable phase [1]. Therefore, theoretically, the oxygen transfer capacity is 5 wt% between the states $FeTiO_3$ and Fe_2TiO_5. Ilmenite has a melting point of 1470°C [2].

Ilmenite was tested in a number of different campaigns involving the FzB and TGA. Ilmenite has also been studied as a potential substrate for a copper oxide-based oxygen carrier. Due to the CLC capabilities and enhanced physical durability of iron oxide and the CLOU capabilities of copper, a material was created in an attempt to create an inexpensive copper-based oxygen carrier.

Ilmenite performed well within the fluidized-bed. It is important to note that ilmenite does not spontaneously decompose and, therefore, must be reduced by a gaseous fuel (i.e., methane, natural gas, hydrogen, synthesis gas etc.). For the redox reactions of ilmenite, air was used as the oxidizer whereas 5% CH_4 in N_2 was used as the fuel.

At lower temperatures, the oxidation of ilmenite proceeds very slowly, but can reach completion within 10 minutes at temperatures above 850°C. Figure 15 shows the completion profile for the oxidation of ilmenite in fluidized-bed whereas Figure 16 shows
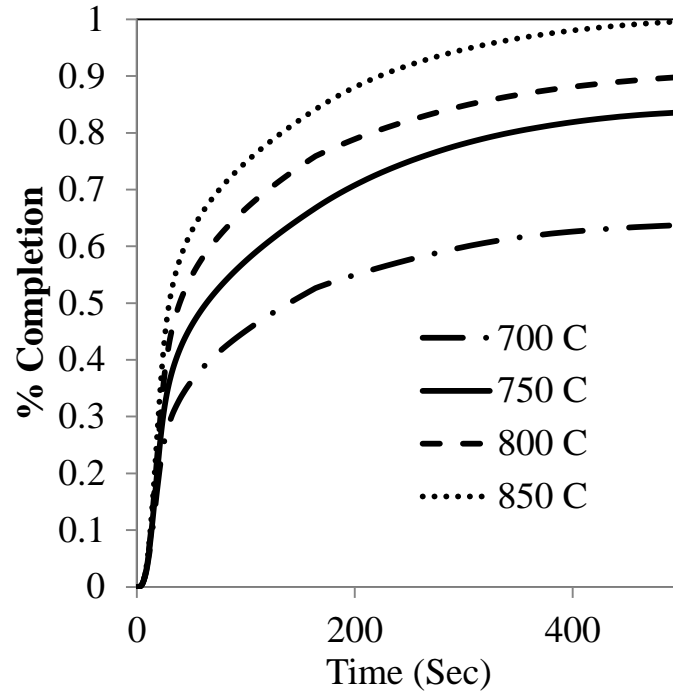
Figure 15: Oxidation of ilmenite at various temperatures in FzB using air.

the rates of oxidation at the corresponding temperatures.

With high physical durability evidenced by low attrition rates and high resistance to agglomeration, ilmenite proved a suitable candidate for a CLC unit employing a fluidized-bed design. It has been reported that ilmenite displays slower redox rates than other oxygen carrier candidates, especially during initial cycles, and displays an activation period after which it shows more attractive reaction rates and has even been shown to increase the rate of gasification of a bituminous coal [2].

4.1.2 Pure Copper

With ilmenite as a comparison, the study of copper-based oxygen carriers commenced. To form a baseline, pure copper was first tested in both TGA and FzB
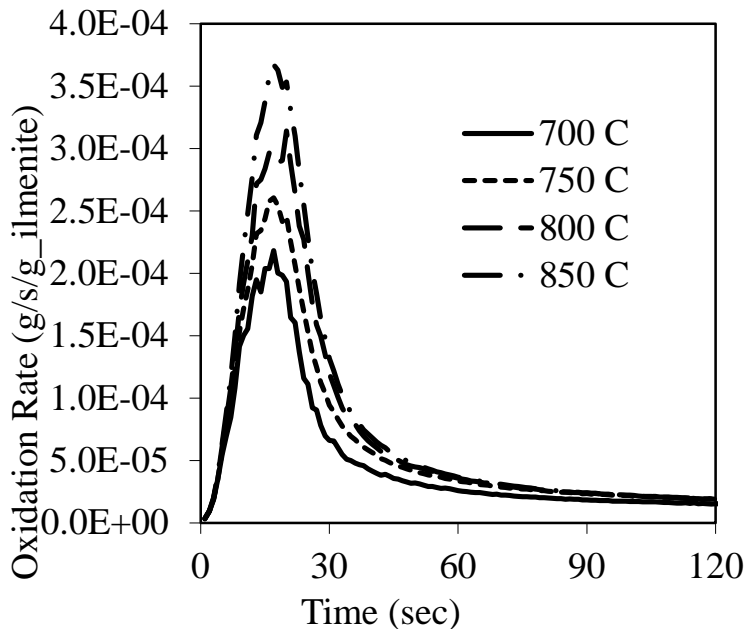
Figure 16: Oxidation rate for ilmenite in TGA under air at several temperatures.

studies. It was quickly understood that the use of copper as an oxygen carrier would be impractical for a fluidized-bed apparatus. Copper has a melting point below 1000°C and becomes soft at temperatures much lower than that. For CLOU operation of copper, the fuel reactor must be above 700°C. This may be understood by inspection of Figure 17. For the spontaneous decomposition of CuO, the kinetic driving force is the difference between the equilibrium partial pressure of oxygen and the actual partial pressure of oxygen in the reaction zone. Therefore, at temperatures below 850°C, reaction rates begin to slow significantly. Because of the need for higher temperature operation, the physical durability of an oxygen carrier must not allow for agglomeration of particles at these temperatures. Agglomeration of oxygen carrier, even prior to sintering, may cause catastrophic failure of the reactor system.

Particulate agglomeration of copper particles was observed at temperatures near
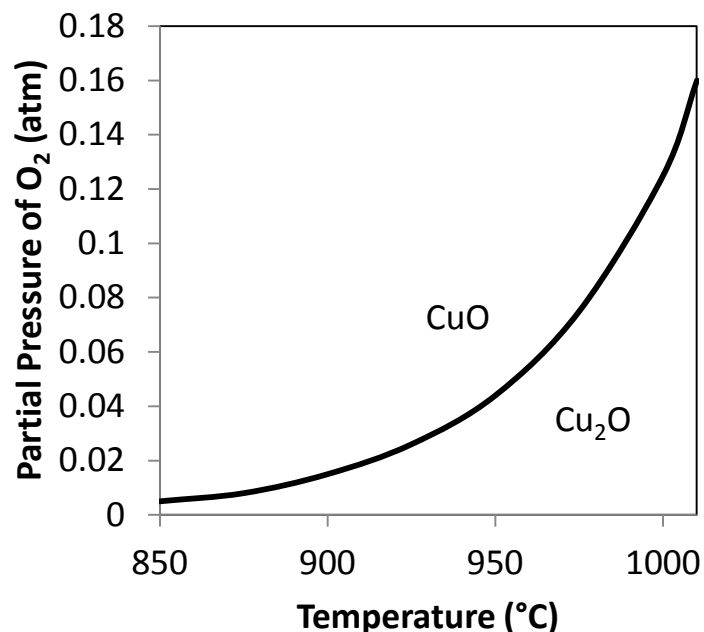
Figure 17: Equilibrium partial pressure of oxygen over the CuO/Cu$_2$O redox pair.

600°C during TGA testing, but that temperature was expected to increase with the harsh

agitation of a fluidized-bed environment, allowing for operation of copper particles at

temperatures near 900°C. Figure 18 shows the agglomeration of 99.9% copper powder

during chemical-looping cycling above 900°C. The agglomeration tendencies of copper

force the use of support materials in a fluidized-bed design.

4.1.3 Supported Copper-based Oxygen Carriers

<u>4.1.3.1 Physical Performance and Characterization</u>

The literature is replete with reports of various materials used as supports for a

variety of oxygen carrier materials. These supports include materials such as: Al$_2$O$_3$,

bentonite, SiO$_2$ and TiO$_2$, ZrO$_2$/MgO, MgAl$_2$O$_4$,YSZ, NiAl$_2$O$_4$, etc. [2,3]. Each of these

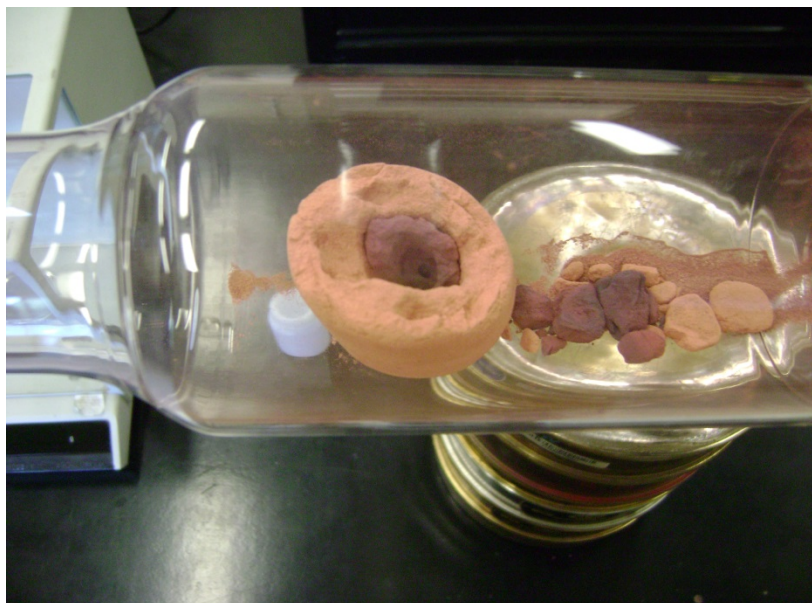supporting materials is reported as having varying levels of success and suitability as

Figure 18: Agglomeration of 99.9% pure copper at 900°C during chemical-looping cycling.

oxygen carriers.

For monetary and availability incentives, it is generally beneficial to find a material that is already in production – either as a primary product or secondary byproduct of another process. A material was obtained from Sigma-Aldrich sold as 13 wt% CuO on Al_2O_3 support (Figure 19). The material is sold as solid spheres in a range of 14-20 mesh (approximately 1,400 to 840 μm). The material was purchased and crushed using a mortar and pestle then sieved to a size range of 75 μm $< D_p <$ 105 μm. The powdered material was then tested at various temperatures under CLOU conditions within the fluidized-bed and TGA. Since the particle size of the material as received was 14-20 mesh, it was necessary to crush and sieve the material to a more suitable size range (75 – 150 μm).

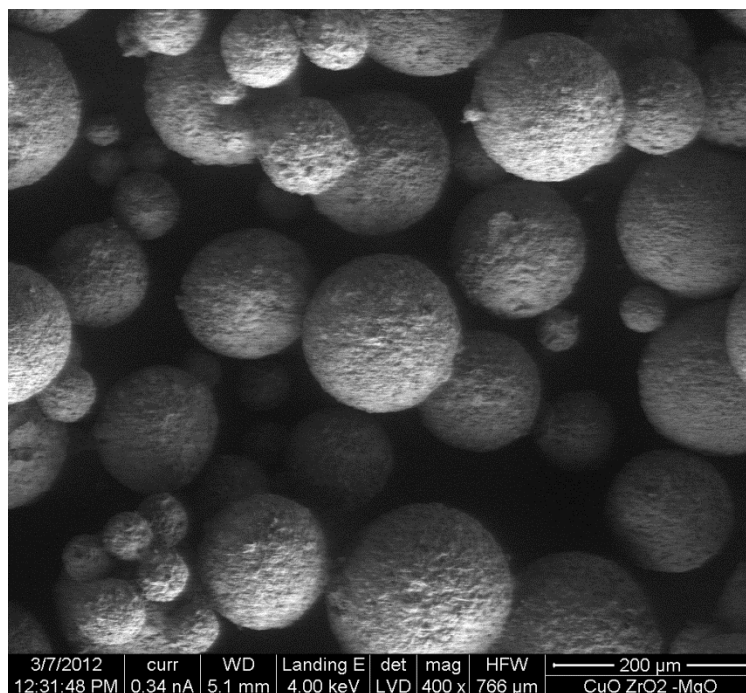From a physical durability standpoint, this material performed rather well. The

Figure 19: SEM micrograph of 13 wt% CuO on Al_2O_3.

material exhibited no agglomeration at the tested temperatures and the observed attrition

rates were comparable to the other materials tested. However, this material performed

poorly from a chemical standpoint. This will be discussed in a subsequent section.

As commercially available copper-based powders suitable for the chemical-

looping process are not overly abundant, the Institute for the Chemical Processing of

Coal (ICPC) in Poland was contracted to prepare a 50 wt% CuO material on a titania

(TiO_2) substrate. The material was produced using a mechanical mixing technique at a

cost of $5,000 USD/kg.   The material was observed using SEM. Figure 20 shows the

SEM micrograph of this material as received. The surface of the material appears very

rough when compared to the alumina material shown in Figure 19. The titania material

was produced using a mechanical mixing technique. This technique employs the use of a

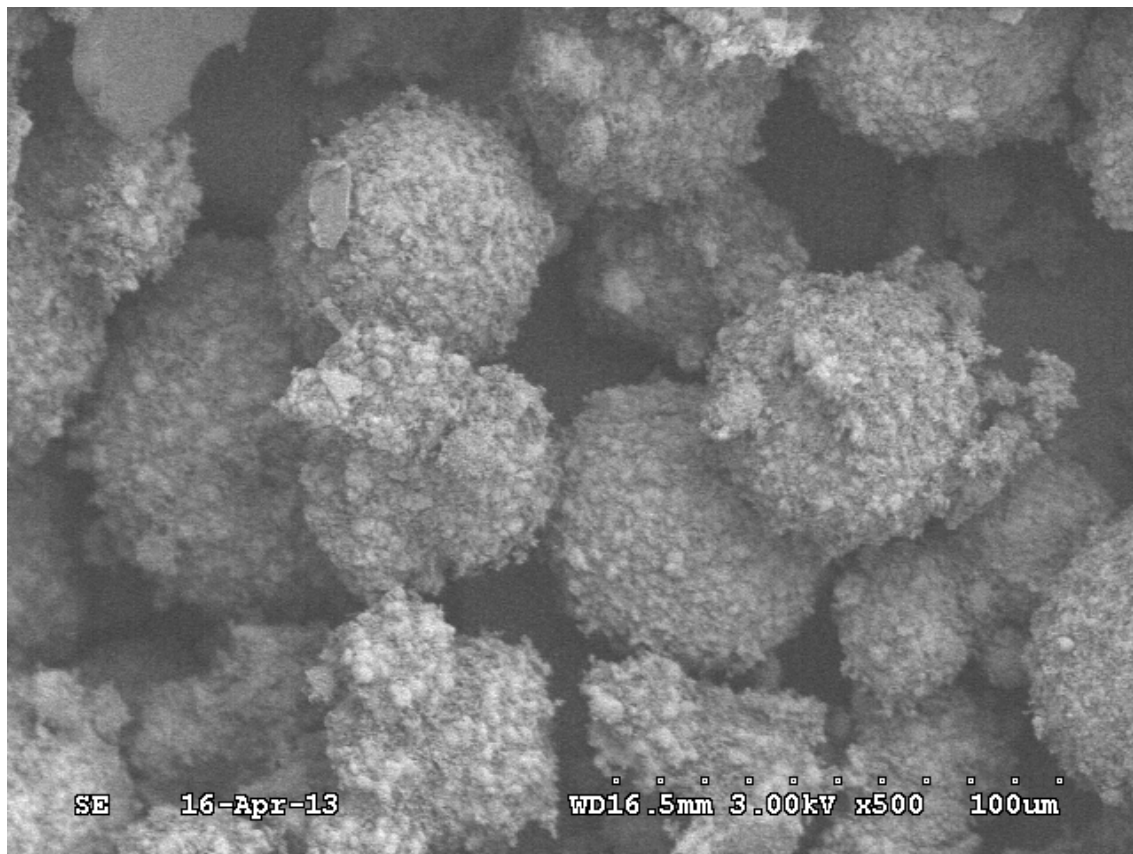machine such as a ball mill or other apparatus that physically forces one material to meld

Figure 20: SEM micrograph of 50 wt% CuO on TiO$_2$.

with another through sheer force of impact. Figure 20 provides the SEM micrograph

images of the titania material. The roughly spherical balls appear to be conglomerates of

much smaller particles. This fragmented topography is likely due to the method of

production.

The titania material did not perform as well in the fluidized-bed as was hoped.

The material was subject to agglomeration at temperatures greater than 850°C and

displayed the largest attrition values recorded compared to the other materials tested. To

combat the poor physical performance of the carrier, a diluent powder was added to help

curb the agglomeration of the material. The material was diluted by 50 wt% zirconia

silicate beads in the size range of 125 microns in diameter. The addition of these beads allowed the material to be tested at temperatures up to 1000°C with minimal agglomeration of particles. The effective CuO loading of the diluted material went from 50 wt% to 25 wt%. The diluted material was used in the testing of solid fuels to be discussed in a subsequent section.

Another acquired material was donated by the Chalmers University of Technology in Sweden. This material (Figure 21) was prepared by a freeze granulation method that involves mixing and binding of the metal oxide and support material and then spraying into a cold bath to create well-mixed spherical particles. Cupric oxide was loaded onto a zirconia-based support which was stabilized by magnesia at a tested loading of 45 wt% CuO using this method. Of all materials tested, this material displayed the greatest physical attributes and was tested at temperatures up to 1000°C without any sign of agglomeration without using diluents for added support.

SEM/EDS micrographs of four of the copper oxide-based materials tested are presented in Table 8. For comparison, rows 1 and 2 show the titania material as a fresh sample as well as after reaction. There appears to be no large qualitative difference between the two. This would seem to suggest that there is no migration of the copper compounds throughout the particle, but, instead, that the copper oxide stays near the surface of the particle. Table 9 displays the corresponding porosity measurements.

Additional characterizations are provided in materials. Some materials show higher attrition at the lower temperature while others show higher attrition at the higher temperature. Gas velocity, expectedly, does appear to have a large influence on the rates of attrition.
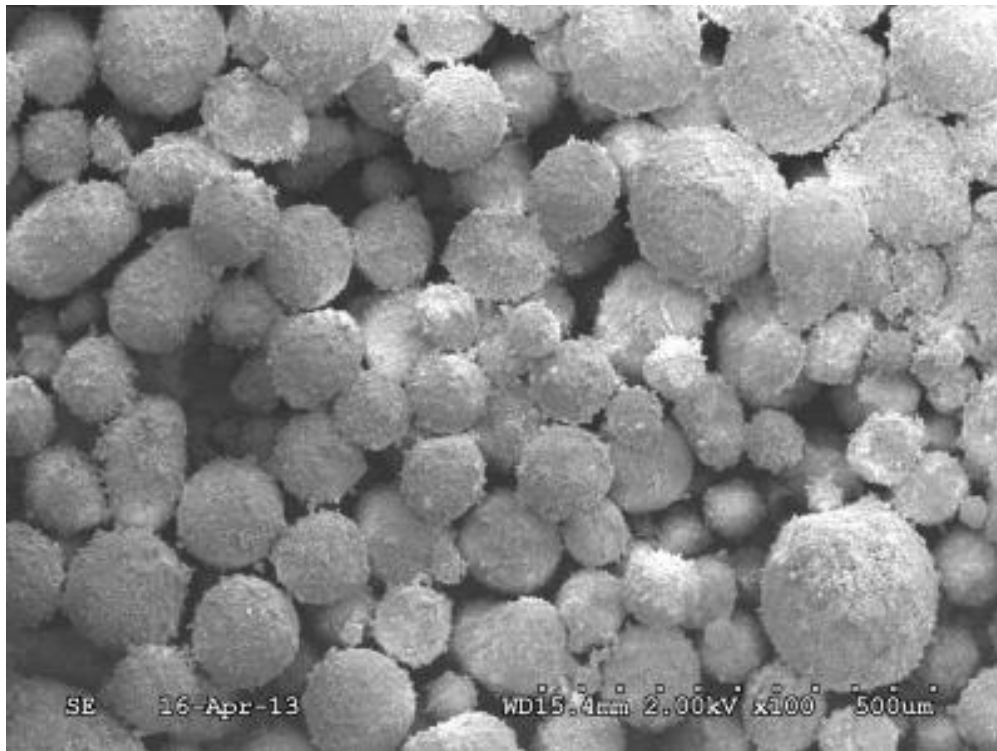
Figure 21: SEM micrograph of 45_ZrO2_FG particles as received.

Attrition results from the collisions between the oxygen carrier particles within the fluidized-bed. In order to compare collisions of equal intensity, the gas velocities used were determined from the minimum fluidization velocity. While a similar particle size was used between the materials, each of the materials tested has a different density and, therefore, a different minimum fluidization velocity. The ratio of the gas velocity (U) to the minimum fluidization velocity (Umf) was varied between 5 and 10. A greater attrition rate was observed for all materials at the higher ratio. Table 10 includes the crushing strength, BET surface area and pore size data. It is interesting to note that the zirconia material exhibited the smallest crushing strength. It has been suggested in the literature that crushing strength may be an indication of attrition rates. Results of an investigation of this claim are presented in Figure 22 – Figure 25.

Table 8: SEM/EDS Micrographs of four copper oxide-based materials tested for oxygen carrier suitability in CLOU operation. Courtesy: Crystal Allen.
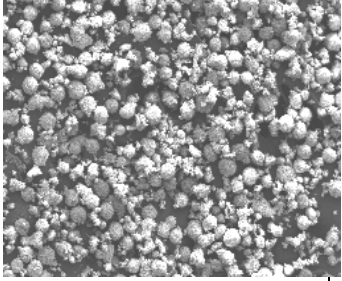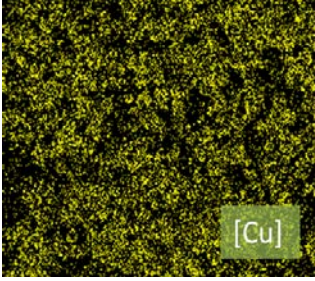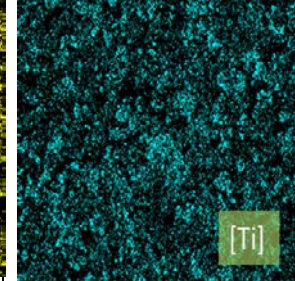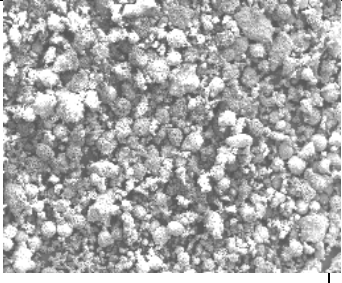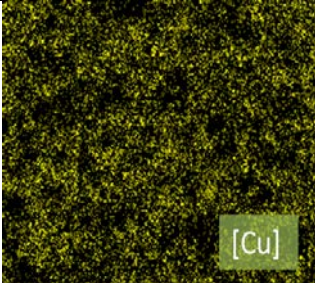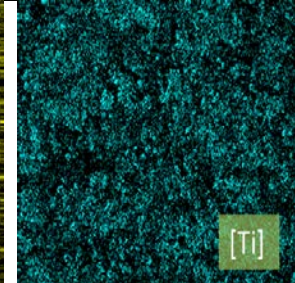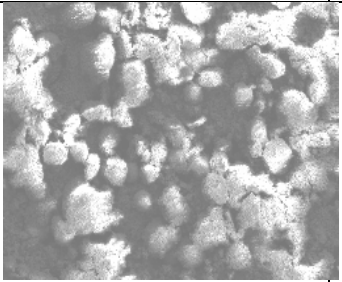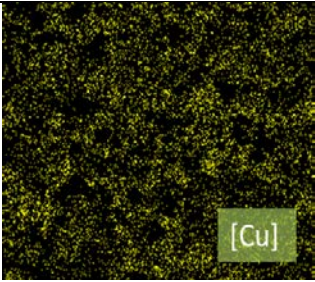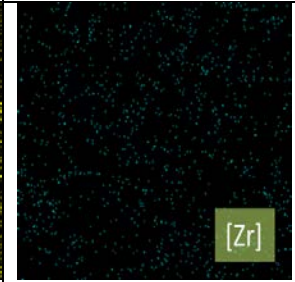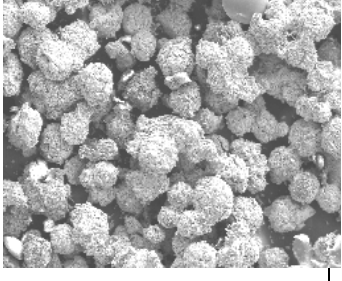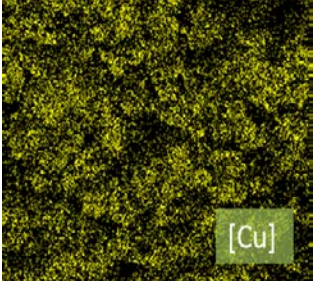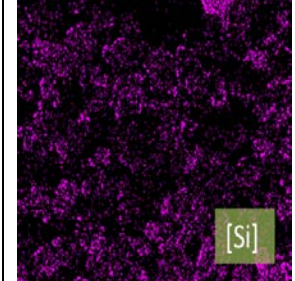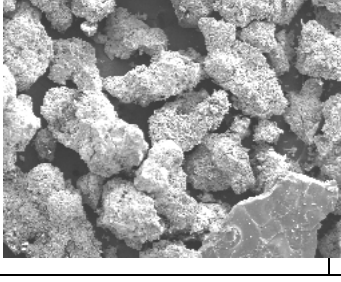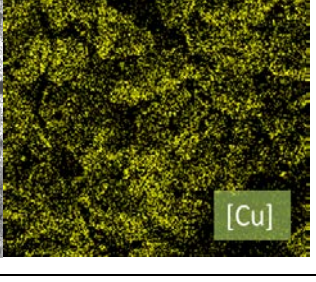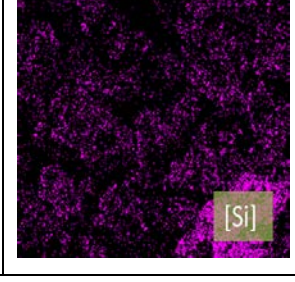
Oxygen Carrier	100×Magnification	Metal	Support
Un-reacted 50_TiO2_MM		[Cu]	[Ti]
Reacted 50_TiO2_MM		[Cu]	[Ti]
Reacted 45_ZrO2/MgO_FG		[Cu]	[Zr]
Reacted 50_SiO2_IW		[Cu]	[Si]
Reacted 70_SiO2_IW		[Cu]	[Si]

Table 9: Surface area and pore size data for four copper based carriers studied as oxygen carriers in CLOU systems. Data courtesy of Crystal Allen.

Oxygen Carrier	Particle Diameter (μm)	BET Surface Area (m2/g)	Total Volume of Pores 1.7-300 nm Width (cm3/g)	Average Pore Width (nm)
Un-reacted 50_TiO2_MM	75 – 105	0.6178	0.001392	10.2463
Reacted 50_TiO2_MM	75 – 105	0.1656	0.000286	27.9278
Reacted 45_ZrO2/MgO_FG	75 – 105	0.8963	0.001926	8.3488
Reacted 50_SiO2_IW	106 – 250	0.0823	0.000375	40.7755
Reacted 70_SiO2_IW	106 – 250	0.0726	0.000883	109.2892

Table 10: Results of crushing strength testing performed on four materials tested for suitability as oxygen carriers in CLOU systems. Courtesy: Crystal Allen

Oxygen Carrier	Particle Diameter (μm)	Crushing Strength (N)	Standard Deviation
Un-reacted 50_TiO2_MM	180 – 250	4.45	1.14
Reacted 50_TiO2_MM	180 – 250	3.94	1.28
Reacted 45_ZrO2/MgO_FG	180 – 250	2.21	0.88
Reacted 50_SiO2_IW	180 – 250	4.10	1.26
Reacted 70_SiO2_IW	180 – 250	4.48	1.02
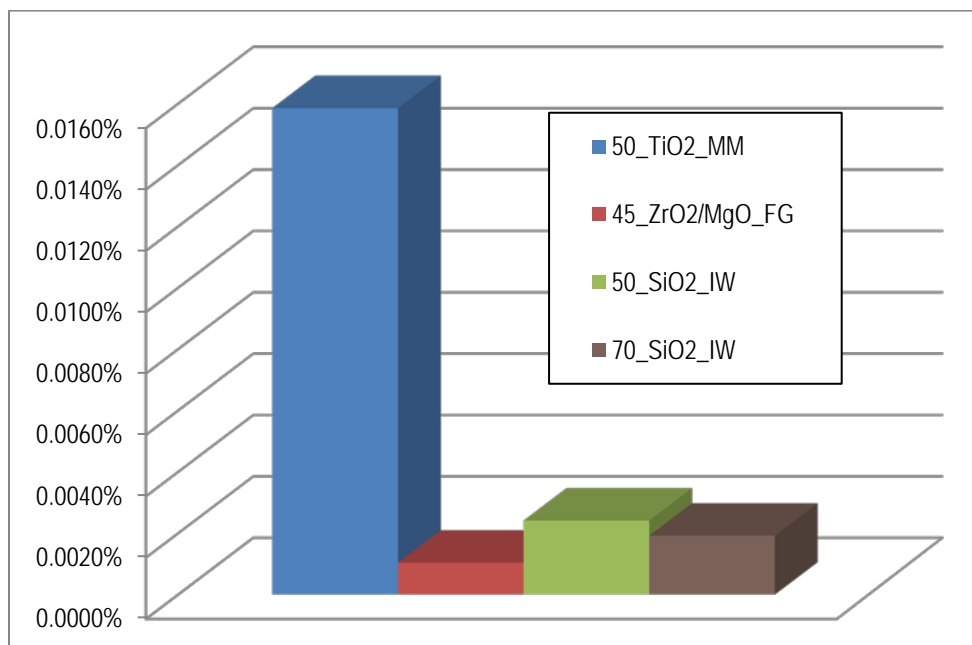
Figure 22: Observed attrition rates during redox cycling of four different materials tested for suitability as oxygen carriers in CLOU systems. Figure courtesy of Crystal Allen.
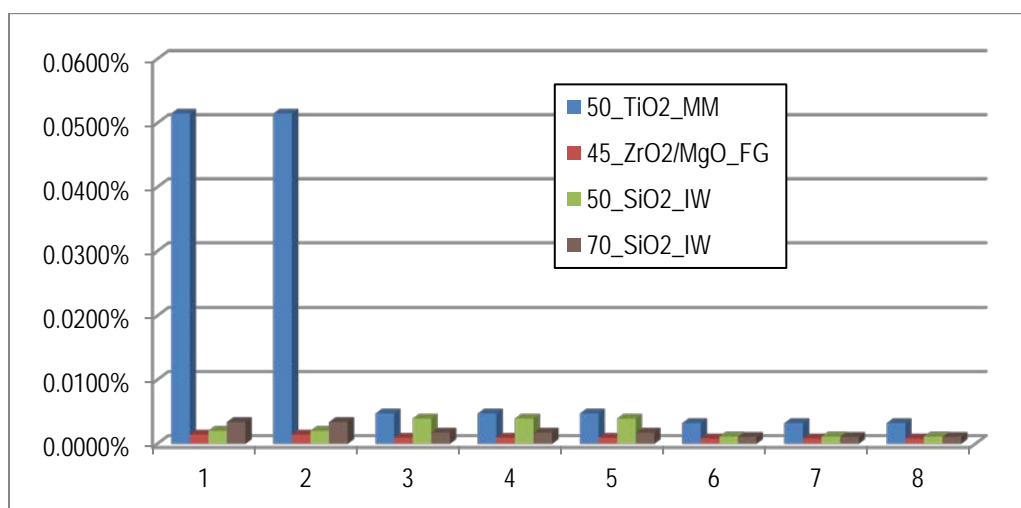
Figure 23: Observed bed weight percent loss per hour of testing for four materials tested for oxygen carrier suitability in CLOU systems. Figure courtesy of Crystal Allen.
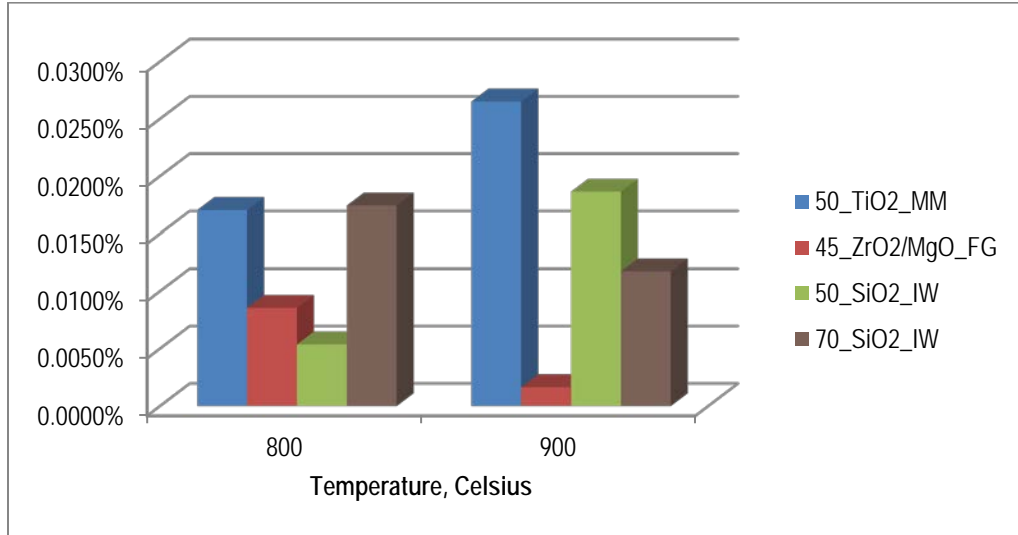
Figure 24: Influence of temperature on attrition of copper oxide-based materials in a fluidized-bed.
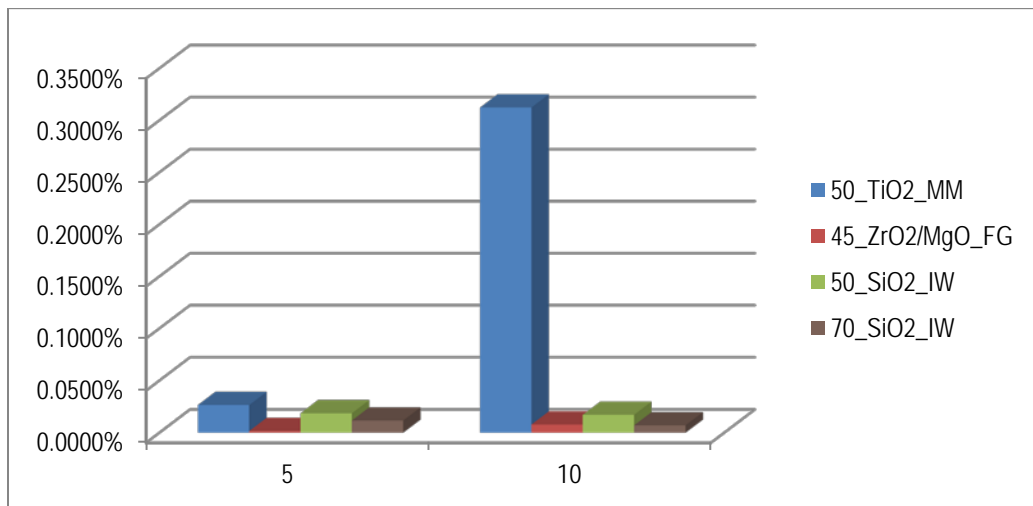
Figure 25: Influence of gas velocity on attrition rates. Gas velocity is given as U/Umf calculated using correlations given by Kunii and Levenspiel. Figure courtesy of Crystal Allen.

Figure 22 displays an overall view of weight loss from the fluidized-bed during CLOU cycling. It is clear that the titania material displayed the lowest attrition resistance while the zirconia material exhibited the highest attrition resistance showing the least amount of bed loss over all conditions. This is especially interesting when considering the crushing strength information given in Table 10. While the zirconia material had the lowest crushing strength, it performed the best when considering attrition. However, demonstrating a much higher crushing strength, the titania material displayed much greater attrition. Therefore, crushing strength is a poor indicator of attrition resistance; at least when considering materials prepared using different methods.

Interestingly, when comparing materials prepared using the same method, crushing strength appears to effectively predict attrition characteristics. The 70_SiO2_IW material has a higher crushing strength than its lower CuO loading counterpart 50_SiO2_IW and shows greater attrition resistance.

Another interesting note is gleaned from Figure 23 which shows the observed weight loss per hour for each of the materials investigated. The results show a very high attrition for the titania material for the first 2 hours followed by a significantly decreased rate. In fact, all four materials showed a decrease in the amount of material leaving the bed over time. Comparing the topographies of the titania material (Figure 20) and the zirconia material (Figure 21), it may be understood that the difference in early stage attrition is due to the very rough nature of the titania material, where the zirconia material is much smoother and exhibited much lower attrition.

Figure 24 displays the influence of temperature on the attrition rates of the materials. It does not appear that there is any effect which is observed by each of the

materials. Some materials show higher attrition at the lower temperature while others show higher attrition at the higher temperature. Gas velocity, however, does appear to have a large influence on the rates of attrition, as may be seen in Figure 25.

Attrition results from the collisions between the oxygen carrier particles within the fluidized-bed. In order to compare collisions of equal intensity, the gas velocities used were determined from the minimum fluidization velocity. While a similar particle size was used between the materials, each of the materials tested has a different density and, therefore, a different minimum fluidization velocity. The ratio of the gas velocity (U) to the minimum fluidization velocity (U_{mf}) was varied between 5 and 10. A greater attrition rate was observed for all materials at the higher ratio.

4.1.3.2 Chemical Characterization Under CLOU Conditions

The failed operation of the pure copper oxide powder due to its poor physical performance merits not going into detail into its chemical performance; therefore, it is not treated here. However, all other carriers performed successfully enough physically to merit some discussion into their respective chemical performances.

While no agglomeration was observed at any temperature during testing of the alumina material, the overall performance of the carrier was very poor as a CLOU material. The % mass change decreased after each redox cycle under CLOU conditions. This is likely due to the formation of Cu-aluminate spinal compounds. These compounds, while still reducible, are not CLOU capable and, therefore, do not spontaneously uncouple oxygen at elevated temperatures and was deemed not optimal for the combustion of solid fuels in a fluidized-bed design of a chemical-looping process.

72

The titania material far outperformed the alumina material when considering CLOU operation. There was no decrease in reactivity after 20 cycles during cycling within TGA which may be seen from Figure 26. The material achieved full conversion under a variety of conditions and temperatures ranging from 600°C to 1000°C.

The trace shown in Figure 27 shows the zirconia-supported material tested for 20 cycles between air and nitrogen at 925°C in TGA. The trace shows a decrease in the mass of the sample over time. While the sample mass slowly decreases, the change in mass between the fully oxidized and fully reduced remains nearly constant. Therefore, this drift is likely just that, a drift in the TGA balance, and does not likely represent a mass loss of the sample.

The ZrO_2/MgO material was tested under many different conditions. The material was tested for use in solid fuels combustion as well as normal CLOU cycling. The results of TGA testing for both the oxidation and decomposition reactions were used to obtain the relevant reaction rate constants and expressions. This information was used in conjunction with the same gathered from TGA results from cycling of the TiO_2 supported material. These rate expressions were used to develop a model that may be applied to predict the characteristic redox patterns of the CuO/Cu_2O pair.

4.1.4 Oxidation and Decomposition Kinetics

The rate expression obtained for the decomposition of CuO using the titania- and zirconia- supported materials was developed using the methods described in Chapter 6. The developed rate expression was then used to predict reaction rates of other materials. These predictions were then compared to rate data obtained during CLOU testing of two
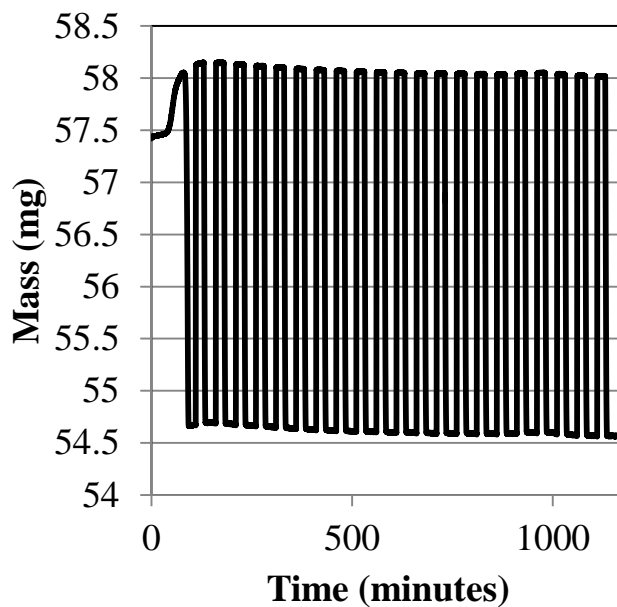
Figure 26: Cycling of 50_TiO2_MM in TGA for 20 loops using air for oxidation and nitrogen during decomposition at 925°C.
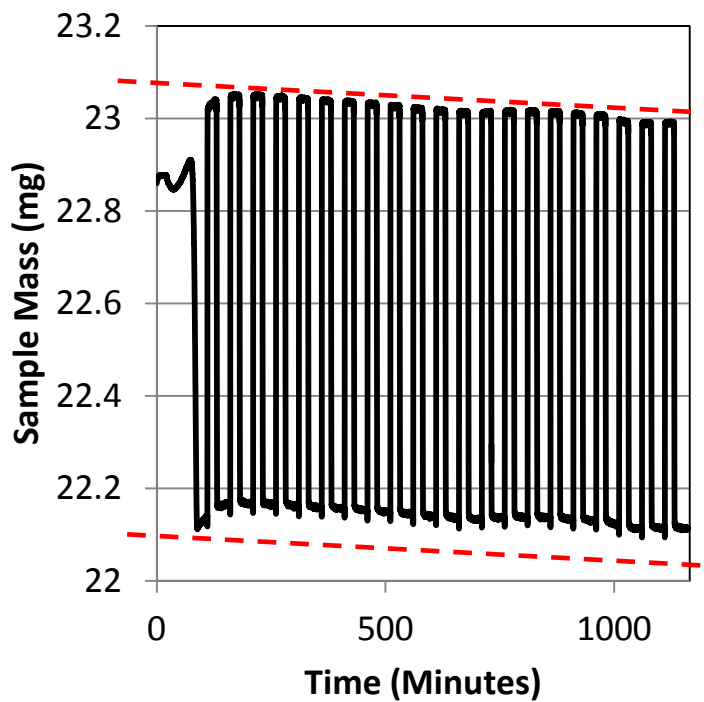

Figure 27: Multiple redox cycling for the 45_ZrO2_FG material at 925°C in TGA under air and nitrogen.

other materials. These other materials differed from the previous two in CuO wt% loading (16 wt% and 64 wt%), production method (Incipient Wetness using a Rotary Evaporator), support type (SiO_2) and area produced (in house at the University of Utah). The CuO/SiO_2 materials exhibited rates and characteristics similar to those observed with the titania and zirconia materials. The obtained model (Table 11) generated Figure 28 which compares the actual extracted decomposition rates of the oxygen carriers and the rates predicted by the model. More information on this study is provided in the manuscript titled Measurement and Modeling of Decomposition Kinetics for Copper-Based Chemical-Looping with Oxygen Uncoupling in Appendix A.

For the modeling and scale-up of copper oxide-based CLOU reactors, it is important to understand the kinetics of both decomposition and oxidation of the oxygen carrier. While it appears that the decomposition of cupric oxide to cuprous oxide may have a universal set of kinetic parameters that may be applied globally for all copper-based oxygen carriers, the same may not be true for the reverse reaction (oxidation of Cu_2O).

Details into this investigation are provided in Appendix B. This section will only serve to highlight the results discussed therein.

Similar to the decomposition reaction of CuO, the oxidation of Cu_2O is largely dependent on a driving force that is a function of the partial pressure of oxygen around the sample and the equilibrium partial pressure of oxygen for the CuO/Cu_2O redox pair at each temperature. For the decomposition of CuO, the reaction rate is accelerated as the temperature is increased by both a direct and indirect affect. The direct affect is explained by use of the activation energy for the reaction, while the indirect affect is

Table 11: Constants for kinetic rate expression modeling the decomposition of CuO.

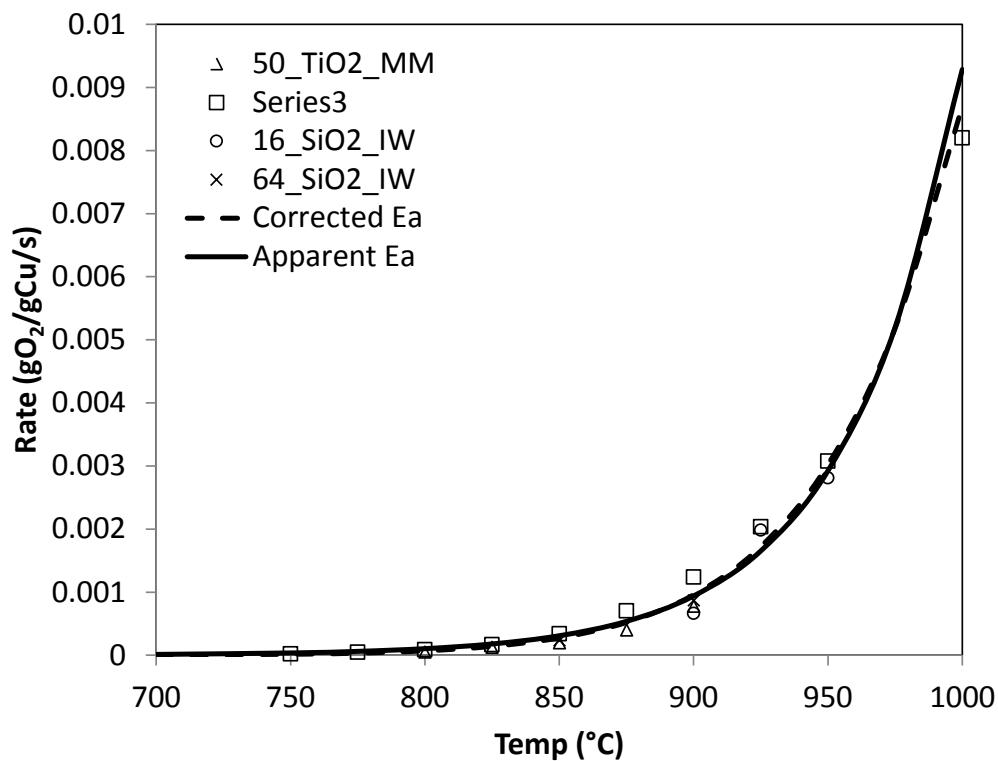| Parameter	50_TiO2_MM	45_ZrO2_FG	Value in Rate Expression
Activation Energy, Ea (kJ/mol)	67	58	62
Frequency Factor, A (atm-1×s-)	$4.15 \times 10\text{-}4$	$3.64 \times 10\text{-}4$	$3.90 \times 10\text{-}4$
Order of P_{O2}, α (atm)	1.0	1.0	1.0
Order of C_{CuO}, β (–)	0	0	0

Figure 28: Rates of decomposition of four different copper-based oxygen carriers at several temperatures using nitrogen as inert purge during decomposition compared with the rates predicted by the developed kinetic rate expression.

caused by the increased equilibrium partial pressure of oxygen with temperature. Unlike decomposition, the reaction rate of oxidation is slowed by the increase of the equilibrium partial pressure of oxygen. Therefore, as the temperature is increased above 850°C, the observed reaction rate begins to slow. This results in a seemingly negative activation energy at high temperatures, but, in reality, is explained within the driving force term. Figure 29 shows the rate of oxidation at several temperatures for the 45_ZrO2_FG material using air as the oxidizer. The decreased reaction rate is readily observed above about 850°C. While this phenomenon is easily explained by the decreased driving force with increased temperature, there are other mechanisms at work during the oxidation of Cu_2O that further complicate determination of an applicable kinetic expression. In fact, while one mechanism appears to be at work during lower temperature oxidation, another mechanism seems to be more representative of the observed kinetics.

For low temperature oxidation of Cu_2O, the pore-blocking model (a logarithmic rate expression) best describes the observed kinetics. This is likely due to an increase in the molar volume of the solid during oxidation from Cu_2O to CuO (approximately 5 vol%). The extracted values describing the pore-blocking kinetic expression are provided in Table 12.

While useful for understanding the oxidation of cuprous oxide, the low temperature kinetic expression is not very applicable to CLOU operation. Generally speaking, the temperatures at which the air reactor will be operated is likely over 900°C. With this in mind, it is obvious that a kinetic expression should be developed closer to the likely temperature range of operation.

For the oxidation of Cu_2O at temperatures above 850°C, the applicable kinetic
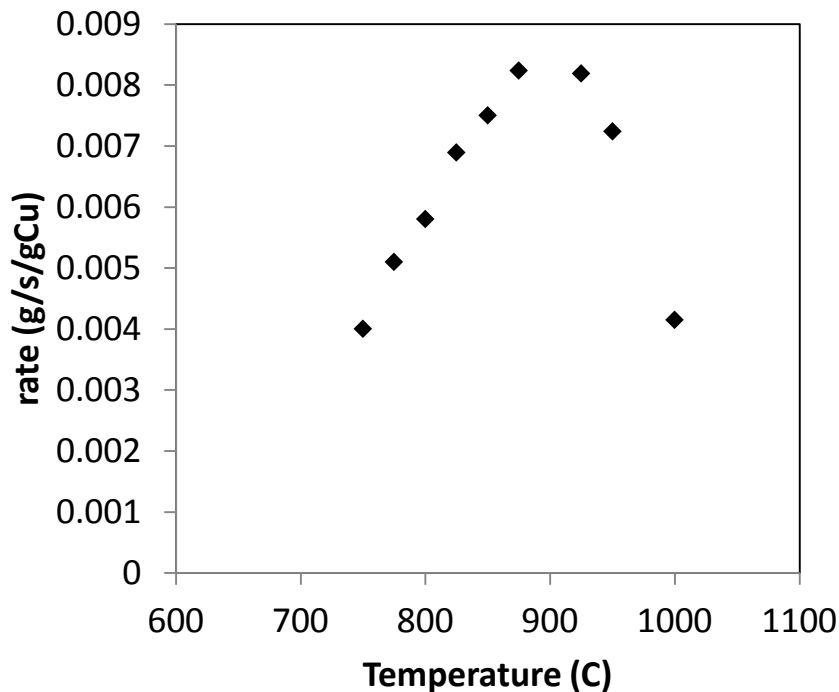
Figure 29: Oxidation rate extracted at 50% conversion for the 45_ZrO2_FG material at temperatures from 750 – 1000°C.

Table 12: Results obtained from modeling of low temperature oxidation of two CLOU materials.

Influence	50_TiO2_MM	45_ZrO2_FG
$f(X): 1/\exp\left(\frac{X}{\lambda}\right)$	$\lambda = -2.95 \times 10^{-4} \times T + 0.34$	$\lambda = -4.16 \times 10^{-4} \times T + 0.48$
$p_{O_2,eq}^{\alpha}$	$P_{O_2}(atm) = 6.057 \times 10^{-11} e^{0.02146\ T(°C)}$	
$f(p_{O_2}): (p_{O_2}^{\alpha} - p_{O_2,eq}^{\alpha})$	$\alpha = 1.3$	$\alpha = 1.3$
$f(T) = A \times \exp\left(-\frac{E_a}{RT}\right)$	A = 6.2×10^{-13} (min-1); E_a = 172 (kJ/mole)	A = 3.4×10^{12} (min-1); E_a = 165 (kJ/mole)

expression was developed assuming the Avrami-Erofeev nucleation/growth kinetics equation. The true scientific nature describing the transition from the pore-blocking kinetic expression to the nucleation/growth kinetic expression is beyond the scope of this work, but is possibly a result of increased diffusion rates to the point at which pores blocked by the expansion of the molar volume do not truly hinder the diffusion of reactive species (likely the diffusion of Cu through CuO). This requires a closer investigation for further understanding.

The kinetic constants used for the completed model are provided in Table 13. The developed model failed to effectively capture the conversion profile of the tested materials at low temperatures, but seemed to capture the higher temperature oxidation of Cu_2O. Figure 30 displays the model compared to the obtained data for both cases.

4.1.5 Production and Evaluation of Novel Materials

Along with the materials obtained from other institutions, a few materials were produced and tested in house at the University of Utah. First among these materials were produced from a high surface area SiC. Due to the oxidation of SiC at CLOU temperatures, the material was baked in air within a muffle furnace for roughly a week. The oxidation of SiC, even at high temperatures, is very slow and required the whole week to form 99% SiO_2. Various productions methods were employed during the creation of this material in an effort to find the optimal loading and distribution of CuO. In the end, the material of choice was produced by first loading CuO onto the surface of the SiC powder using a rotary evaporator. The CuO-coated SiC material was then placed within the muffle furnace to convert the SiC to SiO_2. The method of coating the particle

Table 13: Model used to predict the conversion of Cu$_2$O in two different oxygen carriers using the nucleation/growth kinetics expression Avrami-Erofeev.

Influence	Model Values
$f(X)$	$1 - X$
$p_{O_2,eq}$	$P_{O_2}(atm) = 6.057 \times 10^{-11}e^{0.02146\,T(°C)}$
$f(p_{O_2}): \left(p_{O_2}^\alpha - p_{O_2,eq}^\alpha\right)$	$\alpha = 1.3$
$f(T) = A \times exp\left(-\dfrac{E_a}{RT}\right)$	A = 7.90× 10^4 (min-1); E$_a$ = 69 (kJ/mole)

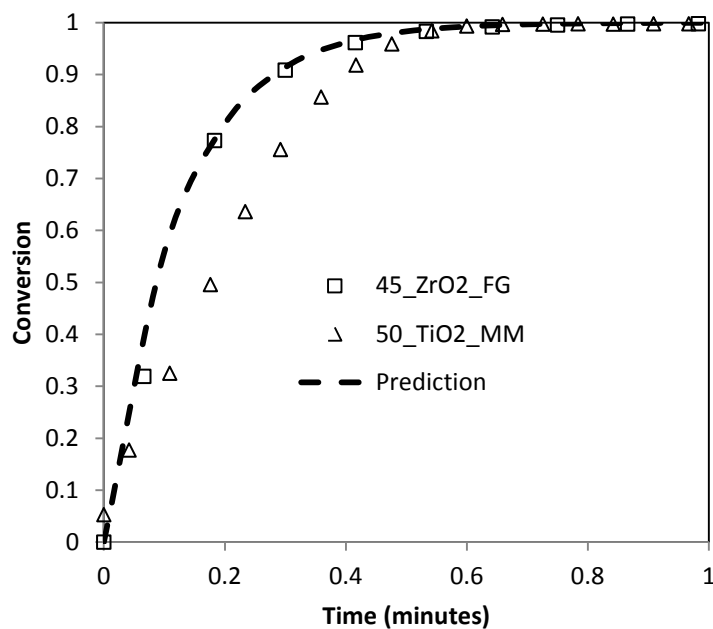Figure 30: Conversion profiles for the oxidation of Cu$_2$O at 925°C for 45_ZrO2_FG (□) and 50_TiO2_MM (Δ) are compared against the model prediction (- - -).

first, then baking within the furnace provided a means whereby the CuO was thermally driven beneath the surface of the particles. This thermally driven migration is evidenced in Figure 31 which shows SEM micrographs of the material before and after baking with the corresponding EDS images. The copper seen in the first row seems to disappear in the figure below. This corresponds to the increased level of Si seen in the second row compared to the first.

By utilizing the coat-then-bake method (CTB) as opposed to the bake-then-coat (BTC) method, the observed agglomeration temperature ceiling was increased from 850°C to over 1000°C for two of the materials. The measured agglomeration temperatures are given in Table 14. The performances of these materials are more adequately presented in Appendix D.

4.2 Conversion of Solid Fuels

The results from the combustion of solid fuels using different oxygen carriers are presented below. Three different fuels (PRB, Illinois #6 and Petroleum Coke) were used for this study and were tested using two different oxygen carriers (50_TiO2_MM and 45_ZrO2_MM). The proximate and ultimate analyses of the tested fuels are provided in Table 6. For the combustion of solid fuels, many factors play major roles in the design of industrial-scale combustors. For example, the selection of an appropriate fuel will have a major impact on the size and design of the boilers. A higher reactivity fuel will require a shorter residence time, allowing for a smaller boiler design. Another factor is the water and/or ash content of the fuel. The higher the water content, the less efficient the fuel, thus requiring more fuel to achieve the same thermal output. A higher ash content can

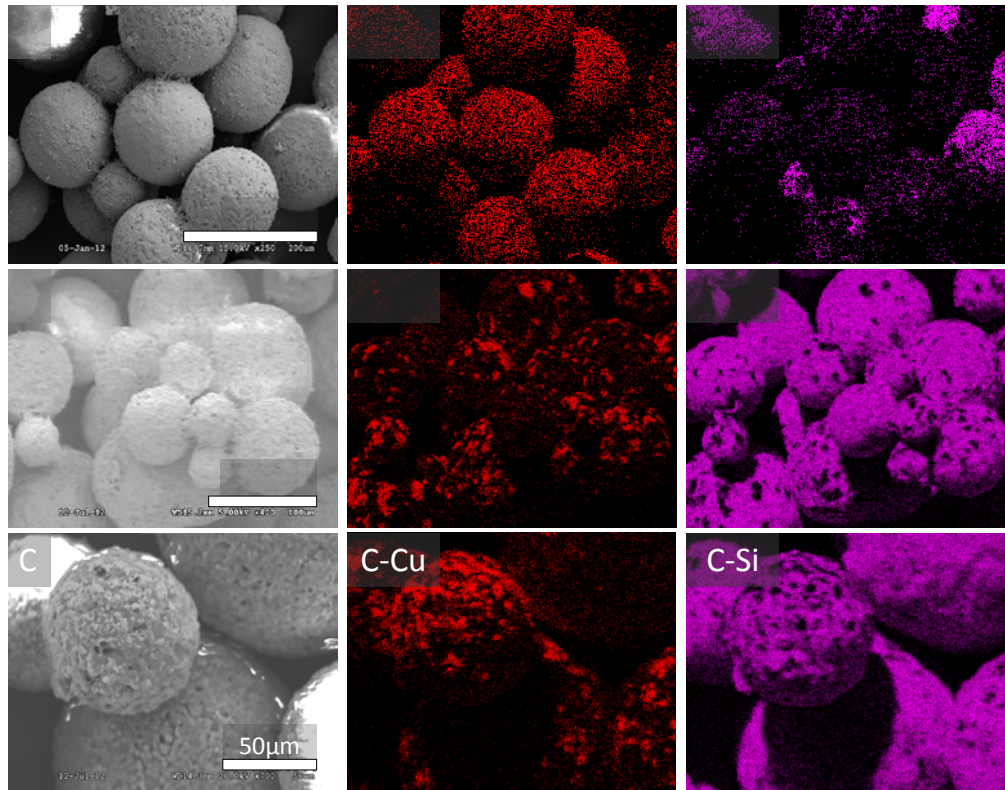Figure 31: SEM and corresponding EDS images for elemental Cu and Si of RV-CTB-15 (a) before baking, (b) after baking, and (c) after fluidization.

Table 14: Measured agglomeration temperature in the fluidized-bed

Oxygen Carrier	CuO loading (wt%)	Agglomeration temp. (°C)
RV-BTC-20	19	850
RV-CTB-15	15	> 1000
RV-CTB-40	40	> 1000
RV-CTB-60	61	950

also affect the thermal efficiency of the boiler, and can also cause great concern due to slagging (collection and cooling of molten bottom ash within the boiler) which reduces heat transfer efficiency to water pipes.

In the case of a chemical-looping combustor, these factors must all be considered. For example, the collection of ash within the fluidized-bed may increase solids inventory and decrease OC circulation rates, thereby decreasing the overall efficiency of the process. Therefore, proper selection of a fuel is critically important to the overall design of a chemical-looping combustor. The following results will help to highlight some of these concerns and potential design considerations to overcome possible challenges.

Petcoke is stripped of most of the volatile content from the creation process, hence, it is less reactive than the coals studied. The Powder River Basin (PRB) coal is a sub-bituminous and thus has a lower rank than the bituminous Illinois #6 coal. The lower rank coals generally have higher reactivities. This ordering may be observed in Figure 32 where the conversion of carbon versus time is displayed for the three fuels during combustion using 50_TiO2_MM material at 930°C. The PRB reacts very quickly, reaching full conversion in just a few seconds. The Illinois #6 coal and petcoke, however, do not reach full conversion. From a stoichiometric standpoint, the oxygen supplied by the metal oxide carrier should be more than sufficient to fully combust all of the fuels. The amount of fuel supplied to the reactor was evaluated by determining the amount of oxygen to be released from the total sample carrier between 80% and 20% conversion of the carrier. Therefore, the amount of oxygen released from the carrier should be 40% more than is necessary for complete carbon burnout of the fuel. A simple explanation could be that the unreacted fuel was simply blown out of the reactor before it
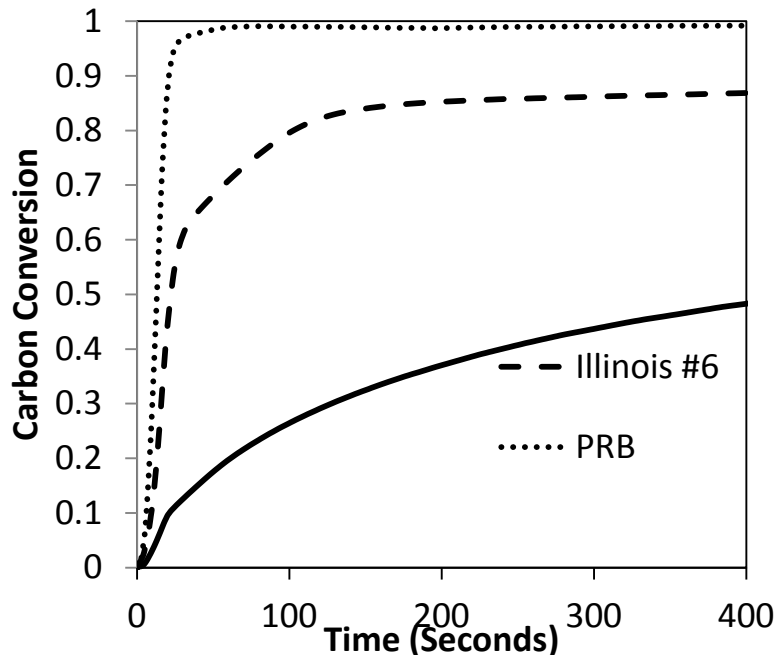
Figure 32: Combustion of three different fuels using 50_TiO2_MM material at 930°C. The conversion is calculated from the mass of carbon (as gas) analyzed and collected by infrared analyzer.

could be consumed. If that is the case, the ensuing oxidation cycle would yield no additional carbonaceous products – or, at least, it would not account for all of the missing carbon. The full conversion profile of the petcoke fuel is given in Figure 33. Clearly, as the conversion approaches 50%, the rate slows considerably and is near zero around 700 seconds of reaction. Air is once again cycled to the reactor around 700 seconds and the missing carbon is burned off. It is clear from this figure that the fuel is not being ejected from the reactor, but is simply not completely reacted within the fluidized-bed. The full reaction profile obtained during the combustion of Illinois #6 coal is very similar to the petcoke, in that it is not fully combusted until the air is once again cycled through the reactor.

Once again, the incomplete combustion of these fuels is not a result of insufficient
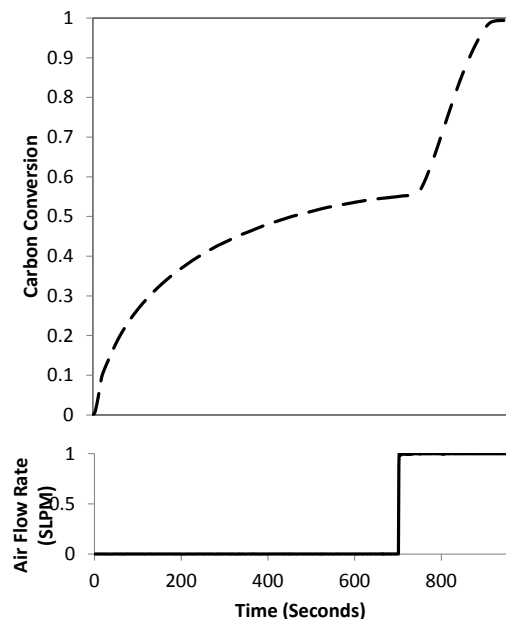
Figure 33: Conversion of carbon during combustion of green petcoke at 930°C using 50_TiO2_MM in a fluidized-bed.

oxygen supply. Certainly, the fuel is oxygen starved, but it is due to the slow reactivity of the fuel and not due to an excessive charge of fuel to the reactor. This characteristic is accentuated and more easily understood by looking at the effects of increasing the fuel particle size.

The combustion of PRB particles ranging from 150 μm to 6,000 μm (0.3 cm) at 930°C using the 45_ZrO2_FG material is given in Figure 34. The three tests were performed by selecting particles that fit the desired size range while having a very similar combined mass. For example, the sample tested in the 6,000 μm range consisted of only one particle. This single particle had a mass very similar to the combined masses of the other two samples individually. While, once again, the combustion of the small particle size (150 μm) was completed very quickly (roughly one minute), the other two samples did not reach full conversion of the carbon even though the masses of each of the three
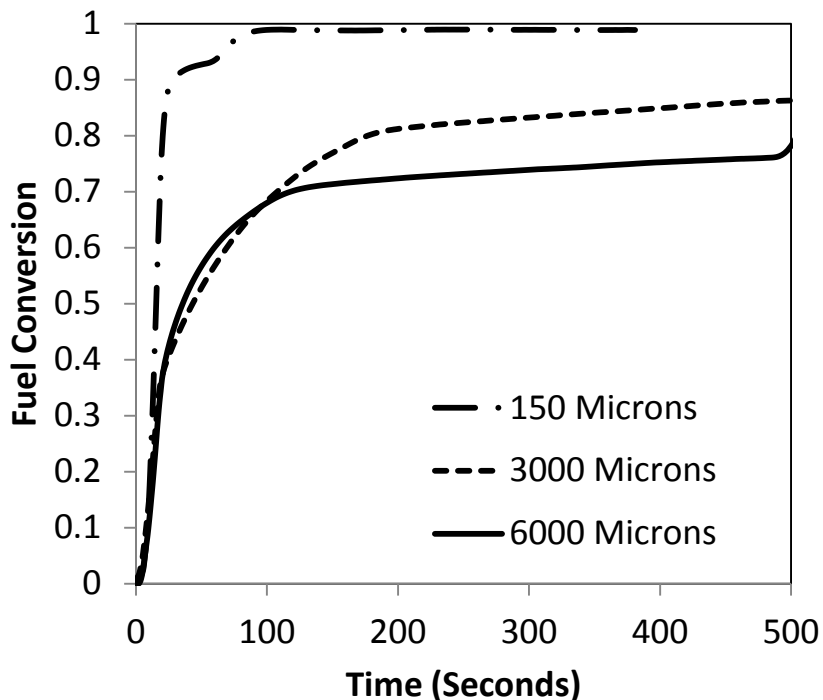
Figure 34: Carbon conversion is tracked during the combustion of PRB at 930°C using 45_ZrO2_FG in a fluidized-bed.

samples was very nearly equal.

Admittedly, it may be possible to have complete burnout of the larger fuel

particles if the amount of oxygen carrier is increased. However, it is likely the case that

this will not be due to the increased amount of available oxygen, but instead, due to an

increase in the reaction time due to a deeper particle bed. The slower decomposition

rates may be achieved by the oxygen carrier simply due to an increased oxygen

partial pressure. The increase in the oxygen partial pressure effectively decreases the

driving force for decomposition. This phenomenon is discussed further in Appendix A

and Appendix B where the kinetic characteristics of both oxidation and decomposition of

the CuO/Cu$_2$O redox pair are discussed in detail, including the effect of the driving force on the reaction.

The reactivity of PRB was previously mentioned as being higher than the other two fuels tested. It may be assumed, however, that even for a more reactive fuel, there exists a particle size threshold, above which a particular oxygen carrier may be ineffective, not because it decomposes too slowly, but to the contrary, because it decomposes too quickly. The higher rates of decomposition then produce oxygen that is unreacted and dilutes the fuel reactor product stream. It should be noted that the driving force fueling the research of technologies such as chemical-looping is the production of a nearly pure CO$_2$ stream which may easily be sequestered. Excess air in the fuel reactor will dilute the CO$_2$, stream making purification of the CO$_2$ more challenging and decreasing the effectiveness of the technology.

Figure 35 shows the conversion of the solid oxygen carrier from CuO to Cu2O during the combustion of large petcoke particles (roughly 3,000 μm) using 45_ZrO2_FG at 930°C and 960°C. The conversion of the solid oxygen carrier material at 960°C, is shown as well. At roughly 200 seconds the oxygen carrier is nearly completely spent and the rate of decomposition slows, essentially to zero. In both cases, the fuel is incompletely combusted and stops as the oxygen is no longer devolved. Due to the increased reactivity of the petcoke at 960°C, the conversion profile for that temperature is extended. Once again, while the amount of oxygen is sufficient for the combustion of this fuel, it is simply released and swept away too quickly to react with the remaining petcoke.

Figure 36 suggests that the oxygen contained within carbonaceous gas evolved
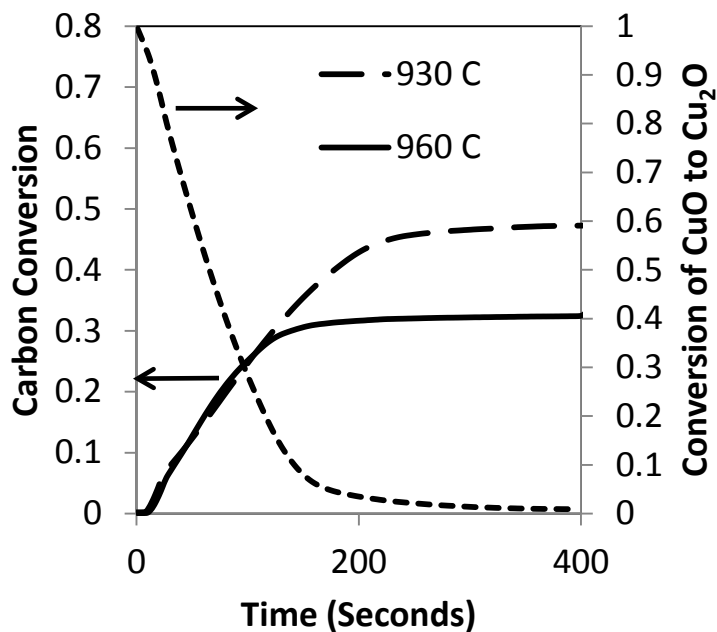
Figure 35: Conversion of carbon during the combustion of petcoke particles with a diameter of roughly 3,000 μm at two temperatures using the 45_ZrO2_FG material as oxygen carrier is compared against the conversion of the oxygen carrier (---),
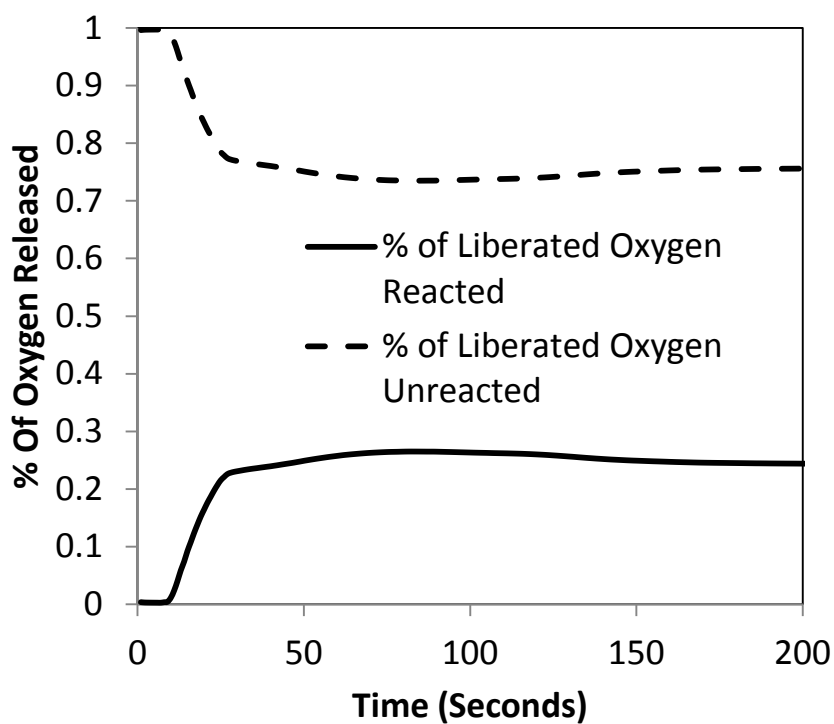

Figure 36: Depiction showing the amount of oxygen liberated from the reactor unreacted compared to the oxygen reacted during combustion of petcoke at 960°C in a fludized-bed with 45_ZrO2_FG as oxygen carrier.

during the combustion of the large petcoke particles accounted for only about 30% of the total evolved oxygen. The remaining near 70% of the liberated oxygen was swept through the outlet as unreacted oxygen. This number actually speaks well to the performance of the oxygen carrier. The challenge of having too much oxygen in the effluent of the fuel reactor may be overcome by simply adding a simple recycle loop. This will deliver unreacted oxygen back to the reactor which will also serve to effectively slow the rate of oxygen carrier decomposition. The slower rates of decomposition would prove more effective for the combustion of less reactive fuels such as petcoke or larger fuel particles; both cases would require a more substantial residence time for complete combustion.

One of the very large challenges in the combustion of solid fuels is understanding how best to deal with the resulting ash. In the case of chemical-looping, the general desire is to handle the separation of oxygen carrier from the ash simply by the differences in their respective fludization characteristics. Generally speaking, the lower the density and smaller the particle, the easier it is to fluidize. In the case of ash associated with solid fuels, that particle sizes are very small and the density is much lower than the solid fuel. Since most oxygen carriers are made from metals (or metal oxides), it can generally be assumed that it is more difficult to fluidize the oxygen carrier than it is to fluidize the resulting ash. By creating an environment where the fluidization properties encourage the expulsion of the smaller ash particles, while still not quite large enough to eject the oxygen carrier, this separation may be effectively and efficiently mitigated.

Unfortunately, the bubbling fluidized-bed did not exhibit such behavior. A set of in-line filters has been installed into the fluidized-bed reactor system with the hope of

catching any elutriated fines (one may hope that coal ash is on that list of elutriated

fines). Unfortunately, as one may see in Figure 37, that hardly anything is collected on

the filter, while the product oxygen carrier is riddled with coal ash.
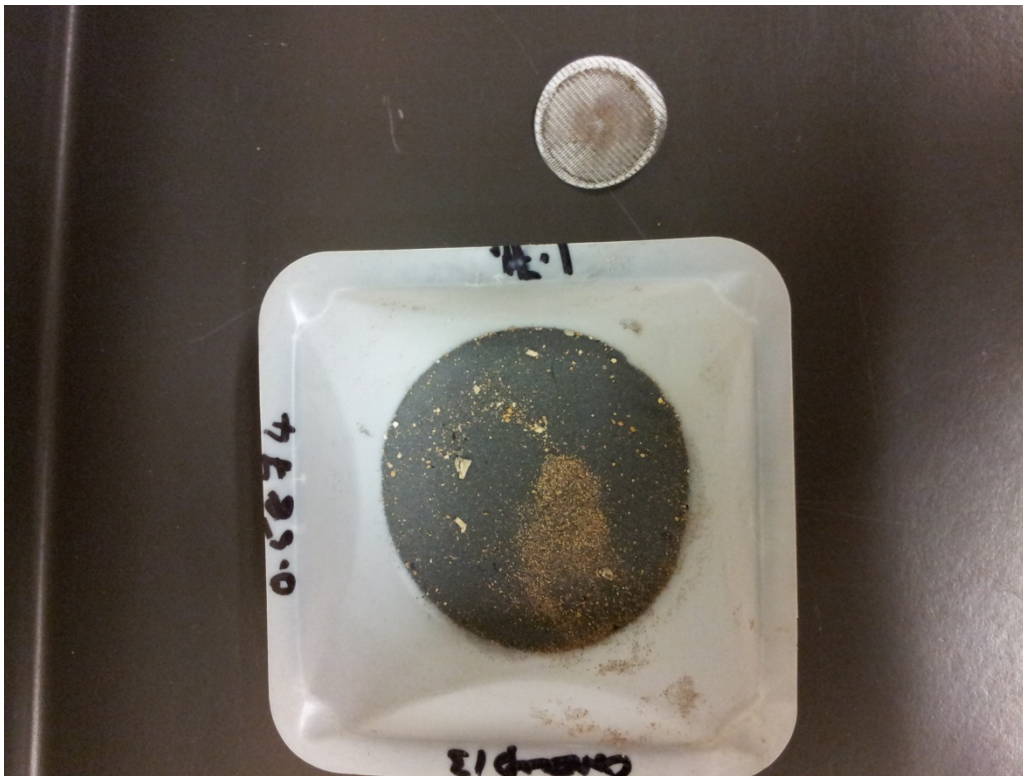
Figure 37: Coal ash that has collected within the particle bed and is not elutriated during the combustion of different solid fuels above 900°C using the 45_ZrO2_FG material shown here.

4.3 References

[1]   Chen, Y. (1997). Low-temperature oxidation of ilmenite (FeTiO3) induced by high energy ball milling at room temperature. J Alloy Compd. 257 (1-2):156 – 160.

[2]   Wang, C. Y., & Zhou, M.-F. (2004). Mineral Chemistry of Fe-Ti oxides from Xinjie PGE-bearing layered mafic ultramafic intrusion in Sichuan, SW China. Mineral Deposit Research, meeting the global challenge (pp. 481-485). Beijing: Springer.

[3]   Cuadrat, A. Chemical-looping Combustion of Coal Using Ilmenite as Oxygen Carrier. Ph.D. Dissertation, Instituto de Carboquimica (ICB-CSIC). Zaragosa, Spain, 2012.

CHAPTER 5

CONCLUSIONS

Chemical-looping is quickly becoming a suitable alternative for the cleaner combustion of fossil fuels. While there is still much that needs to be understood before this technology may be commercialized, the promise that this technology holds gives hope to those involved in its development.

Several materials have been suggested as possible suitable candidates for use in a chemical-looping system. Among these, copper oxide stands out toward the front. Copper oxide has a relatively high oxygen carrying capacity, high reactivity and creates an overall endothermic reaction in the fuel reactor when oxidizing a number of fuel sources. The most notable characteristic of copper oxide is that it is CLOU capable. This means that at certain temperatures, both an oxidized state (CuO) and a reduced state (Cu_2O) are thermodynamically favored, depending on the partial pressure of oxygen within the system. This characteristic enables the cycling between CuO and Cu_2O without a fluid fuel. Much improved reaction rates are observed during the combustion of solid fuels without the need for initial gasification of the fuel.

A seemingly plethora of potential copper oxide-based material have been suggested as suitable materials for use in a chemical-looping system. Among them, the use of high surface area SiC and ilmenite have proven effective due, in large part, to their

ease of production and relatively low cost. Other prepared materials may possibly exhibit slightly better physical durability, but it is challenging to compete with a cost-effective support such as the abundantly available ilmenite.

The ilmenite-supported oxygen carrier performed very well both physically and chemically. There was no long-term decrease in reactivity and it has the added benefit of being available for CLC combustion. The future of chemical-looping will be shaped using metal blended oxygen carriers. These type of carriers can be highly cost effective while providing the positive benefits from both metal oxide sources.

Because copper oxide is such an attractive material for a chemical-looping system, it becomes necessary to more adequately understand the mechanisms responsible for both the oxidation and decomposition of the CuO/Cu_2O redox pair. An effective model describing the kinetics of oxidation and another describing the kinetics of decomposition have been developed. These models adequately describe the observed behavior of the relevant copper oxide states while remaining simple enough to be effectively utilized in larger-scale modeling of a copper oxide-based chemical-looping system. Moreover, a single equation which adequately describes the decomposition of CuO over a wide range of supports and production methods has been developed. This, in particular, is useful for larger-scale modeling applications to effectively compare the theoretical performance of a host of copper-based carriers.

The decomposition of CuO under CLOU conditions is adequately described with an activation energy 62 kJ/mol and a pre-exponential constant of $3.9 \times 10\text{-}4$. The order of reaction with respect to the partial pressure of oxygen is 1 and the reaction is independent of the solid conversion.

The oxidation of Cu_2O, on the other hand, is not so easily modeled. For low temperatures, the oxidation mechanism appears to obey a pore-blocking rate law while there appears to be a transition around 700 - 800°C where the conversion profile begins to more accurately follow a nucleation/growth rate model. The Avrami-Erofeev model adequately described the conversion profile with n = 1. The influence of the solid, unlike the reverse reaction, appears to be pseudo-first order. This pseudo-first order influence incorporates potential underlying mechanisms such as solid state Cu+ diffusion.

Copper oxide-based materials have been proven suitable as oxygen carriers for the combustion of solid fuels. The successful combustion of solid fuels was shown in this work while using two different oxygen carrier materials. The fuels with lower reactivities create challenges that are easily overcome with simple engineering strategies, whereas the higher reactivity fuels may successfully employ the use of larger particles.

The combustion of PRB at 930°C is completed very rapidly – around 30 seconds for 0.1 g. This equates to a consumption rate of 0.003 g_{fuel}/s. The developed kinetic equation predicts an oxygen release rate of 0.0036 g_{O2}/s-g_{Cu}. For the lower reactivity fuels, while the oxygen release rate remains essentially the same, the combustion rate drops thereby releasing unspent oxygen into the flue gas.

There are still plenty of opportunities for the continued research of chemical-looping technologies. A great many topics relating to this technology still have yet to be adequately researched. Among those topics needing the most attention:

1. Determining the most cost-effective oxygen carrier production method.

2. At what rate are the oxygen carrier particles "poisoned" by different solid fuels?

3. How does one go about separating the ash produced from the combustion of

   solid fuels from the oxygen carrier materials?

APPENDIX A

MEASUREMENT AND MODELING OF DECOMPOSITION KINETICS FOR

COPPER OXIDE-BASED CHEMICAL LOOPING

WITH OXYGEN UNCOUPLING

AppliedEnergy

Measurement and modeling of decomposition kinetics for copper oxide-based chemical looping with oxygen uncoupling

CrossMark

Christopher K. Clayton *, Kevin J. Whitty

Dept. of Chemical Engineering, The University of Utah, 50 S. Central Campus Dr., Room 3290, Salt Lake City, UT, 84112, USA

HIGHLIGHTS

- By experimental approach kinetic equations of two copper-based oxygen carriers were defined.
- The dual effects of temperature (kinetic and thermodynamic) were separated.
- The developed kinetic equations were then used to predict the rates of two other carriers.
- It may be reasonable to assume a universal rate equation for all copper-based oxygen carriers.

ARTICLE INFO

ABSTRACT

Chemical looping combustion with oxygen uncoupling (CLOU) is a promising CO_2-capture ready energy technology that employs oxygen carriers with thermodynamic properties that cause oxygen to be spontaneously liberated as gaseous O_2 in the fuel reactor, where it can react directly with solid fuels. One of the promising CLOU carrier metals is copper, cycling between CuO and Cu_2O. Experimentally-determined rate expressions for these reactions are needed for proper development, modeling and scale-up of CLOU technology. The $CuO–Cu_2O$ system presents an interesting challenge in that the rate of decomposition depends on the thermodynamic driving force imparted by the difference between equilibrium and actual partial pressures of oxygen, and the equilibrium partial pressure is strongly temperature dependent in the range useful for combustion. This study investigates decomposition of two different copper-based oxygen carriers, from CuO to Cu_2O oxidation states, to develop a universal kinetic expression to describe the observed rate of reaction as a function of temperature, conversion and gas environment. The kinetic model developed is compared to results of a third support type (silica) using two different CuO wt% loadings (64 wt% CuO and 16 wt% CuO) to demonstrate applicability to other support types and copper oxide loadings.

1. Introduction

Chemical looping combustion (CLC) is promising technology for CO_2-capture ready processing of carbonaceous fuels for energy production, and has been recognized as having potentially lower energy demand and offering a lower cost of electricity than oxy-fuel combustion, IGCC and flue gas CO_2 removal by amine scrubbing [1,2]. The most common configuration for a CLC system involves two interconnected fluidized beds, the so-called air reactor and fuel reactor, with metal-based "oxygen carrier" particles cycling between them [3]. The metal is oxidized in the air reactor, the product gas of which is oxygen-depleted air. The oxidized carrier particles are transported to the fuel reactor via a loop seal, thus keeping nitrogen from entering the fuel reactor. In the fuel reactor, the oxygen carrier is reduced by a gaseous fuel such as natural gas, effectively combusting the fuel to CO_2 and H_2O, resulting in a product stream of nearly pure CO_2 once water vapor is condensed. The reduced carrier is returned to the air reactor.

Because solid–solid reactions are inefficient, CLC is not suitable for processing solid fuels unless the fuels are converted to syngas in an upstream reactor or in situ in the fuel reactor. Another, more promising approach is so-called Chemical Looping with Oxygen Uncoupling (CLOU), a variant of CLC, that involves use of specific metal–metal oxide complexes to spontaneously release ("uncouple") oxygen as gaseous O_2 in the fuel reactor [4]. This is possible because the equilibrium behavior of the carrier oxidation/reduction reaction is such that gaseous O_2 is favored at high temperature, low-O_2 conditions such as those existing in the fuel reactor of a CLC system. In the air reactor, the high O_2 partial pressure favors the oxidized metal. The advantage of CLOU carriers

---
* Corresponding author. Tel.: +1 8047885724.
  E-mail address: chris.clayt@gmail.com (C.K. Clayton).

over conventional CLC carriers is that the released oxygen can react directly with solid fuel or char, thereby avoiding the need to convert the solid to gas through relatively slow gasification reactions.

Only a few metal complexes that exhibit this CLOU behavior in the range of chemical looping combustion temperatures have been identified. Mattisson et al. [4] discussed the ability of CuO, MnO and CoO to perform the spontaneous liberation of oxygen. CLOU Copper oxide is attractive due its fast reaction rates and it is thermodynamically favored to completely convert gaseous hydrocarbons to CO_2 and H_2O [5]. Most notably, however, copper oxide looping is overall exothermic in both the air reactor and fuel reactor, whereas other materials are exothermic in the air reactor, but would require heat input to the fuel reactor since the heat required to reduce the carrier exceeds that given off by the fuel as it combusts [6].

When used as a CLOU carrier, copper cycles between the Cu^{+2} cupric (CuO) and Cu^{+1} cuprous (Cu_2O) states:

$$Cu_2O(s) + 1/2O_2(g) \leftrightarrow 2CuO(s) \qquad (1)$$

The equilibrium curve for this reaction is shown in Fig. 1. At temperatures above approximately 800 °C, in otherwise low-O_2 environments (such as the fuel reactor of a chemical looping system), the left side of the above reaction is favored, generating O_2. If the O_2 continues to be consumed (e.g., by reaction with fuel), the CuO decomposition reaction will continue to progress. The use of the Cu_2O-CuO system to generate carbon dioxide was first recognized by Lewis and Gilliland in 1954 [7]. Application to CLC was first demonstrated by Mattisson et al. [4], who showed that conversion of petcoke by CLOU is as much as 50 times faster than conversion by conventional CLC with an iron-based carrier, which requires in situ conversion of petcoke to syngas by relatively slow gasification reactions. Several groups have since continued in the investigation of CLOU using either Co, Mn or Cu-based carriers in their studies ultimately concluding that either Mn or Cu may be suitable choices [8–13].

For proper design and modeling of chemical looping systems, it is valuable to understand the intrinsic chemical kinetics of both the forward (oxidation) and reverse (reduction) reactions shown in reaction (1). Ideally, it would be useful to develop general rate expressions applicable across a broad range of conditions, for example of the form below for cupric oxide decomposition:

$$rate = A\exp(-E_a/RT)[CuO]^{\alpha}(P_{O_{2,eq}} - P_{O_2})^{\beta} \qquad (2)$$

where A is a pre-exponential constant, E_a is the activation energy and α and β are reaction orders. The challenge lies in experimentally determining these constants. The inclusion of the oxygen concentration term in Eq. (2) may not initially be obvious. Because reaction (1) is reversible, the thermodynamic behavior shown in Fig. 1
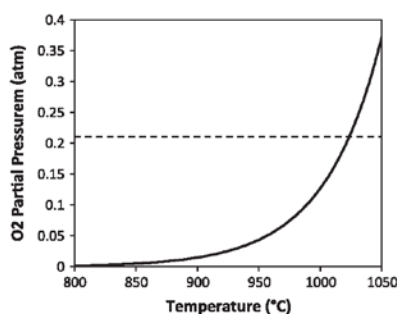
affects the rate of the carrier oxidation and decomposition (uncoupling) reactions. It is well understood that rates of reversible reactions such as reaction (1) are affected by the difference between the actual and equilibrium concentrations of reacting species, the so-called "driving force." This has also been observed to occur with copper-based oxygen carriers operating in the CLOU regime [14]. Due to the effect of temperature on the equilibrium partial pressure of oxygen the oxygen concentration term in Eq. (2) takes the form shown as a difference between the equilibrium partial pressure and the observed partial pressure of oxygen.

The dependence of Cu_2O oxidation and CuO decomposition on the oxygen driving force makes identification of intrinsic kinetics of the respective oxidation and reduction reactions challenging. For example, several groups studying CLOU have reported a decrease in the rate of oxidation by air at higher temperatures [12,14–16], which is due at least in part to a decrease in the difference between the equilibrium O_2 partial pressure and air's partial pressure of 0.21 atm. Similarly, in certain types of experiments the rate of cupric oxide reduction to release O_2 is affected by that released O_2. Adánez-Rubio et al. [17] demonstrated a decrease in the decomposition rate of CuO with an increase in the supplied partial pressure of oxygen. They suggested that the decrease in reaction rate be ascribed to a decrease in the driving force between the equilibrium partial pressure and supplied partial pressures of oxygen.

Using results obtained from the decomposition of a zirconia-supported copper oxide-based carrier in a batch fluidized bed with Mexican Petcoke as a fuel Sahir et al. [18] suggested that the apparent activation energy observed during CuO decomposition is a combined effect from the activation energy as well as the influence of the oxygen partial pressure driving force. Their analysis suggests that the energy required to overcome both the thermodynamic (oxygen partial pressure driving force) and kinetic (activation energy) barriers to reaction is 280 kJ/mole. They report that by separating the influences of these two barriers they were able to obtain a kinetic barrier of 20 kJ/mole and a thermodynamic barrier of 260 kJ/mole. This work reports results obtained using a sample of the oxygen carrier material used in that analysis.

It has been observed that the rate of CuO decomposition is slower than that of Cu_2O oxidation in the temperature range of interest to copper looping systems, so it is especially critical for proper design of the fuel reactor that decomposition rates are well understood and can be modeled. The objective of this study is therefore to gain a better understanding of the chemical mechanisms associated with decomposition of cupric oxide. The desired kinetic model should adequately represent the characteristics of a copper-based oxygen carrier regardless of variability in characteristics such as support type, copper loading and production method. It is the goal of this work to provide such a model.

2. Experimental

In order to gain a better understanding of the decomposition mechanism and to compare carriers under a variety of conditions, two copper-based oxygen carriers were studied under a variety of experimental conditions.

2.1. Samples

Two different CuO-based carriers, prepared by different methods, were evaluated. Properties of the carriers are presented in Table 1. The MgO stabilized ZrO_2 material was produced using a freeze granulation method and provided by Chalmers University, Sweden. This material was reported to be very stable while maintaining physical strength and high chemical reactivity. Johansson

Fig. 1. Equilibrium curve for Cu_2O–CuO system. From data in Ref. [4].

Table 1
Copper-based carriers used in this study.

Carrier	Source	Preparation method	CuO loading (wt%)
50_TiO2_MM	ICPC, Poland	Mechanical mixing	50
45_ZrO2_FG	Chalmers, Sweden	Freeze granulation	45
16_SiO2_IW	University of Utah	Incipient Wetness	16
64_SiO2_IW	University of Utah	Incipient Wetness	64

et al. [19] reported that an inverse relationship exists between support strength and reactivity and that, when compared to other supports, the ZrO_2/MgO compound exhibited the best combination of reactivity and strength for a Mn-based carrier. To evaluate a range of Cu-based carriers a titania-supported material was also tested. The titania material was produced by the Institute for the Chemical Processing of Coal, Poland, and was prepared by mechanical mixing of titania and cupric oxide followed by extrusion and curing. Two silica-based materials were produced at the University of Utah using wet impregnation to deposit CuO to 64 wt% and 16 wt% loadings.

Three of the materials had a CuO loading over 40 wt%, which is particularly high for copper-based materials due to its affinity toward agglomeration/sintering at CLC temperatures. It is desirable to minimize the solids inventory in an industrial-scale reactor to keep both capital costs (smaller reactors) and operating costs (carrier material, energy lost to ΔP for fluidization) down. So, it is important to use oxygen carriers with the highest practical loading of the reaction participating species (copper in this case). This work focuses the development of an overall kinetic equation on the results of the titania- and zirconia-based materials while the silica-based materials are reported for comparison and justification of the reported kinetic model.

2.2. Experimental system and procedures

For conventional CLC carriers, reduction of the solid oxygen carrier requires reaction with a gaseous fuel. In the case of CLOU a fuel is not required; thermodynamics force reduction through oxygen uncoupling at high temperatures and when the gas O_2 partial pressure is below the equilibrium partial pressure. The term "reduction" may be better understood by replacing with "decomposition" in the case where a fuel is not used. In this study, the decomposition of CuO to Cu_2O is reported for both the titania- and zirconia-based carrier materials. Decomposition was carried out under a variety of atmospheres ranging from 0% O_2 to 4% O_2 at various temperatures. Efforts were made to avoid having any of the sample material exposed to oxygen evolved during reduction, as that would reduce the driving force of decomposition for the reasons described previously.

A TA Instruments Q500 thermogravimetric analyzer (TGA), with a maximum operating temperature of 1000 °C, was used for this study. In the Q500, gas flows upwards around a small, shallow sample pan which is suspended from a microbalance with a sensitivity of 0.01 mg. The sample is positioned in a furnace, the temperature of which is controlled based on a sensitive thermocouple positioned immediately above the sample layer.

For the experiments, samples ranging from 10 to 50 mg were loaded into small sample pans made of platinum or quartz. In order to maximize gas–solid contact and minimize mass transfer effects, small diameter particles (<45 μm) and a shallow layer of particles (nearly a monolayer in the bottom of the pan) were used. 100 ml/min of either air or nitrogen was fed into the TGA and the progression of mass loss was analyzed to determine the rate

of CuO decomposition. Experiments were conducted between 600 and 1000 °C.

The TGA records data in true real-time giving measurements that are a direct representation of what is happening within the sample as mass and temperature change. The specified reaction rate may be directly calculated from observed mass gain or loss, normalized by the mass of reactive material (copper).

Several experimental campaigns were designed specifically to determine individual kinetic parameters for decomposition of cupric oxide. Prior to decomposition, the carrier was oxidized completely, as evidenced by the cessation of mass increase. Decomposition times varied from 10 min to 120 min, and the oxygen concentration during decomposition was adjusted to between 0% and 4%.

Referring to Eq. (2) there are four constants that must be identified to complete the rate expression: A, E_a, α and β. As noted previously, experimental evaluation of reaction kinetics for the CuO–Cu_2O system is more challenging than for other gas–solid reactions due to the dependence of rate on oxygen driving force and the strong dependence of oxygen partial pressure on temperature. To account for this, several sets of experiments were performed to isolate each constant in the rate expression with the aim of minimizing secondary influences.

Experimental conditions used to determine the activation energy are summarized in Table 2. Generally speaking, the determination of activation energy for a given reaction is performed simply by varying the operating temperature for an experimental campaign while holding all other variables constant. The same is the case here; only, this time the influence of the partial pressure of oxygen driving force must be taken into consideration. At higher temperatures (above 900 °C) the equilibrium partial pressure of oxygen begins to increase rapidly with temperature. The higher the equilibrium partial pressure means the greater the driving force experienced by the sample. In order to mitigate this effect runs 1–5 were conducted where the total change in the driving force between these tests is less than 0.005 atm. While the total change in driving force seems rather small the difference between the driving force at 750 °C (Experiment #1) and 850 °C (Experiment #5) changes by about a factor of 10, which may be significant. Therefore, temperature plays two roles in the determination of reaction rates: first, it shows up in the exponential function as combined with the inherent activation energy; second, it affects the driving force, which is a function of temperature due to the equilibrium partial pressure of oxygen within that term. Thus, the determined apparent activation energy in this study reflects the combined effect of both traits. For the modeling of industrial-sized applications this approach may be more useful than an intrinsic activation energy as the effect of temperature is built into a single term. This may be utilized when the partial pressure of oxygen in the bulk surrounding the particles is near zero thereby simplifying the driving force term within the kinetic expression. However, when the partial pressure of oxygen is not zero this

Table 2
Experiments to determine the activation energy for the decomposition of CuO to Cu_2O.

Experiment number	Temperature (°C)	Equilibrium O_2 part. press. (atm)
1	750	0.0005
2	775	0.0010
3	800	0.0016
4	825	0.0029
5	850	0.0050
6	875	0.0085
7	900	0.0150
8	925	0.0250
9	950	0.0430

method is less accurate requiring the distinction of the multiple temperature effects (i.e. activation energy and equilibrium partial pressure of oxygen within the driving force term).

In large fluidized bed reactors where the particle bed may be several meters deep, oxygen released by the particles near the bottom of the bed may inhibit the decomposition of the particles higher in the bed. This phenomenon must be better understood in order to enable more accurate modeling of industrial-scale reactors. In order to determine the effect of oxygen partial pressure, a series of experiments was performed in which the temperature was held constant and the gas concentration was varied as shown in Table 3.

3. Results and discussion

For most of the results presented here, the reaction rate was reported at 50% conversion. The mass loss data between 20% and 80% conversion was fit to a polynomial expression using regression analysis in order to smooth the data and remove any noise associated. The regression curve represented the data very well with a typical coefficient of determination (R^2) value of 0.998. The reaction rates were calculated as follows:

$$r = -\frac{dm}{dt} \frac{1}{m_{Cu}} \tag{3}$$

where dm/dt represents the rate of mass change corresponding to oxygen loss and is normalized by the mass of copper (m_{Cu}) in the sample.

Fig. 2 displays the raw data obtained from the TGA during decomposition of the 50_TiO2_MM material at 900 °C. The decomposition of CuO is endothermic, which may be seen by the slight initial temperature decrease in Fig. 2. It was important for this work to maintain isothermal conditions in order to extract the kinetic constants. The small mass of sample used and the very shallow, nearly monolayer of sample in the sample pan, helped maintain isothermal conditions. As seen in Fig. 2 the observed temperature drop during decomposition was only about 0.25 °C. This small temperature difference does not affect the reaction rate at 50% conversion, since the furnace temperature controller had adjusted the sample temperature back to the target 900 °C by this point (Fig. 2).

In addition to maintaining isothermal conditions this work also sought to remain within the kinetically controlled regime and away from any mass transfer affects. Sahir et al. [18] investigated the applicability of the Law of Additive Reaction times describing the observed kinetics of reaction for CuO-based oxygen carriers. The Law of Additive Reaction Times weighs the influence of intrinsic kinetics, pore diffusion and bulk diffusion in describing the overall observed rate. They concluded that the Law was effectively applicable and described well the observed rates and conversion profiles at lower temperatures. They showed that while reactions of particles in the size range of 855–1000 μm were definitely influenced by mass transfer resistances that particles in the size range of 100–300 μm were well described without any influence from mass transfer up to 800 °C [20]. The particles used in this study were sieved to well below the 100 μm cutoff reported by Sahir

Table 3
Experiments to explicate influence of O$_2$ "driving force" on kinetics of CuO decomposition reaction.

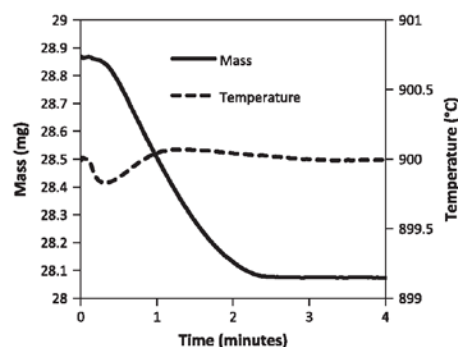| Experiment number	Temperature (°C)	Equilibrium O$_2$ part. press. (atm)	Supplied O$_2$ part. press. (atm)	O$_2$ "driving force" (atm)
1	950	0.045	0.00	0.045
2	950	0.045	0.020	0.025
3	950	0.045	0.034	0.011

Fig. 2. Raw TGA data during the decomposition of CuO in the 50_TiO2_MM material.

et al. as having no influence from mass transfer. Bulk diffusion concerns were further mitigated by using a near mono-layer of particles in a very low-profile pan.

3.1. Activation energy for CLOU decomposition

The degree of CuO decomposition versus time, measured in a pure N$_2$ atmosphere, is presented in Fig. 3. Clearly, as the temperature increases the time required for conversion decreases. The rates of decomposition for the four samples, measured at 50% conversion, are shown as a function of temperature in Fig. 4. The rates of the two materials compared favorably at each temperature, suggesting that one kinetic expression may be used for modeling rates in these types of copper-based oxygen carriers despite differences in substrates and preparation methods. Fig. 5 displays the Arrhenius plot for the decomposition of the titania- and zirconia-based materials. The apparent activation energy for the zirconia material (45_ZrO2_FG) is 264 kJ/mole while it is 284 kJ/mole for the titania-based material (50_TiO2_MM). As previously mentioned, using Mexican Petcoke as a fuel Sahir et al. [18] reported the observed activation energy of the zirconia material as 281 kJ/mole giving excellent correspondence to the value reported here.

These high activation energies represent both effects of temperature on the reaction rate (i.e. intrinsic activation energy and equilibrium partial pressure of oxygen). In order to effectively model the decomposition of CuO when the bulk partial pressure of oxygen is greater than zero the separation of these effects is required. In order to separate these effects the reaction rate was divided by the driving force and the resulting term was plotted against 1000/T to extract the corrected apparent activation energy of CuO decomposition for the zirconia- and titania- based materials. This will only be correct if the reaction order of the partial pressure of oxygen is equal to 1. The determination of the reaction order of the partial pressure of oxygen is given in Section 3.3. The resulting Arrhenius plot may be observed in Fig. 6. The corrected activation energies are 58 kJ/mole and 67 kJ/mole for the titania- and zirconia-based materials respectively. Sahir et. al. [18] reported that the corrected value was 20 kJ/mole.

3.2. Reaction order with respect to CuO

The order of the concentration of cupric oxide, α in reaction (2), was determined by analyzing the shape of the mass loss curve. Fig. 3 shows a plot of data representing the conversion versus time of the decomposition of CuO to Cu$_2$O for the 45_ZrO2_FG material. The straightness of the curves between 10% and 90% conversion
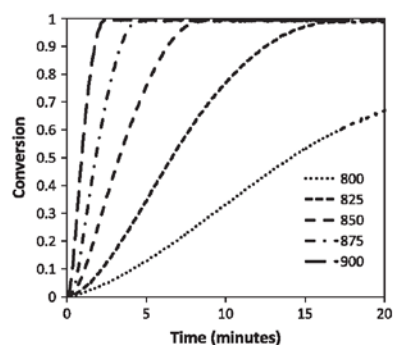
101

Fig. 3. Conversion versus time for the decomposition of CuO. Carrier: 50_TiO2_MM.
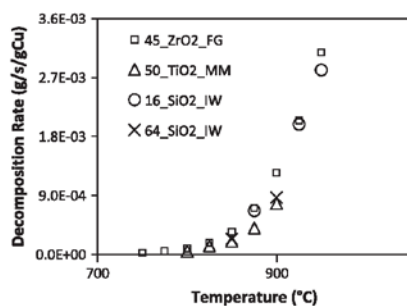

Fig. 4. Rates of decomposition of CuO under N_2 measured in the TGA using 50_TiO2_MM and 45_ZrO2_FG.
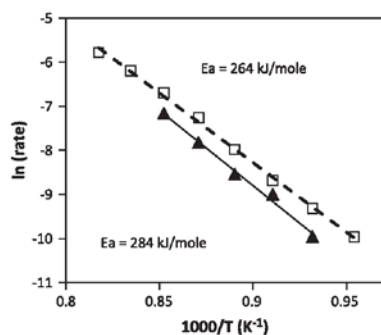

Fig. 5. Arrhenius plot for decomposition of CuO in 45_ZrO2_FG and 50_TiO2_MM. The apparent activation energies are calculated to be 257 kJ/mole and 284 kJ/mole for the zirconia and titania-supported materials, respectively.

Fig. 6. Arrhenius plot for the decomposition of 45_ZrO2_Fg and 50_TiO2_MM. This data attempts to separate the dual effect of temperature on the kinetic equation (i.e. influence on the activation energy and driving force) thereby generating the corrected activation energies for both materials.

Fig. 7. Conversion versus time for CuO decomposition of the 45_ZrO2_FG material under a nitrogen atmosphere at several temperatures.

(the range of interest for CLOU processes) indicates that the rate is independent of CuO concentration suggesting that the reaction is zero order in CuO. This can also be observed for the 45_ZrO2_FG material in Fig. 7, particularly at higher temperatures.

The reaction may be determined graphically to be either zero, first or second order in CuO by integrating the rate expressions and plotting the term for concentration of CuO of the integrated rate expression versus time and identifying if any yield a straight line. If the reaction were zero order in CuO concentration (represented by [CuO]), the rate of CuO consumption, $d[CuO]/dt$, would
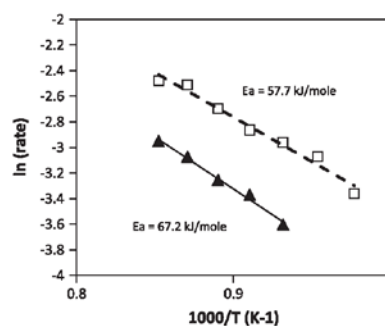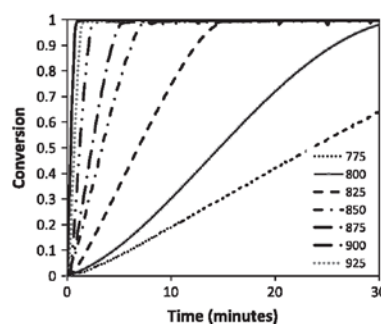
be constant, resulting in the following relation for [CuO] as a function of time:

$$[CuO] = Ct \tag{4}$$

where C represents a constant. Thus, if the reaction were zero order in CuO, a plot of [CuO] versus time would yield a straight line. Similarly, the rate expressions for first and second order in CuO concentration,

$$\frac{d[CuO]}{dt} = C[CuO] \tag{5}$$

and

$$\frac{d[CuO]}{dt} = C[CuO]^2 \tag{6}$$

respectively yield, upon rearrangement and integration,

$$\ln[CuO] = Ct \tag{7}$$

and

$$\frac{1}{[CuO]} = Ct \tag{8}$$

So a first order reaction would yield a straight line if ln[CuO] were plotted versus time, and a second order reaction would produce a straight line if 1/[CuO] were plotted versus time. In Figs. 8 and 9 the data is taken from the 800 °C and 900 °C tests and plotted

to determine reaction order. As can be seen in the plots, the reaction order in CuO concentration appears to be approximately zero.

The graphical approach in this case seems to fit very agreeably, yet it was still prudent to compare to both a numerical approach as well as compare the data to the other carrier material. The order of reaction with respect to the solid was fit to a plot of rate versus concentration of CuO and a regression analysis revealed α to be equal to zero with a coefficient of determination (R^2) of 0.97. Results obtained from analysis of the 50_TiO2_MM material (Fig. 9) also agree well. As with the zirconia-based material, the reaction appears to be zero order in CuO concentration.

3.3. Reaction order with respect to oxygen partial pressure

As noted previously, in industrial-scale fuel reactors where the bed material may be several feet deep, oxygen released from the particles may create an appreciable oxygen partial pressure either locally or in regions of little fuel. This in turn will reduce the driving force for decomposition, which may slow the decomposition rate. The tests outlined in Table 3 were used to isolate the influence the oxygen driving force has on the decomposition reaction and to determine the reaction order with respect to oxygen partial pressure. By holding the temperature constant and supplying a partial pressure of oxygen to the sample lower than the equilibrium partial pressure, decomposition still proceeds from CuO to Cu₂O. Using thermogravimetric analysis Wen et al. [21] verified the equilibrium partial pressure of oxygen versus temperature for CuO/Cu₂O in the range of 600 < T < 950 °C calculated by performing a Gibb's energy minimization. An exponential regression curve was fit to the equation reported by Wen et al. with a coefficient of determination (R^2) value of 0.999. The regression curve used in this work for the equilibrium partial pressure of oxygen was:

$$P_{O2}(atm) = 6.057 \times 10^{-11} e^{0.02146\,T} \tag{9}$$

where T is in units of degrees Celcius. Fig. 10 displays the decomposition of 45_ZrO2_FG as well as 50_TiO2_MM at 950 °C under 3 different oxygen partial pressure atmospheres (0 atm, 0.020 atm and 0.034 atm) in nitrogen. It is clear that as the supplied partial pres-
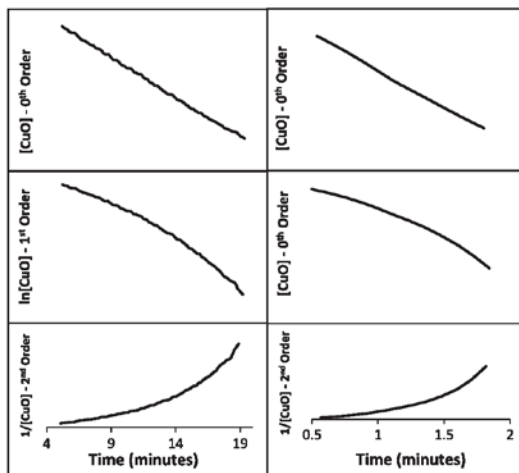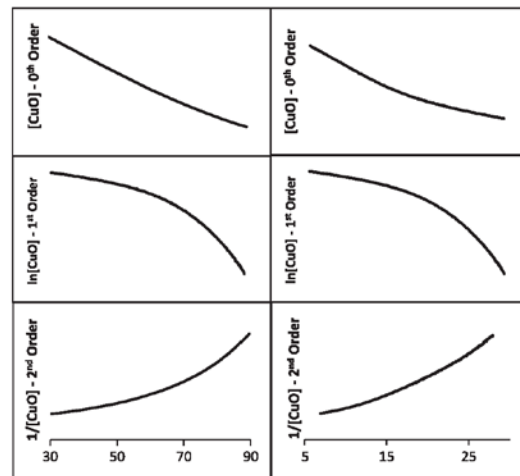

Fig. 9. Plots to determine the order of reaction with respect to the solid (CuO) the 50_TiO2_MM material. The trends suggest the reaction to be zero order in CuO concentrations. The left three figures are obtained at 800 °C while the right three figures are obtained at 900 °C.
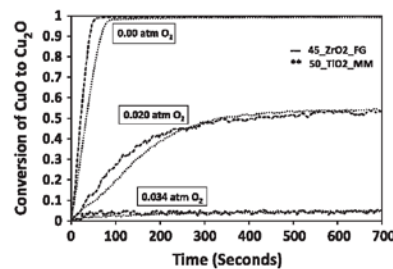
Fig. 10. Decomposition of CuO at 950 °C under 3 different supplied oxygen pressures (0.00, 0.020 and 0.034 atm) for both the zirconia- (–) and titania-supported (**) carriers.

sure of oxygen increases, thus reducing the thermodynamic driving force, both the reaction rate and extent of reaction decrease.

While the observed decrease in the reaction rate with decreased driving force was expected, the observed decrease in the extent of reaction was not. Additional testing was performed confirm this observation. Both the titania- and zirconia-based materials were subjected to an atmosphere of 0.03 atm of oxygen at 950 °C. Upon reaction completion (identified by cessation of mass loss) the oxygen partial pressure was decreased to 0.01 atm, thus increasing the driving force, and the sample was once again allowed to react to completion. After reaction ceased at this O₂ partial pressure, pure nitrogen was fed to the reactor. Fig. 10 displays the mass versus time data for these experiments. It may be understood from Fig. 10 that the increase in oxygen partial pressure at levels less than the equilibrium pressure, inhibits the decomposition extent of CuO. It is unclear why this occurs, but a similar effect may have been shown by Wen et al. They reported the decomposition of CuO at set partial pressures of oxygen and recorded mass versus time data while the temperature was increased. They show that for each subsequent increase in oxygen partial pressure supplied that an increase in temperature was needed for full decomposition [21].

Fig. 8. Plots to determine the order of reaction with respect to the solid (CuO) the 45_ZrO2_FG material. The trends suggest the reaction to be zero order in CuO concentrations. The left three figures are obtained at 800 °C while the right three figures are obtained at 900 °C.

Due to the reduced extent of reaction, using the rate of reaction at 50% conversion of the material at each of the different supplied oxygen partial pressures was impossible; therefore, the reaction rate was extracted from a portion of the curve where the reaction appears to be progressing most quickly from the data obtained under 0.020 atm of oxygen. The order of reaction with respect to oxygen driving force was calculated to be 1.01 for 45_ZrO2_FG material. A similar analysis of the 50_TiO2_MM material resulted in an identical reaction order of 1.0. The reaction therefore appears to be first order in $(P_{O2,eq} - P_{O2})$.

3.4. Preexponential factor

After the other values had been determined the preexponential constant A (frequency factor) was calculated. For the corrected activation energies it was determined to be 4.15×10^{-4} and 3.64×10^{-4} for the titania and zirconia materials respectively. It was then determined that 3.90×10^{-4} gave the best fit to both sets of data. In order to verify the method of obtaining the corrected activation energies the preexponential constant for the apparent activation energies were also obtain as 2.09×10^{9} for the titania material and 9.53×10^{8} for the zirconia material while the value used in modeling was 1.52×10^{9}.

3.5. Model testing

The constants of the kinetic expressions for the two carriers are summarized in Table 4. The resulting rate expression for decomposition of CuO was determined by selecting values near the average of obtained from the results of the titania- and zirconia-based materials that best fit both sets of data.

Decomposition rates for the two materials were slightly different. Average values of the two materials were used to form a general rate expression, which predicts the mass release rate of oxygen, per mass of copper (Cu) in the carrier, as a function of temperature and oxygen partial pressure:

$$\text{rate}\left(\frac{g}{s}\frac{1}{g_{Cu}}\right) = 3.90 \times 10^{-4} \exp\left(-\frac{62,000}{R \times T}\right)[P_{O2,eq} - P_{O2}] \quad (10)$$

where T is in units of Kelvin and pressure is in units of atmospheres.

The temperature dependency of $P_{O2,eq}$ modeled by Eq. (4) can be incorporated into this model to present an expression for rate solely as a function of temperature and surrounding O_2 partial pressure:

$$\text{rate}\left(\frac{g}{s}\frac{1}{g_{Cu}}\right) = 3.90 \times 10^{-4} \exp\left(-\frac{62,000}{R \times T}\right)[6.057$$
$$\times 10^{-11} \exp^{0.02146 \times (T-273)} - P_{O2}] \quad (11)$$

Fig. 11 compares the model presented in Eq. (6) with rates obtained from experimental data from the titania- and zirconia-supported oxygen carriers tested over the temperature range

Table 4
Constants for kinetic rate expression.

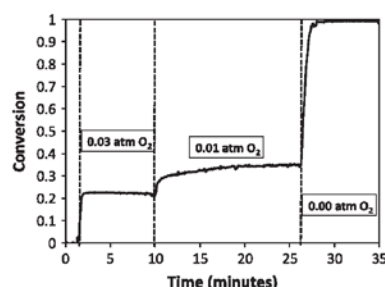| Parameter	50_TiO2_MM	45_ZrO2_FG	Value in rate expression
Activation energy, E_a (kJ/mole)	67	58	62
Frequency factor, A ($atm^{-1} \times s^{-1}$)	4.15×10^{-4}	3.64×10^{-4}	3.90×10^{-4}
Order of P_{O2}, α (atm)	1.0	1.0	1.0
Order of C_{CuO}, β (–)	0	0	0

Fig. 11. Decomposition of 45_ZrO2_FG at 950 °C under 3 different O2 atmospheres (0%, 1% and 3% oxygen).
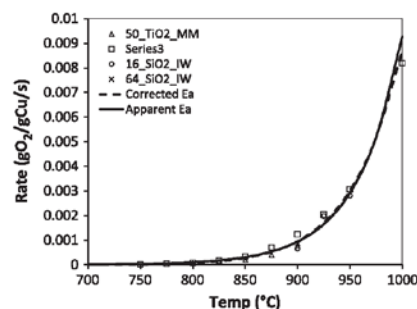

Fig. 12. Plot of reaction rate versus temperature for 4 different CuO-based oxygen carriers in TGA at 4 different temperatures along with the rates predicted by the determined rate expression (□ 45_ZrO2_FG, △ 50_TiO2_MM, ○ 16_SiO2_IW and × 64_SiO2_IW, – kinetic models).

800–950 °C. It also compares models derived using the two different activation energies.

For the apparent activation energies the driving force term is incorporated within the activation energy itself and therefore is not expressed in the kinetic equation (Eq. (7)). Use of this equation must be limited to where the partial pressure of oxygen in the bulk is near zero.

$$\text{rate}\left(\frac{g}{s}\frac{1}{g_{Cu}}\right) = 3.90 \times 10^{-4} \exp\left(-\frac{274,000}{R \times T}\right) \quad (12)$$

For comparison, the rates obtained from decomposition data from two silica-supported carriers containing 16 and 64 wt% CuO
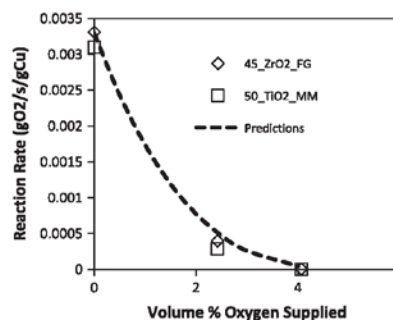

Fig. 13. The rates of decomposition of two oxygen carriers are given with the model predictions as a function of volume% of oxygen supplied during decomposition at 950 °C.

are included in Fig. 12. As seen from the line showing the model, rate expression in Eq. (5) also matches those carriers well. By observing the results shown in Fig. 12 it may be seen that the model reasonably predicts the rates of all 4 carriers especially in the range between 900 and 950 °C. This range of temperature is likely to be the temperature range of a copper-based CLOU system when considering reaction rates, equilibrium influence driving force as well as physical stability of the material (agglomeration resistance). Both the model using the corrected activation energy and model using the apparent activation energy predict well the behavior of the decomposition rates of CuO in inert atmospheres. It is believed that only Eq. (6) will accurately represent the decomposition of CuO in an atmosphere where the partial pressure of oxygen is greater than zero but less than the equilibrium partial pressure. Fig. 13 gives the reaction rates of the zirconia and titania supported materials under different oxygen partial pressure conditions. The model reasonably predicts the rates of decomposition of these two materials.

4. Conclusions

The decomposition rates of two copper-based oxygen carrier materials were determined experimentally using a TGA, and the resulting data was used to develop a kinetic expression to estimate the rate of oxygen release as a function of temperature, conversion and oxygen partial pressure. The analysis indicated that the rate is essentially independent of CuO concentration (i.e. zero order). The decomposition rate decreases when oxygen is present in the surrounding gas due to a decrease in thermodynamic driving force, defined as the difference between the equilibrium oxygen partial pressure at a given temperature and the gas O_2 partial pressure. The developed kinetic equation was then used to model the reaction of four copper-based oxygen carriers. The four samples differ in loading of CuO, support material, preparation method and location of production. With these differences between the carrier materials it may be reasonably expected that the decomposition rate for each of them would vary somewhat as well. When normalized to copper content, some variability between the rates and conversion profiles of the samples was observed, but the proposed rate expression reasonably predicts behavior for all four carriers under a variety of conditions. This suggests that it may be possible to extend the developed equation to the modeling of any copper-based oxygen carrier.

The developed kinetic expression was designed for use in industrial applications by focusing on the conversion interval from 20% to 80% of the solid carrier. The observed activation energy is the result of two effects caused by temperature, the direct influence of temperature on reaction rate according to the Arrhenius expression as well as an indirect affect where temperature changes affect the driving force by affecting the equilibrium partial pressure of oxygen. The separation of these two effects is necessary for the correct prediction of CuO decomposition within the fuel reactor of a CLOU unit.

Acknowledgements

References

[1] Ekström C, Schwendig F, Biede O, Franco F, Haupt G, De Koeijer G, et al. Techno-economic evaluations and benchmarking of pre-combustion CO_2 capture and oxy-fuel processes developed in the European ENCAP project. Energy Proc 2009;1(1):4233–40.
[2] Marion J, Mohn N, Liljedahl GN, Nsakala N, Morin J-X, Henriksen P. Technology options for controlling CO_2 emissions from fossil-fuelled power plants. In: Third annual conference on carbon capture and sequestration, 3–6 May 2004, Alexandria, VA; 2004.
[3] Lyngfelt A, Leckner B, Mattisson T. A fluidized-bed combustion process with inherent CO_2 separation: application of chemical looping combustion. Chem Eng Sci 2001;56:3101–13.
[4] Mattisson T, Lyngfelt A, Leion H. Chemical-looping with oxygen uncoupling for combustion of solid fuels. Int J Greenh Gas Con 2009;3:11–9.
[5] Garcia-Labiano F, de Diego LF, Adanez J, Abad A, Gayan P. Reduction and oxidation kinetics of a copper-based oxygen carrier prepared by impregnation for chemical-looping combustion. Ind Eng Chem Res 2004;43(26):8168–77.
[6] De Diego LF, Garcia-Labiano F, Gayan P, Celaya J, Palacios JM, Adanez J. Operation of a 10 kW$_{th}$ chemical-looping combustor during 200 h with a CuO–Al_2O_3 oxygen carrier. Fuel 2008;86:1036–45.
[7] Lewis WK, Gilliland ER. Production of pure carbon dioxide. U.S. Patent Nos. 2,665,971 and 2,665,972; 1954.
[8] Chuang S, Dennis JS, Hayhurst AN, Scott SA. Development and performance of Cu-based oxygen carriers for chemical-looping combustion. Combust Flame 2008;154:109–21.
[9] Lyngfelt A, Johansson M, Mattisson T. Chemical-looping combustion – status of development. In: 9th International conference on circulating fluidized beds, May 13–16, Hamburg, Germany; 2008.
[10] Leion H. Capture of CO_2 from solid fuels using chemical-looping combustion and chemical-looping with oxygen uncoupling. Dissertation. Chalmers University of Technology, Goteburg, Sweden; 2008.
[11] Abad A, Mattisson T, Lyngfelt A, Ryden M. Chemical-looping combustion in a 300 W continuously operating reactor system using a manganese-based oxygen carrier. Fuel 2006;85:1174–85.
[12] Chuang S, Dennis J, Hayhurst A, Scott S. Kinetics of the oxidation of a co-precipitated mixture of Cu and Al_2O_3 by O_2 for chemical-looping combustion. Energy Fuel 2010;24:3917–27.
[13] Adánez-Rubio I, Abad A, Gayán P, de Diego L, García-Labiano F, Adánez J. Identification of operational regions in the chemical-looping with oxygen uncoupling (CLOU) process with a Cu-based oxygen carrier. Fuel 2012.
[14] Gayan P, Adánez-Rubio I, Abad A, de Diego LF, García-Labiano F, Adánez J. Development of Cu-based oxygen carriers for chemical-looping with oxygen uncoupling (CLOU) process. Fuel 2012;96:226–38.
[15] Eyring EM, Konya G, Lighty JS, Sahir AH, Sarofim AF, Whitty K. Chemical looping with copper oxide as carrier and coal as fuel. Oil Gas Sci Tech 2010. 10.2516/ogst/2010028.
[16] Brandt B, Gruene P, Rosowski F, Farrauto RJ, Castaldi MJ. Oxygen uptake and release kinetics of Cu/Cu_2O/CuO on Al_2O_3 and ZrO_2–SiO_2 as materials for chemical looping combustion. In: AlChE annual meeting, 16–21 October 2011, Minneapolis, MN, USA; 2011.
[17] Adánez-Rubio I, Gayán P, Abad A, de Diego LF, García-Labíano F, Adánez J. Evaluation of a spray-dried CuO/$MgAl_2O_4$ oxygen carrier for the chemical looping with oxygen uncoupling process. Energy Fuel 2012;26:3069–81.
[18] Sahir AH, Sohn HY, Leion H, Lighty JS. Rate analysis of chemical-looping with oxygen uncoupling (CLOU) for solid fuels. Energy Fuel 2012;26:4395–404.
[19] Johansson M, Mattisson T, Lyngfelt A. Investigation of Mn_2O_4 with Stabilized ZrO_2 for chemical-looping combustion. Chem Eng Res Des 2006;84(A9):807–18.
[20] Sahir AH, Lighty JS, Sohn HY. Kinetics of copper oxidation in the air reactor of a chemical looping combustion system using the law of additive reaction times. Ind Eng Chem Res 2011;50(23):13330–9.
[21] Wen YY, Li ZS, Xu L, Cai NS. Experimental study of natural Cu ore particles as oxygen carriers in chemical looping with oxygen uncoupling (CLOU). Energy Fuel 2012;26(6):3919–27.

APPENDIX B

OXIDATION KINETICS OF CU$_2$O IN OXYGEN

CARRIERS FOR CHEMICAL LOOPING

WITH OXYGEN UNCOUPLING

Oxidation Kinetics of Cu$_2$O in Oxygen Carriers for Chemical Looping with Oxygen Uncoupling

Christopher K. Clayton,*[,†] H. Y. Sohn,[‡] and Kevin J. Whitty[†]

[†]Department of Chemical Engineering, The University of Utah, 50 S. Central Campus Drive, Room 3290, Salt Lake City, Utah 84112, United States

[‡]Department of Metallurgical Engineering and of Chemical Engineering, The University of Utah, 135 S. 1460 E., Room 412, Salt Lake City, Utah 84112, United States

ABSTRACT: Chemical looping with oxygen uncoupling (CLOU) is a promising CO$_2$-capture ready energy technology that employs oxygen carriers with thermodynamic properties that cause oxygen to be spontaneously liberated as gaseous O$_2$ in the fuel reactor, where it can react directly with solid fuels. One of the promising CLOU carrier materials is copper oxide, cycling between CuO and Cu$_2$O. Experimentally determined rate expressions for these reactions are needed for proper development, modeling, and scale-up of CLOU technology. The evaluation of rates for this system is not straightforward, however, since the equilibrium partial pressure of oxygen is appreciable and varies significantly in the temperature range of interest. This in turn affects the driving force for oxidation, and also affects rates of reduction. The study presented here aims to better understand the oxidation conversion characteristics, to decouple the influence of temperature and driving force for a range of carrier materials, and to offer suitable rate expressions. It is concluded that the well-documented decrease in oxidation rate at higher temperatures cannot be explained solely by the decrease in driving force, but that physical development of copper boundaries likely plays a more significant role at high temperatures.

1. INTRODUCTION

Chemical looping combustion (CLC) is a promising technology enabling CO$_2$-capture ready processing of carbonaceous fuels for energy production, and has been recognized as having potentially lower energy demand and offering a lower cost of electricity than oxy-fuel combustion, IGCC, and flue gas CO$_2$ removal by amine scrubbing.[1] CLC utilizes the redox behavior of certain materials, in particular metal oxides, to scavenge oxygen in an air reactor and deliver that oxygen as a metal oxide into a second reactor where a fuel is also present. By this inherent in situ separation of oxygen, the flue gas from the fuel reactor contains no nitrogen, but primarily CO$_2$ and H$_2$O, which is easily condensed producing a nearly pure CO$_2$ stream[2−4] suitable for sequestration with little additional processing.

Chemical looping with oxygen uncoupling (CLOU), a variant of chemical looping combustion (CLC) technology, involves the use of specific metal−metal oxide complexes to spontaneously release ("uncouple") oxygen as gaseous O$_2$ in the fuel reactor. This is possible because the equilibrium behavior of the carrier oxidation/reduction reaction is such that gaseous O$_2$ is favored at high temperature, low-O$_2$ conditions such as those existing in the fuel reactor of a CLC system. In the air reactor, the high O$_2$ partial pressure favors the fully oxidized metal. The advantage of CLOU carriers over conventional CLC carriers is that the released oxygen can react directly with solid fuel or char, thereby avoiding the need to convert the solid to gas through relatively slow gasification reactions.

Only a few metal complexes that exhibit this CLOU behavior in the range of chemical looping combustion temperatures have been identified.[5] Copper oxide is attractive because of its fast

reaction rates, and it is thermodynamically favored to completely convert gaseous hydrocarbons to CO$_2$ and H$_2$O.[6] In addition, copper oxide looping is overall exothermic in both the air reactor and fuel reactor since the heat required to reduce the carrier and liberate oxygen is less than the heat produced during combustion of the fuel. This simplifies thermal integration of a full scale CLC system. Where other materials are exothermic in the air reactor, many still require heat input to the fuel reactor since the heat required to reduce the carrier exceeds that given off by the fuel as it combusts.

When used as a CLOU carrier, copper cycles between the Cu^{1+} cuprous (Cu$_2$O) and Cu^{2+} cupric (CuO) states:

$$2Cu_2O + O_2 \leftrightarrow 4CuO \qquad (1)$$

The equilibrium curve for this reaction is shown in Figure 1. At temperatures above approximately 800 °C, in otherwise low-O$_2$ environments (such as the fuel reactor of a chemical looping system), the left side of the above reaction is favored, generating O$_2$. If the O$_2$ continues to be consumed (e.g., by reaction with fuel), the CuO decomposition reaction will continue to progress. The efficient use of the Cu$_2$O−CuO system to generate oxygen, which then reacts with a carbonaceous fuel to produce carbon dioxide was first recognized by Lewis and Gilliland in 1954.[7] Application to CLC was first demonstrated by Mattisson et al.,[8] who showed that the release of oxygen allows conversion of petcoke by CLOU to be as much as 50 times faster than conversion by
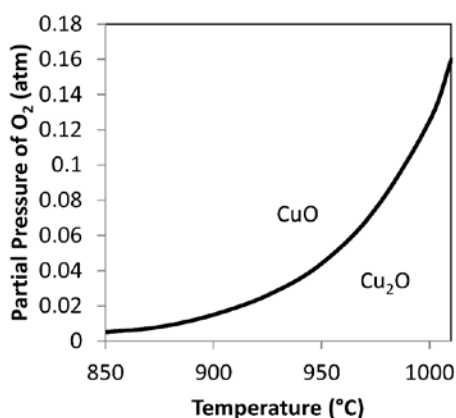
Figure 1. Equilibrium partial pressure of oxygen over the CuO/Cu$_2$O redox pair.

conventional CLC with an iron-based carrier, which requires in situ conversion of petcoke to syngas by relatively slow gasification reactions. Several groups have since continued in the investigation of CLOU using either Co, Mn, or Cu-based carriers in their studies, ultimately concluding that Mn and Cu are promising choices for the CLOU carrier base material.[9−14]

For proper design and modeling of chemical looping systems, it is valuable to understand the intrinsic chemical kinetics of both the forward (oxidation) and reverse (reduction) reactions shown in reaction 1. Ideally, it would be useful to develop general rate expressions applicable across a broad range of conditions, for example, of the form below for cuprous oxide oxidation:

$$\text{rate} = A \exp(-E_a/RT) f[Cu_2O][P_{O_2}^\beta - P_{O_2,eq}^\beta] \qquad (2)$$

where A is a pre-exponential factor, E_a is the activation energy, β is a reaction order. $P_{O_2,eq}$ represents the equilibrium partial pressure of oxygen and is dependent on temperature, and P_{O_2} is the actual partial pressure of oxygen. The exponents, β, on the two partial pressure terms contained within the driving force expression must be equal to each other, constrained by the equilibrium relation obtained from the correctly balanced form of eq 1, as explained below:

$$K = \frac{a_{CuO}^4}{a_{Cu_2O}^2 \times a_{O_2}} \qquad (3)$$

where a_i represents the activity of the individual species. Because CuO and Cu$_2$O are pure solids the activity may be assumed to be 1 and the activity of O$_2$ is more correctly expressed as the fugacity of oxygen which, using units of atm, is equal to the partial pressure of oxygen. Therefore the equilibrium relation is simplified to

$$K = \frac{1}{p_{O_2}} \qquad (4)$$

Owing to the fact that eq 4 is the definition of the equilibrium constant, K, it may be noted that at equilibrium $p_{O_2} = p_{O_2,eq}$. For this to be mathematically consistent, the exponents must be equal.

The challenge lies in experimentally determining these constants. Equation 2 can be more easily manipulated in a more general form, as shown in eq 5 where the rate equation is displayed as a combination of functions separating each of the dependent variables into a distinct function such that $f(T)$ represents the effect of temperature, $f(X)$ represents the effect of the solid conversion over time, and $f(P_{O_2})$ which represents the role of the driving force.

$$\text{rate} = f(T) f(X) f(P_{O_2}) \qquad (5)$$

Interestingly, the thermodynamic behavior shown in Figure 1 affects the rate of the carrier oxidation and decomposition (uncoupling) reactions. It is well understood that rates of reversible reactions such as reaction 1 are affected by the difference between the actual and equilibrium concentrations of the reacting species. This has also been observed to occur with copper-based oxygen carriers operating in the CLOU regime,[15] which makes identification of intrinsic kinetics of the respective oxidation and reduction reactions challenging. For example, several groups studying CLOU have reported a decrease in the rate of oxidation by air at higher temperatures,[10,12,16,17] which is due at least in part to a decrease in the difference between the equilibrium O$_2$ partial pressure and air's partial pressure of 0.21 atm (at sea level). Similarly, in certain types of experiments the rate of O$_2$ release by cupric oxide reduction is affected by that released O$_2$.

It has been reported that the oxidation rate of Cu$_2$O does not increase continually with temperature, but increases to a maximum around 800 °C and then begins to slow down resulting in an apparent negative activation energy.[12−14] Several mechanisms have been suggested to explain this behavior, including (1) a reduced driving force caused by the increased equilibrium partial pressure of oxygen with temperature, (2) sintering of grain boundaries, and (3) decreased grain boundary diffusion caused by the increased molar volume of CuO as compared to that of the reduced state of Cu$_2$O.[12,18,19]

The objective of this study is to develop kinetic expressions aimed at better describing the observed oxidation profiles of cuprous oxide-based oxygen carriers.

2. EXPERIMENTAL SECTION

To gain a better understanding of the mechanisms involved in the oxidation of Cu$_2$O and to compare carriers under a variety of conditions, several complementary experiments and oxygen carriers were studied. This study bases the developed kinetic expression on results obtained from the experimental study of two different oxygen carriers. The results of the comparison between measured and predicted rates are also presented.

2.1. Experimental System. A TA Instruments TGA Q500 with a maximum operating temperature of 1000 °C was used for this study. Samples ranging from 10 to 50 mg were loaded into small sample pans made of platinum or quartz. To maximize gas−solid contact and minimize mass transfer effects, small diameter particles (<45 μm) and a shallow layer of particles (nearly a monolayer in the bottom of the pan) were used. Approximately 100 mL/min of either air or nitrogen was fed into the TGA and the progression of mass gain or loss was analyzed to determine rates of Cu$_2$O oxidation and CuO reduction, respectively.

2.2. Samples. Two very different CuO-based carriers, prepared by different methods, were evaluated. Properties of these carriers are presented in Table 1. The MgO-stabilized

Table 1. Copper-Based Carriers Used in This Study

carrier	source	preparation method	CuO loading (wt %)	size range (μm)
50-TiO2-MM	ICPC, Poland	mechanical mixing	50	37–45
45_ZrO2_FG	Chalmers, Sweden	freeze granulation	45	37–45

ZrO_2 material was reported to be very stable while maintaining physical strength and high chemical reactivity. Johansson et al. reported that an inverse relationship exists between support strength and reactivity and that, when compared to other supports, the ZrO_2/MgO compound exhibited the best combination of reactivity and strength on a Mn-based carrier.[20] They discussed that as the physical strength increased a decrease in the surface area and porosity was also observed; thereby decreasing the reactivity of the material. The extension to a copper-based oxygen carrier was made assuming similar performance characteristics of the ZrO_2/MgO substrate. To evaluate the extension to the Cu-based carrier a titania-supported material was also tested. The developed kinetic expression for the oxidation of supported Cu_2O was determined based on the experimentally obtained results of the zirconia and titania materials.

2.3. Experimental Analysis and Procedures. The experiments were conducted between 600 and 1000 °C. Flow in the TGA was approximately 0.1 SLPM into a reaction chamber with an approximate ID of 1.25 cm.

Experiments were designed specifically to determine kinetic parameters for oxidation of cuprous oxide. The oxidation cycle times were set to between 10 and 120 min. Oxygen concentrations were varied from about 1% to 21% O_2.

Referring to eq 2 there are three constants that must be identified to complete the rate expression: A, E_a, and β. Several sets of experiments were performed to determine each of these constants.

The activation energy (E_a) was first determined using moderate temperature oxidation to avoid any influence of the decreasing oxygen driving force on the rate at higher temperatures. The experiments used to determine the low temperature activation energy are summarized in Table 2. To

Table 2. Experiments to Determine the Activation Energy for the Oxidation of Cu_2O to CuO at Low Temperatures

expt no.	temp (°C)	equilibrium O_2 partial pressure (atm)	supplied O_2 partial pressure (atm)	O_2 "driving force" (atm)
1	600	<0.01	0.21	0.21
2	625	<0.01	0.21	0.21
3	650	<0.01	0.21	0.21
4	675	<0.01	0.21	0.21
5	700	<0.01	0.21	0.21

determine the effect of oxygen partial pressure, a series of experiments was performed in which the temperature was held constant and the gas concentration was varied as shown in Table 3. Similarly, to focus solely on the effect of temperature at elevated levels, a series of experiments was performed in which the partial pressure "driving force" (difference between oxygen partial pressure and equilibrium partial pressure) was held constant while temperature was varied, as shown in Table 4.

Table 3. Experiments to Explicate Influence of O_2 "Driving Force" on Kinetics of Cu_2O Oxidation Reaction

expt no.	temp (°C)	equilibrium O_2 partial pressure (atm)	supplied O_2 partial pressure (atm)	$f(P_{O_2})$
1	825	0.005	0.0286	0.0236
2	825	0.005	0.0232	0.018
3	825	0.005	0.0089	0.004

Table 4. Experiments to Explicate Influence of Temperature on Kinetics of Cu_2O Oxidation Reaction at Elevated Temperatures by Maintaining a Constant Partial Pressure Driving Force

expt no.	temp (°C)	equilibrium O_2 partial pressure (atm)	supplied O_2 partial pressure (atm)	$f(P_{O_2})$
1	785	0.0412	0.0012	0.040
2	855	0.0446	0.0056	0.040
3	885	0.051	0.011	0.040
4	923	0.064	0.024	0.040
5	976	0.116	0.076	0.040

3. RESULTS AND DISCUSSION

Evaluation of the oxidation experiments and determination of the rate expressions are described below. The rate of oxidation
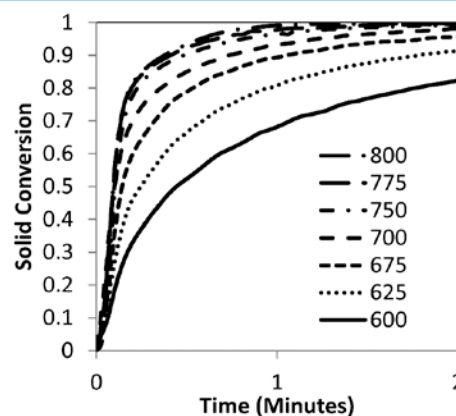
Figure 2. Oxidation of 50_TiO2_MM material at various temperatures under air inside TGA.

was calculated from the mass change data obtained from the TGA using the following:

$$\text{rate} = \frac{dm}{dt} \frac{1}{m_{Cu}} \tag{6}$$

where m is the total mass of the sample at time (t) as measured by the TGA and m_{cu} is the mass of copper in the sample.

3.1. Selection of Applicable Models. The selection of the correct kinetic model is critical to obtain a clear understanding of the mechanisms responsible for observed kinetic behaviors. A general rate expression as given by eq 2 is simple and easily understood, so the generalized rate expression is often used, and the applicable parameters are fit to the observed data.

In the case of Cu_2O oxidation, however, this simple model does not adequately explain nor capture the mechanisms responsible for the observed kinetics. Figure 2 shows the conversion of 50_TiO2_MM from Cu_2O to CuO under air at
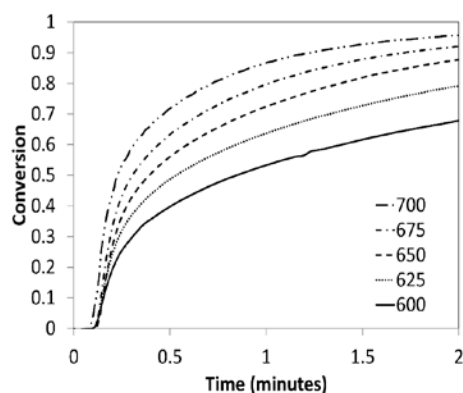
Figure 3. Oxidation of 45_ZrO2_FG in TGA using air at several temperatures.
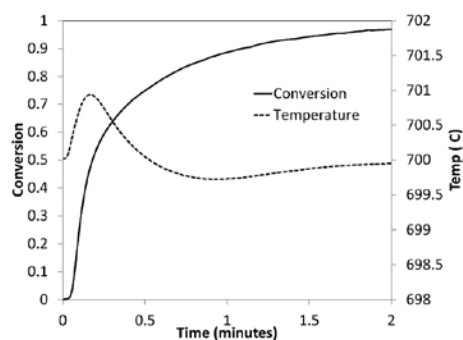

Figure 4. Oxidation of 45_ZrO2_FG in TGA at 700 °C in air. Figure shows a 1 °C change in temperature during the reaction.
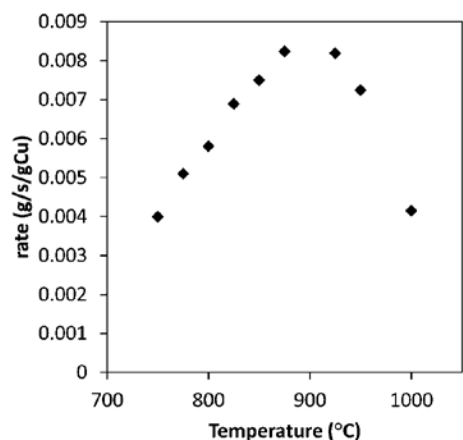

Figure 5. Oxidation rate extracted at 50% conversion for the 45_ZrO2_FG material at temperatures from 750 to 1000 °C.

Figure 6. Conversion profile for the 45_ZrO2_FG material under three different supplied oxygen volume percentages.
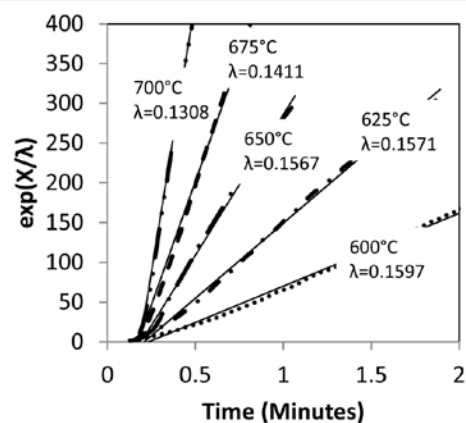
Figure 7. Pore-blocking kinetics for the low temperature oxidation of Cu_2O in 50_TiO2_MM.
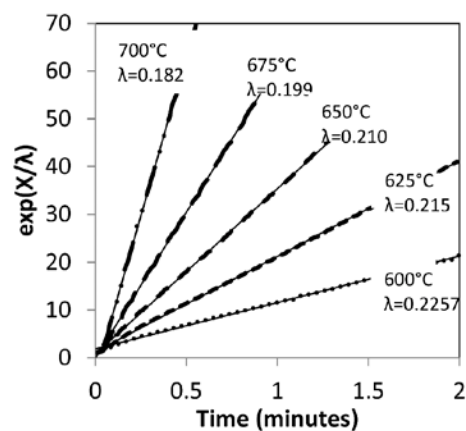
Figure 8. Pore-blocking kinetics for the low temperature oxidation of Cu_2O in 45_ZrO2_FG.

several temperatures between 600 and 800 °C using a thermogravimetric analyzer (TGA). It may be seen in the figure that the traces at the lower temperatures have a dramatic shift in reaction rate long before nearing full conversion. Sohn and Kim[27] suggest that this dramatic change prior to nearing full conversion is indicative of a pore-blocking mechanism
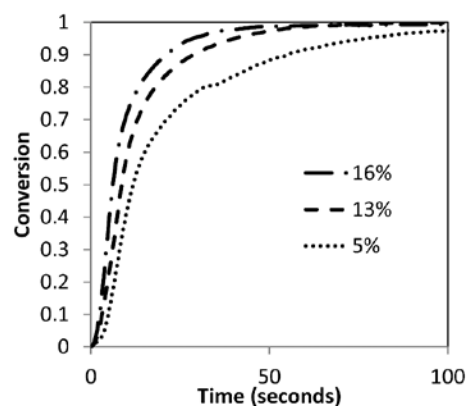
controlling the reaction rate. However, at the higher temperatures (above 700 °C) the conversion profiles reach over 80% conversion prior to the change in reaction rate. This

Figure 9. Arrhenius plot with the associated apparent activation energies of the logarithmic rate laws describing the low-temperature oxidation of Cu_2O in the 50_TiO2_MM ($\square$) and 45_ZrO2_FG ($\diamond$) materials.

Figure 10. Plot of observed and predicted profiles using the pore-blocking kinetic rate expression for the 45_ZrO2_FG material at three different temperatures.
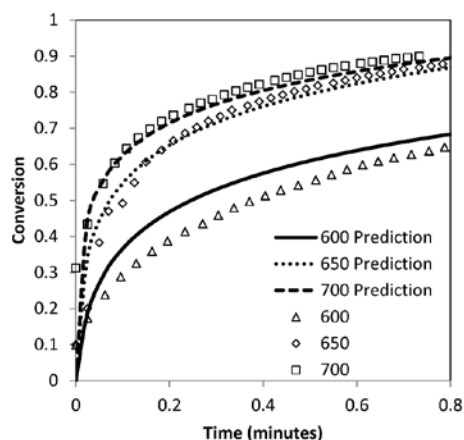
phenomenon is more easily seen in Figure 3 where the conversion profile of the zirconia material is given.

Oxidation of the carrier at the higher temperatures is therefore unlikely controlled by a pore-blocking mechanism because the reaction nears complete conversion before the effects of pore-blocking are observed. This regime, then, must be described by another mechanism. Commonly, for the redox reactions of metals the Avrami−Erofeev equation is used describing nucleation and growth kinetics.[21,22] This approach will be used to model the rates obtained at temperatures above 700 °C, while the pore-blocking model will be utilized for the lower temperature rates (temperatures below 750 °C).

3.2. Oxidation Rates. The rate of reaction was determined from eq 6. Because of the uncertainty of the initial rate data resulting from rapid reaction rates as well as a slight temperature increase resulting from the exothermic nature of copper oxidation, the initial rates were not used to determine coefficients in the kinetic expression. Instead, the rates were extracted at 50% of total theoretical conversion of the carrier from Cu_2O to CuO. The weight percent increase from Cu_2O to CuO is 10%, which must then be adjusted to reflect the specific weight loading of CuO in each of the different materials.

For this work two important assumptions were made: first, that mass transfer effects due to diffusion from the bulk gas to the particle surface as well as intraparticle gas diffusion may be neglected, and second, the temperature of the tested samples remains isothermal through the duration of the reaction cycle.
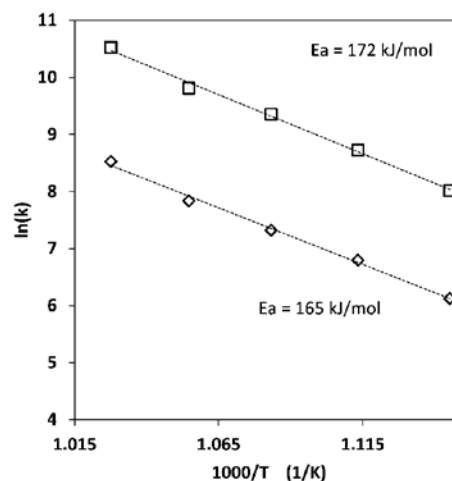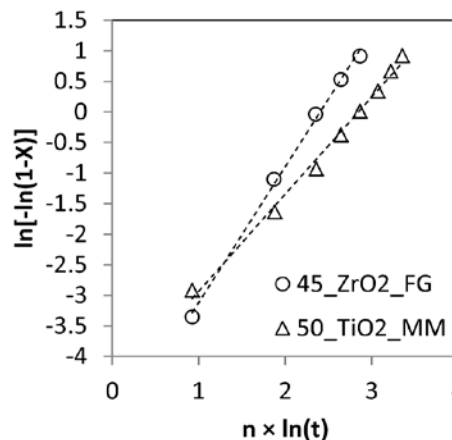

Figure 11. Nucleation and growth kinetics for the oxidation of Cu_2O in the 45_ZrO2_FG and 50_TiO2_MM materials at 925 °C. The best fit was found at $n = 1$.

The assumption that temperature during oxidation remains isothermal is perhaps questionable, since heat released during oxidation of these carriers is enough to increase the temperature by more than 500 °C. However, the relatively high gas flow rate, small sample size, and shallow layer in the

Table 5. Results Obtained from Modeling of Low Temperature Oxidation of Two CLOU Materials

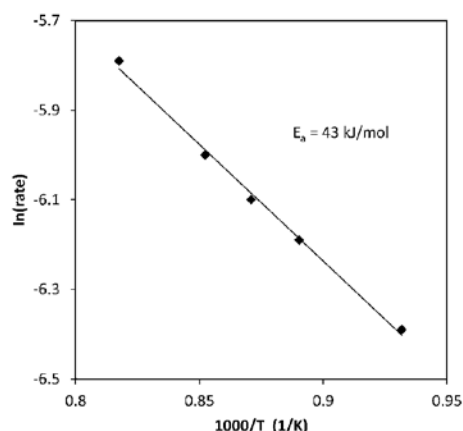| influence	50_TiO2_MM (T °C)	45_ZrO2_FG (T °C)	average values (T °C)
$f(X)$: $1/\exp\left(\dfrac{X}{\lambda}\right)$; λ	$-2.95 \times 10^{-4}T + 0.34$	$-4.16 \times 10^{-4}T + 0.48$	$-3.55 \times 10^{-4}T + 0.41$
$f(p_{O_2})$: $(p_{O_2}^{\beta} - p_{O_2,eq}^{\beta})$	$\beta = 1.3$	$\beta = 1.3$	$\beta = 1.3$
$p_{O_2,eq}^{\beta}$		$p_{O_2}(\text{atm}) = 6.057 \times 10^{-11}\, e^{0.02146T(°C)}$	
$f(T) = A \times \exp\left(-\dfrac{E_a}{RT}\right)$	$A = 6.2 \times 10^{-13}$ (g/s·atm$^{1.3}$); $E_a = 172$ (kJ/mol)	$A = 3.4 \times 10^{-12}$ (g/s·atm$^{1.3}$); $E_a = 165$ (kJ/mol)	$A = 2.0 \times 10^{-12}$ (g/s·atm$^{1.3}$); $E_a = 168$ (kJ/mol)

Figure 12. Arrhenius plot of results obtained during the oxidation of 45_ZrO2_FG in TGA under constant driving force conditions. The calculated apparent activation energy is 43 kJ/mol.
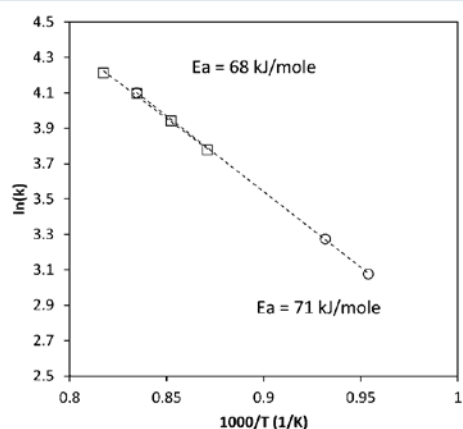

Figure 13. Activation energy for the high temperature oxidation of Cu$_2$O using the zirconia (□) and titania (○) based oxygen carriers. The activation energy is determined using the Avrami−Erofeev nucleation and growth kinetic expression.

sample pan, which acts as a heat sink, help avoid excessive temperature rise. Figure 4 displays a conversion profile for the oxidation of 45_ZrO2_FG along with its measured temperature obtained at the same time. During oxidation the temperature of the sample rises very quickly in the reaction, but the total rise is only about 1 °C. The faint dip below 700 °C at approximately 0.75 min is a result of a slight lag in the dynamic temperature control of the TGA instrument. That is a

Table 7. Model Used to Predict the Conversion of Cu$_2$O in Two Different Oxygen Carriers Using the Nucleation/Growth Kinetics Expression Avrami−Erofeev. This Model Is Only Used to Predict Conversions at Higher Temperatures ($T > 800$ °C)

influence	model values
$f(X)$	$1 - X$
$p_{O_2,eq}^{\alpha}$	$P_{O_2}(atm) = 6.057 \times 10^{-11} e^{0.02146 T(°C)}$
$f(p_{O_2})$: $(p_{O_2}^{\beta} - p_{O_2,eq}^{\beta})$	$\beta = 1.3$
$f(T) = A \times \exp\left(-\dfrac{E_a}{RT}\right)$	$A = 8.50 \times 10^4$ (g/s·atm$^{1.3}$); $E_a = 69$ (kJ/mol)
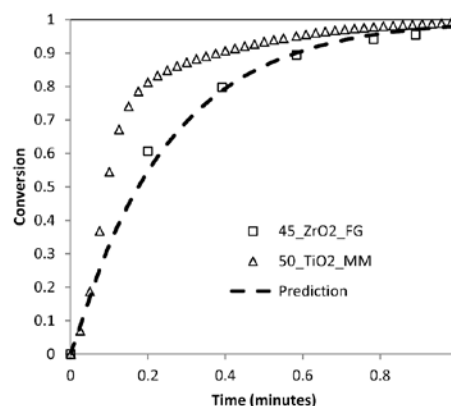
Figure 14. Conversion profiles for the oxidation of Cu$_2$O at 800 °C for 45_ZrO2_FG (□) and 50_TiO2_MM (△) are compared against the model prediction (- - -).

change of 0.1% of the total temperature and corresponds to a change in the equilibrium partial pressure of oxygen from 0.0202% to 0.0207% (a 2% change). Because of a limited effect, the temperature was treated as isothermal.

To avoid mass transfer resistances a low profile sample pan was employed. The height-to-diameter ratio of the sample pans used in this work was 1:6. In addition to the low profile pan, the sample was placed in the pan such that a very near monolayer of solid material was placed in the bottom. To minimize mass transfer resistance due to the intraparticle diffusion of gases, very small particles were used ($D_P < 45$ μm). During their analysis of reaction rates and the roles of intrinsic kinetics vs bulk and diffusion limitations, Sahir et al.[23] were able to define a particle size range beneath which they were able to effectively model the conversion of copper-based oxygen carriers without accounting for mass transfer resistances. They concluded that,

Table 6. Results Obtained from Modeling of High Temperature Oxidation of Two CLOU Materials

| influence	50_TiO2_MM	45_ZrO2_FG
$f(X)$	$1 - X$	
$p_{O_2,eq}^{\alpha}$	$P_{O_2}(atm) = 6.057 \times 10^{-11} e^{0.02146 T(°C)}$	
$f(p_{O_2})$: $(p_{O_2}^{\beta} - p_{O_2,eq}^{\beta})$	$\beta = 1.3$	$\beta = 1.3$
$f(T) = A \times \exp\left(-\dfrac{E_a}{RT}\right)$	$A = 5.60 \times 10^4$ (g/s·atm$^{1.3}$); $E_a = 68$ (kJ/mol)	$A = 5.65 \times 10^4$ (g/s·atm$^{1.3}$); $E_a = 71$ (kJ/mol)
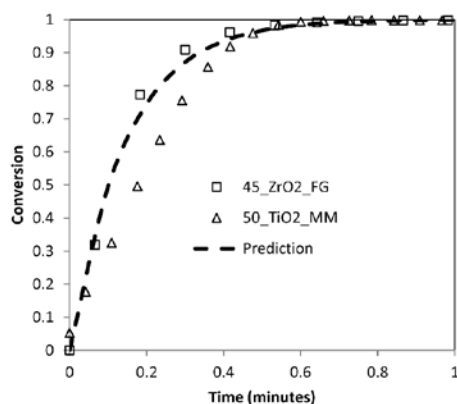
Figure 15. Conversion profiles for the oxidation of Cu_2O at 925 °C for 45_ZrO2_FG (□) and 50_TiO2_MM (△) are compared against the model prediction (- - -).

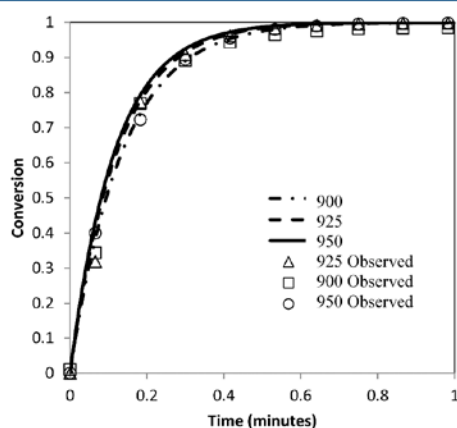**Figure 16.** Comparison of the predicted and observed conversion profiles for the 45_ZrO2_FG material.

while reactions of particles in the size range of 855−1000 μm were definitely influenced by mass transfer resistances, particles in the size range of 100−300 μm were well described without any influence from mass transfer up to 800 °C. The particles in this study were sieved well below the 300 μm threshold described therein.

3.3. Influence of the Partial Pressure of Oxygen on Reaction Kinetics. The partial pressure of oxygen plays a significant role in the oxidation of Cu_2O. From Figure 5 it may be seen that the rates of oxidation increase with temperature until reaching an observed maximum around 875 °C and then begin to decrease. This has been explained by different groups as being the result of a decrease in the driving force of oxidation.[10,12−14] The driving force, as defined herein, is given by the difference between the actual partial pressure of oxygen and the equilibrium partial pressure of oxygen:

$$f(p_{O_2}) = (p_{O_2}^\beta - p_{O_2,eq}^\beta) \qquad (7)$$

The partial pressure of oxygen at equilibrium for the CuO/Cu_2O redox pair is given in Figure 1 and is represented in eq 8.[31]

$$P_{O_2}(atm) = 6.057 \times 10^{-11} e^{0.02146 \times T} \qquad (8)$$

The data obtained during completion of the testing displayed in Table 3 was used to numerically determine the influence of the partial pressure driving force on the observed conversion profiles. By comparing the oxidation rates taken at 50% conversion for the results from varying the supplied oxygen partial pressures, the influence associated with the partial pressure driving force, (β), was determined to be 1.3. Figure 6 shows the observed conversion profiles for these tests. It is clear that the supplied partial pressure of oxygen significantly affects the conversion profile.

3.4. Low Temperature Oxidation. Zhu et al.[22] suggested that at low temperatures the oxidation of cuprous oxide followed a logarithmic rate law and the resulting activation energy was 38 kJ/mol which compares very well with the value reported here obtained using the constant driving force approach. These authors suggested that while the logarithmic rate law held true at low temperatures (up to 800 °C), the activation energy became very small or negative at higher temperatures. During their discussion several theories for the logarithmic characteristics of the oxidation rate were dismissed including (1) electric fields developed across oxide layers, (2) the tunneling of electrons, (3) and the possible nucleation and growth processes. They were able to describe the mechanism responsible for the apparent logarithmic nature of the reaction rate as a pore-blocking mechanism resulting from the 5% volume increase from Cu_2O to CuO. Zhu et al. recommended the use of the model described by Davies et al.[24] as follows:

$$m = k_1 \ln(k_2 t + k_3) \qquad (9)$$

where m represents the mass of the reacting species and k_1, k_2, and k_3 represent fitting constants which may be thought of physically as relating to the number of open low-resistance pathways (i.e., pores, grain boundaries, cracks, etc.).[21]

Evans, coauthor of the work of Davies et al.,[25] developed a more easily understandable expression along these same lines. In the case of mutually blocking pores (blocking of neighboring pores through compression) the expression appears as follows:[25]

$$X = \lambda \ln\left(1 + \frac{k_d t}{\lambda}\right) \qquad (10)$$

Equation 10 shows that conversion is a function of a blocking constant, λ, and a second constant, k_d.

Utilizing this method several groups were able to show that the effect of pore-blocking is commonly a function of temperature. Won and Sohn[26] successfully accounted for the effect of pore-blocking as did Sohn and Kim[27] and Sohn et al.[28] for very different types of materials. These groups were able to show that the pore-blocking influence may be readily recognized by two separate regimes of reaction rates: the first regime is characterized by quick initial rates and is followed quickly by the second as the reaction rate slows well before full conversion. This phenomenon may be seen in Figure 2 and Figure 3 for the case of cuprous oxide oxidation. Therefore, the low temperature activation energy may be determined when this pore-blocking effect is taken into account.

By rearranging eq 10 and plotting the left-hand side, $\exp(X/\lambda)$, against time the blocking constant is resolved by finding the value of λ that gives the "best-fit" straight line using regression analysis at each temperature. Figure 7 and Figure 8 display the

results of the pore-blocking analysis. The pore-blocking constant λ varies from 0.226 at 600 °C to 0.182 at 700 °C.

3.4.1. Influence of the Solid Conversion on Reaction Kinetics. In simple cases the influence of the solid conversion on the overall kinetic expression is determined by simply using a regression analysis to fit the conversion curve or by determining the "straightest" line of plots given by X, $\ln(X)$ or $1/X$ versus time. The straightest figure represents either zero, first, or second order, respectively. The oxidation of cuprous oxide, however, is not a simple case.

After regression analysis the order of reaction with respect to the solid (Cu_2O) ranges between 4 and 2 at temperatures from 600 to 700 °C, respectively. A fourth order reaction is unlikely to be the case; therefore, some other mechanism must be influencing the conversion of the solid. It is, however, more likely that the molar volume change from one mole of copper I oxide (Cu_2O, cuprous oxide) at 23.87 cm^3/mol to that of two moles of copper II oxide (CuO, cupric oxide) at 12.52 cm^3/mol (see eq 1) causes a pore-blocking phenomenon that must be understood for proper understanding of the reaction order. The increase from 23.87 cm^3 (Cu_2O) to 25.04 cm^3 ($2CuO$) creates a volume change in the solid of about 5%.

It was shown in the previous section that a pore-blocking kinetics model may well represent the effects observed such as the two regime rates seen in Figure 2 and Figure 3. Pore-blocking mechanisms are commonly functions of temperature and create a very significant decrease in the reaction rate after a very short reaction time. This effect may be seen in the same figures as the initial rate of mass change is relatively quick, but after just a very short reaction time (less than 30 s) the rates at each of the temperatures tested decreases very quickly. Therefore, in order to understand the influence the solid has in the reaction kinetics the proposed kinetic eq 2 must be revisited.

Applying eq 5, the generalized form of the rate equation, and the pore-blocking kinetic eq 10 the corrected rate equation can be developed. By rearranging eq 10 creating a time explicit function we arrive at

$$\exp\left(\frac{X}{\lambda}\right) = 1 + \frac{k_d t}{\lambda} \tag{11}$$

By differentiating we get

$$\exp\left(\frac{X}{\lambda}\right)\frac{dX}{\lambda} = \frac{k_d}{\lambda}\,dt \tag{12}$$

Rearranging eq 12 we arrive at the rate equation using pore-blocking kinetics.

$$\text{rate} = \frac{dX}{dt} = \frac{k_d}{\exp\left(\frac{X}{\lambda}\right)} \tag{13}$$

We can equate eq 13 to the general rate eq 5 from which we can understand that the apparent rate constant k_d is related to the influence of both the temperature and partial pressure of oxygen, $f(T)$ and $f(P_{O_2})$, respectively, given in eq 14.a, while $f(X)$ is described by $1/\exp(X/\lambda)$ given in eq 14.b.

$$\frac{dX}{dt} = \frac{k_d}{\exp\left(\frac{X}{\lambda}\right)} = f(T)\,f(X)\,f(P_{O_2}) \tag{14}$$

$$k_d = f(T)\,f(P_{O_2}) = k[P_{O_2}{}^{\beta} - P_{O_2,eq}{}^{\beta}] \tag{14.a}$$

$$f(X) = \frac{1}{\exp\left(\frac{X}{\lambda}\right)} \tag{14.b}$$

The resulting rate equation may then be written as:

$$\frac{dX}{dt} = k\frac{1}{\exp\left(\frac{X}{\lambda}\right)}[P_{O_2}^{\beta} - P_{O_2,eq}^{\beta}] \tag{15}$$

Where k is the true rate constant and may be expressed as

$$k = A\exp\left(-\frac{E_a}{RT}\right) \tag{16}$$

The pore-blocking constant, λ, was determined for each temperature and an expression was developed for extrapolation or prediction. Figure 7 and Figure 8 show the results of fitting the pore blocking constant (λ) to the observed conversion data for both the 50_TiO2_MM and 45_ZrO2_FG materials, respectively.

The observed pore blocking constants for the 2 materials may be estimated by the following expressions:

45_ZrO2_FG:

$$\lambda = -4.16 \times 10^{-4}(T\ °C) + 0.48 \tag{17}$$

50_TiO2_MM:

$$\lambda = -2.95 \times 10^{-4}(T\ °C) + 0.34 \tag{18}$$

3.4.2. Influence of Temperature on Reaction Kinetics. Generally speaking, the influence of temperature on a reaction is reflected in the activation energy, and determination of the activation energy generally involves measuring the reaction rate for experiments at different temperatures when the reactant concentration, the partial pressure of oxygen in this case, is held constant. But as noted earlier, for cuprous oxide oxidation temperature has an indirect effect as well. The partial pressure of the oxygen driving force is a function of the difference between the partial pressure of oxygen and the equilibrium partial pressure of oxygen. The equilibrium partial pressure of oxygen is a function of temperature, and at elevated temperatures (above 800 °C) the equilibrium partial pressure of oxygen becomes increasingly important.

The oxygen driving force influence is not much of a concern at the lower temperature where the pore-blocking kinetics are used to describe the conversion profiles due to the very small influence from the equilibrium partial pressure of oxygen. Because of the influence of temperature on the pore-blocking constant shown earlier, the activation energy must be explicated while taking that into account.

The activation energy may be determined by rearranging equation 14.b (13) and solving for the function $f(T)$:

$$\frac{k_d}{f(P_{O_2})} = f(T) = A \times \exp\left[-\frac{E_a}{RT}\right] \tag{19}$$

thereby allowing for calculation of the associated activation energy. Using the slopes of the lines created in Figure 7 and Figure 8 k_d is readily determined at each temperature. By dividing k_d by $f(P_{O_2})$ the reaction rate constant (k) is found. The activation energy is then obtained by plotting $\ln(k)$ vs $1/T$ and is shown in Figure 9.

The activation energy obtained for each of the materials is very similar. For the titania-based material the relevant activation energy is 172 kJ/mol while it is 165 kJ/mol for the

zirconia material. The similarity between these values suggests that the true activation energy for the low-temperature oxidation of Cu_2O may be universal regardless of support or production method. By average the resulting activation energy is 168 kJ/mol.

3.4.3. Resulting Kinetic Expressions. Using the influences given in the previous sections the resulting kinetic equations are given in Table 5 and correspond to the generalized rate expression given as eq 5.

The comparison between the predicted and observed conversion profiles for the 45_ZrO2_FG material is given in Figure 10. While average values are used for the prediction model the comparison between the predicted values and the observed values are favorable. The conversion profiles are well predicted by the presented equation.

3.5. High Temperature Oxidation. For the high temperature oxidation of Cu_2O the pore-blocking kinetic equation does not adequately describe the observed rates over the range of conversion. It is unclear why the oxidation mechanism is observed to change at elevated temperatures. It has been suggested that the diffusion mechanism for the growth of the CuO layer may or may not be attributed to the diffusion of the copper through the oxide layer instead of the diffusion of oxygen. This would seem to satisfy the observations shown here in this work as the diffusion rate of metal ions increases with temperature.

Commonly, for metals and powders, the nucleation and growth kinetics equation developed by Avrami[29] is used to model the redox characteristics.[18,19] The expression is given by

$$[-\ln(1 - X)]^{1/n} = k_{app} \times t \tag{20}$$

where n is considered a constant used to describe the type of nucleation and growth that is occurring. By rearranging:

$$\ln[-\ln(1 - X)] = n \times \ln(k_{app}) + n \times \ln(t) \tag{21}$$

Figure 11 allows determination of the growth constant n by plotting $\ln[-\ln(1 - X)]$ against $n \times \ln(t)$ and determining the straightest line for n = 1, 2, 3, or 4. Figure 11 shows n = 1 as the best fit for both the titania and zirconia materials. A value of 1 for n is traditionally associated with constant nucleation/growth throughout the reaction.

3.5.1. Influence of the Solid Conversion on Reaction Kinetics. The influence of the solid conversion on the reaction kinetics at high temperatures is noticeably different from the influence for low temperature oxidation. This may be due to a mechanism such as solid state diffusion of Cu^{2+} through CuO. It is not, however, within the scope of this work to determine the exact mechanisms involved, but instead to develop a set of equations that adequately describe the overall mechanism involved in the oxidation of Cu_2O.

For n = 1 the rate expression is determined by differentiating X with respect to t. After rearranging the result gives:

$$\frac{dX}{dt} = (1 - X) \times k_{app} \tag{22}$$

By equating to eq 5 it may be understood that the individual influences are described by

$$f(X) = 1 - X \tag{23}$$

$$k_{app} = f(T)f(P_{O_2}) \tag{24}$$

The dependence of the kinetics on the solid appears first order, but is more accurately described as a pseudo-first-order dependence which incorporates, globally, the potential submechanisms mentioned previously.

3.5.2. Influence of Temperature on Reaction Kinetics. The falsification of the activation energy refers to an incorrect interpretation of the observed activation energy and has been identified and discussed by Sohn[30] where the influences from both the thermodynamic and the kinetic barriers were identified. To effectively create a model to predict the reaction rates of Cu_2O oxidation the effect of these two influences must be separated, thereby uncovering the true activation energy. By maintaining a constant driving force over a variety of temperatures the thermodynamic effect of temperature is effectively mitigated. To maintain a constant driving force the difference between the partial pressure of the supplied oxygen and the equilibrium partial pressure must be maintained by adjusting the supplied oxygen at each temperature (see Table 4). The results of this testing campaign for the 45_ZrO2_FG material are presented in Figure 12 as an Arrhenius-type plot. The apparent activation energy of this material is 43 kJ/mol.

By utilizing eq 24 the activation energy may be determined by dividing k_{app} by $f(P_{O_2})$ which effectively takes into account the influence by the partial pressure of oxygen at every supplied oxygen partial pressure.

The value for k_{app} at each temperature may be determined using a regression plot such as Figure 11. The linear regression expression of $y = mx + b$ gives $b = n [\ln(k_{app})]$. After k_{app} has been determined the activation energy calculation follows the procedure given in section 3.4.2 for k_d. The resulting determined apparent activation energies are given in Figure 13 with an average of 69 kJ/mol. The average value for the pre-exponential factor is 5.62×10^4 s^{-1}. The obvious difference between the activation energy calculated from Figure 12 and Figure 13 may be explained by the testing procedures for the constant driving force tests. The tests assumed a first order dependence on the partial pressure of oxygen driving force. Subsequent testing to uncover the actual dependence resulted in 1.3 order dependence; this gave rise to the difference in the activation energy values. Ideally, this would have been determined prior to selecting the constant driving force testing conditions.

3.5.3. Resulting Kinetic Expressions. The kinetic expression resulting from the work above is given in Table 6.

3.6. Application of Developed Equations. Efforts were made to develop an equation that fit the conversion of both materials reasonably. The experimentally determined constants were used to determine values that best described the effects of both materials, which are given in Table 7. Figure 14 shows the comparison of the prediction against the conversion profiles for both materials at 800 °C. The conversion of the titania material is faster than the prediction. This may be explained by the change from the low temperature oxidation mechanism (pore-blocking kinetics) to the high temperature mechanism (nucleation and growth kinetics). There may be some transition period where neither expression accurately describes the true mechanism. The evaluated temperature, 800 °C, is lower than what is considered a target for operation of an industrial scale CLOU reactor, but it may be in the realm of operating temperatures for other CLC technologies. The higher temperatures (above 900 °C) are more in the expected target range for industrial CLOU reactors.

Figure 15 displays the conversion profiles for the titania and zirconia materials along with the predicted values at 925 °C. This figure shows the model is better at predicting the higher temperature conversion profiles. Figure 16 displays the conversion profiles for the zirconia material at three different temperatures in the higher regime: 900, 925, and 950 °C.

4. CONCLUSIONS

The kinetics of oxidation for Cu_2O are challenging to accurately describe and model. Many mechanisms play significant roles at different temperatures making it difficult to assign a simple expression that accurately models this reaction over a large range of temperatures. By separating the oxidation into two regimes (regime 1 below 700 °C and regime 2 above 800 °C) and using two separate models for each regime, the oxidation kinetics for two different metal oxide carriers are adequately described. The higher temperature predictions more accurately describe the conversion profiles of both materials.

For temperatures below 700 °C the average apparent activation energy is given as 168 kJ/mol for use in a pore blocking model. For the higher temperatures ($T > 800$ °C) the average apparent activation energy is given as 69 kJ/mol for modeling using the Avrami−Erofeev equation.

■ AUTHOR INFORMATION

Corresponding Author
*E-mail: Chris.clayt@gmail.com.

Notes
The authors declare no competing financial interest.

■ ACKNOWLEDGMENTS

■ NOMENCLATURE

Abbreviation Name

CLC = chemical looping combustion
CLOU = chemical looping with oxygen uncoupling
TGA = thermogravimetric analysis

Symbol Name Units

A = preexponential constant, $g/s \cdot atm^{1.3}$
E_a = activation energy, J/mol
a_i = activity coefficient of species i, -
R = gas constant, J/mol-K
T = temperature, K or C
p_{O_2} = partial pressure of oxygen, atm
$p_{O_2,eq}$ = partial pressure of oxygen at equilibrium, atm
β = order of reaction with respect to partial pressure of oxygen, -
K = equilibrium constant, -
$f(T)$ = influence of temperature on the reaction rate, units consistent with definition of rate
$f(X)$ = influence of solid conversion on the reaction rate, -

$f(p_{O_2})$ = influence of the partial pressure of oxygen on the reaction rate, units based on partial pressure dependence to be determined by experiment
λ = pore blocking constant, -
k_d = fitting parameter for pore blocking equation, 1/s
t = time, s
X = conversion, -
k_{app} = fitting paramter for Avrami−Erofeev equation, 1/s
n = nucleation constant, -

■ REFERENCES

(1) Marion, J.; Mohn, N.; Liljedahl, G. N.; Nsakala, N.; Morin, J.-X.; Henriksen, P.-P. Technology options for controlling CO_2 emissions from fossil-fuelled power plants. Third Annual Conference on Carbon Capture and Sequestration, Alexandria, VA, May 3−6, 2004.

(2) Ishida, M.; Jin, H. A novel combustor based on chemical looping reactions and its reaction kinetics. *J. Chem. Eng. Jpn.* **1994**, 27 (3), 296−301.

(3) Lyngfelt, A.; Leckner, B.; Mattisson, T. A fluidized-bed combustion process with inherent CO_2 separation: Application of chemical-looping combustion. *Chem. Eng. Sci.* **2001**, 56 (10), 3101−3113.

(4) Mattisson, T.; Lyngfelt, A.; Cho, P. The use of iron oxide as an oxygen carrier in chemical-looping combustion of methane with inherent separation of CO_2. *Fuel* **2001**, 80 (13), 1953−1962.

(5) Mattisson, T. Materials for chemical-looping with oxygen uncoupling. *ISRN Chem. Eng.* **2013**, 1, 1−19.

(6) Garcia-Labiano, F.; de Diego, L. F.; Adanez, J.; Abad, A.; Gayan, P. Reduction and oxidation kinetics of a copper-based oxygen carrier prepared by impregnation for chemical-looping combustion. *Ind. Eng. Chem. Res.* **2004**, 43 (26), 8168−8177.

(7) Lewis, W. K.; Gilliland, E. R. *Production of pure carbon dioxide.* U.S. Patent Nos. 2,665,971 and 2,665,972, 1954.

(8) Mattisson, T.; Lyngfelt, A.; Leion, H. Chemical-looping with oxygen uncoupling for combustion of solid fuels. *Int. J. Greenhouse Gas Control* **2009**, 3, 11−19.

(9) Chuang, S.; Dennis, J. S.; Hayhurst, A. N.; Scott, S. A. Development and performance of Cu-based oxygen carriers for chemical-looping combustion. *Combust. Flame* **2008**, 154, 109−121.

(10) Lyngfelt, A.; Johansson, M.; Mattisson, T. *Chemical-Looping Combustion − Status of Development.* 9th International Conference on Circulating Fluidized Beds, Hamburg, Germany, May 13−16 2008.

(11) Leion, H. Capture of CO_2 from solid fuels using chemical-looping combustion and chemical-looping with oxygen uncoupling. Ph.D. Thesis, The Chalmers University of Technology, Sweden, 2008.

(12) Abad, A.; Mattisson, T.; Lyngfelt, A.; Ryden, M. Chemical-looping combustion in a 300 Wth continuously operating reactor system using a manganese-based oxygen carrier. *Fuel* **2006**, 85, 1174−1185.

(13) Chuang, S.; Dennis, J.; Hayhurst, A.; Scott, S. Kinetics of the oxidation of a co-precipitated mixture of Cu and Al_2O_3 by O_2 for chemical-looping combustion. *Energy Fuel* **2010**, 24, 3917−3927.

(14) Adánez-Rubio, I.; Abad, A.; Gayán, P.; de Diego, L.; García-Labiano, F.; Adánez, J. Identification of operational regions in the chemical-looping with oxygen uncoupling (CLOU) process with a Cu-based oxygen carrier. *Fuel* **2012**, 102, 634−645.

(15) Gayan, P.; Adánez-Rubio, I.; Abad, A.; de Diego, L. F.; García-Labiano, F.; Adánez, J. Development of Cu-based oxygen carriers for chemical-looping with oxygen uncoupling (CLOU) process. *Fuel* **2012**, 96, 226−238.

(16) Eyring, E. M.; Konya, G.; Lighty, J. S.; Sahir, A. H.; Sarofim, A. F.; Whitty, K. Chemical looping with copper oxide as carrier and coal as fuel. *Oil Gas Sci. Technol.* **2010**, 10.

(17) Brandt, B.; Gruene, P.; Rosowski, F.; Farrauto, R. J.; Castaldi, M. J. Oxygen uptake and release kinetics of $Cu/Cu_2O/CuO$ on Al_2O_3 and ZrO_2-SiO_2 as materials for chemical looping combustion. Oct 16−21 2011, AIChE Annual Meeting, Minneapolis, MN, USA.

Article

(18) Zhu, Y.; Mimura, K.; Isshiki, M. Oxidation mechanism of Cu_2O to CuO at 600–1050 C. *Oxid. Met.* **2004**, *62* (3), 207–222.

(19) Prisedsky, V. V.; Vinogradov, V. M. Fragmentation of diffusion zone in high-temperature oxidation of copper. *J. Solid State Chem.* **2004**, *177*, 4258–4268.

(20) Johansson, M.; Mattisson, T.; Lyngfelt, A. Investigation of Mn_2O_4 with stabilized ZrO_2 for chemical-looping combustion. *Chem. Eng. Res. Des.* **2006**, *84* (A9), 807–818.

(21) Wimmers, O. J.; Arnoldy, P.; Moulijn, J. A. Determination of the reduction mechanism by temperature-programmed reduction: application to small iron oxide (Fe_2O_3) particles. *J. Phys. Chem. Solids* **1986**, *90* (7), 1331–1337.

(22) Lin, H.; Chen, Y.; Li, C. The mechanism of reduction of iron oxide by hydrogen. *Thermochim. Acta* **2003**, *400* (1–2), 61–67.

(23) Sahir, A. H.; Lighty, J. S.; Sohn, H. Y. Kinetics of copper oxidation in the air reactor of a chemical looping combustion system using the law of additive reaction times. *Ind. Eng. Chem. Res.* **2011**, *50* (23), 13330–13339.

(24) Davies, D. E.; Evans, U. R.; Agar, J. N. The oxidation of iron at 175 to 350 °C. *Proc. R. Soc. London, A* **1954**, *225*, 427–443.

(25) Evans, U. R. *The Corrosion and Oxidation of Metals*; Edward Arnold Ltd: London, 1960.

(26) Won, S.; Sohn, H. Y. Kinetics of the reaction between hydrogen sulfide and lime particles. *Metall. Tran. B* **1985**, *16B*, 164–168.

(27) Sohn, H. Y.; Kim, B. S. A novel cyclic reaction system involving CaS and $CaSO_4$ for converting sulfur dioxide to elemental sulfur without generating secondary pollutants. 2. Kinetics of the reduction of sulfur dioxide by calcium sulfide powder. *Ind. Eng. Chem. Res.* **2002**, *41*, 3087–3091.

(28) Sohn, H. Y.; Savic, M.; Padilla, R.; Han, G. A novel cyclic reaction system involving BaS and $BaSO_4$ for converting SO_2 to elemental sulfur without generating pollutants: Part 1. Feasibility and kinetics of SO_2 reduction with BaS. *Chem. Eng. Sci.* **2006**, *61*, 5088–5093.

(29) Avrami, M. Kinetics of phase change. I. General theory. *J. Chem. Phys.* **1939**, *7*, 1103–1113.

(30) Sohn, H. The influence of chemical equilibrium on fluid–solid reaction rates and the falsification of activation energy. *Metall. Mater. Trans. B* **2004**, *35* (1), 121–131.

(31) Clayton, C. K.; Whitty, K. J. Measurement and modeling of decomposition kinetics for copper oxide-based chemical looping with oxygen uncoupling. *Appl. Energy* **2013**, DOI: 10.1016/j.apenergy.2013.10.032.

APPENDIX C

CHARACTERISTICS AND CLOU PERFORMANCE OF

A NOVEL SIO$_2$-SUPPORTED OXYGEN CARRIER

PREPARED FROM CUO AND β-SIC

energy&fuels

Characteristics and CLOU Performance of a Novel SiO$_2$-Supported Oxygen Carrier Prepared from CuO and β-SiC

Sean B. Peterson,*[,†] Gabor Konya,[†] Christopher K. Clayton,[‡] Robert J. Lewis,[†] Blake R. Wilde,[†] Edward M. Eyring,[†] and Kevin J. Whitty[‡]

[†]Department of Chemistry, The University of Utah, 315 S. 1400 East, Room 2020, Salt Lake City, Utah 84112, United States
[‡]Department of Chemical Engineering, The University of Utah, 50 S. Central Campus Drive, Room 3290, Salt Lake City, Utah 84112, United States

ABSTRACT: An effective copper-based oxygen carrier for use in chemical looping with oxygen uncoupling (CLOU) has been developed, and its physical and reactive properties have been evaluated. The preparation method involves coating β-SiC support material with CuO and then baking the coated material at 980 °C which causes the β-SiC to convert to SiO$_2$, thus enveloping the CuO. Variations of the preparation technique, including different forms of SiC, methods of CuO addition, and the order of CuO addition and baking, were tested. It was determined that preparation by rotary evaporation CuO deposition and final sintering produced superior carrier particles. Loadings as high as 60 wt % CuO were achieved. The carrier particles fluidized well, and for loadings to 40 wt % CuO, no agglomeration was observed at temperatures as high as 1000 °C. The particles retained reactivity over many oxidation and reduction cycles. The coat-then-bake preparation method using β-SiC is a viable candidate to be used as oxygen carrying material in CLOU.

1. INTRODUCTION

Chemical looping combustion (CLC) is a promising energy generation technology that involves cycling a solid, metal-based "oxygen carrier" between two fluidized bed reactors and offers inherent separation of CO$_2$ with comparatively little energy penalty.[1,2] An advanced form of CLC, chemical looping with oxygen uncoupling (CLOU, Figure 1), is particularly suitable
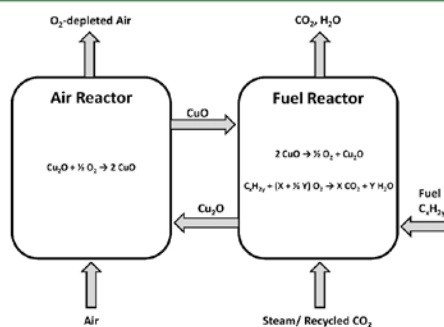

Figure 1. Schematic of the copper-based CLOU process. Solid fuel is represented by C$_x$H$_{2y}$.

for solid fuels such as coal, petroleum coke, and biomass. In the air reactor, the metal is oxidized by oxygen, resulting in an O$_2$-depleted effluent stream. The oxidized carrier is transported to a fuel reactor fluidized by steam and/or CO$_2$, where the thermodynamics of CLOU carriers are such that the release of gaseous oxygen is favored. The released O$_2$ combusts the fuel, resulting in a product gas of mostly CO$_2$ and steam. Condensation of the steam results in a nearly pure stream of CO$_2$ suitable for sequestration with little additional processing required. CLOU is recognized as one of the most promising

CO$_2$ capture-ready technologies for energy production from coal, and research in this area has accelerated rapidly in recent years.

A key consideration of CLOU technology is the oxygen carrier material. Several pure and mixed metals have been identified as having suitable thermodynamics for oxygen release in the fuel reactor.[3−6] Many investigations have focused on copper cycling between cupric (CuO) and cuprous (Cu$_2$O) oxide:

$$2CuO \leftrightarrow Cu_2O + \frac{1}{2}O_2 \tag{1}$$

In thermogravimetric (TGA) experiments, pure copper oxide powder can be oxidized to CuO in an air environment and reduced to Cu$_2$O in an inert environment over many cycles.[7] However, in fluidized bed conditions similar to those that would be used in a commercial CLOU system, CuO agglomerates, which makes it unsuitable for use in a fluidized system. Support materials such as alumina,[8] titania,[9] zirconia,[10] ceria,[11] sepiolite,[12] and combined supports[13] have been investigated to act as inert binders that allow the use of CuO in the fluidized conditions required for CLOU.[4] While the main concern that justifies the need of a support material is agglomeration, the support material may also improve the kinetics of the oxidation and reduction reactions of the copper oxides.[9]

In terms of the entire chemical looping process, it is desirable to operate with the highest possible loading of active carrier material to minimize necessary solids circulation rates and equipment size. According to eq 1, 10.1% of the mass of pure

CuO can be released as O_2. For a typical U.S. eastern bituminous coal containing 70% carbon, 5% hydrogen, 3% sulfur, 8% oxygen, and 14% ash and inerts, complete combustion requires 2.2 kg of O_2 per kg of coal. That would require 22 kg of pure CuO or 55 kg of oxygen carrier containing a 40% loading of CuO. It is unreasonable to target complete oxidation of all Cu_2O to CuO in the air reactor and full conversion of all CuO to Cu_2O in the fuel reactor since fluidized beds act as stirred tank reactors and reaction rates slow considerably at high conversions. A reasonable target is that 30% of the copper exists as CuO exiting the fuel reactor and 75% exists as CuO exiting the air reactor.[14] With that assumed performance, the circulation rate becomes 122 kg carrier per kg of coal. Although that ratio is comparable to what is used in circulating fluidized bed combustors and gasifiers today,[1] decreasing the carrier/fuel ratio by increasing the loading of active metal or improving oxidation and reduction rates will improve performance and process economics.

A simple method for introducing CuO to a support material to prepare oxygen carriers for CLOU experiments is incipient wetness impregnation. The incipient wetness method has provided supported CuO that performed well in TGA experiments. However, de Diego et al. has reported that CuO on the external surface of the support material can be worn off in a fluidized environment, contributing to agglomeration of the material.[15] This means that the CuO content is limited by the pore volume of the support material for oxygen carriers prepared by incipient wetness. Compounds that are stable in both oxidizing and reducing environments at temperatures up to 1000 °C and have a significant pore volume are not readily available. Other methods for preparing copper-based oxygen carriers, such as mechanical mixing,[12,16] spray drying,[17] and freeze granulation[10] have shown promise. In some cases these methods have produced materials that lack the mechanical strength needed to be viable candidates for use in CLOU.[16,17]

The aim of the present study was to develop a novel copper-based oxygen carrier for CLOU that exhibits sustained reactivity, has high mechanical strength for processing in fluidized beds, and does not have copper concentrated on the surface so as to minimize agglomeration risk. This was achieved by impregnating β-SiC support material with CuO. High surface area β-SiC converts to SiO_2 in oxidizing environments at temperatures above 800 °C.[18] Once CuO is loaded onto the β-SiC support, the material is calcined in air at 980 °C to promote conversion of silicon carbide to silicon dioxide. As the β-SiC converts to SiO_2 it envelops and secures the CuO. The CuO is not concentrated on the external surface of the material and therefore should not be worn off or encourage agglomeration in fluidized beds. Industrial-grade silicon carbide powder is readily available and used for grinding and sandblasting. Ideally, the silicon carbide should have high porosity and internal surface area to promote gas–solid reactions. Engineered high surface area β-SiC is available as a catalyst support for gas-to-liquid conversion processes.[19]

2. EXPERIMENTAL SECTION

2.1. Preparation of Oxygen Carriers. *2.1.1. Raw Materials.* Two sources of silicon carbide were used as starting material for carrier preparation. Initial development was performed using SiC powder (Pfaltz & Bauer, 99% pure, −40 mesh). Once the production technique was refined, the support material was changed to 100 μm spheres of β-SiC catalyst support (SICAT Catalysts, Inc.). Details of the SiC support materials are presented in Table 1. The raw β-SiC and

Table 1. Properties of SiC Support Materials

support	SiC powder	β-SiC spheres	SiO_2 spheres[a]
particle size range (μm)	390–450	125–200	125–200
bulk density (kg/m^3)	3200	3200	2100
BET surface area (m^2/g)	<1	25.9	10.8
pore volume (cm^3/kg)	~0	146	64

[a]The SiO_2 spheres were prepared by baking the β-SiC spheres at 980 °C for 7 days, thus oxidizing the SiC to SiO_2.

the sintered and oxidized SiO_2 material are ultimately different and have been characterized separately in the table. Several different SiO_2-supported oxygen carriers, with CuO loadings as high as 60 wt %, were prepared and subjected to physical characterization, reactivity testing, and fluidized bed performance analysis.

2.1.2. Oxygen Carriers with SiC Powder as Support. Initial carriers containing 20 wt % CuO were prepared on SiC powder using a wet impregnation technique and also by impregnation using a rotary evaporator. In both procedures described below, copper(II) nitrate was mixed with SiC using acetone as the solvent. The carriers made using SiC powder were produced using one, two, four, or eight impregnation cycles. Within a given series, the copper(II) nitrate was added in equal amounts for each impregnation cycle so that the sum of the CuO from all of the impregnation cycles would yield a carrier with the target CuO content of 20 wt %.

Oxygen carriers prepared by the wet impregnation (WI) method were prepared by mixing the SiC support and copper(II) nitrate in acetone. Enough acetone was added to completely submerse the SiC powder. After sufficient stirring, the sample was dried in an oven at 110 °C. The dry materials were then calcined at 180 °C overnight. After complete calcination, if the oxygen carrier was to be prepared by multiple additions, the next addition of CuO then took place.

A second method used to prepare oxygen carriers was impregnation by rotary evaporation (RV). These carriers were prepared similarly to wet impregnation samples. However, the whole process utilized a rotary evaporator. The lower pressure provided by the rotary evaporator promoted faster evaporation of the acetone, allowing for quick and even deposition of copper(II) nitrate on the SiC powder. Once the materials in the flask had dried, the temperature was increased at a rate of 25 °C/min to a final external temperature of about 350 °C. The material was left rotating on the rotary evaporator at this high temperature until the calcination of copper(II) nitrate was complete, indicated by a completely black material left in the flask. After the flask had cooled, the next addition of CuO took place.

2.1.3. Oxygen Carriers with SICAT Spheres as Support. After properties and performance of the initial carriers were evaluated, a second group of carriers was produced using the SICAT spheres as the support material. These carriers were prepared through multiple impregnation cycles using the rotary evaporation technique described above. Two different routines were used for preparation using the SICAT β-SiC spheres. Since β-SiC converts to SiO_2 in oxidizing environments above 800 °C, the material was baked for seven days at 980 °C in air. Moene et al. reported that this conversion can reach 60 to 70% completion in 10 h, but complete conversion is very slow.[18] For this reason, the material was baked for seven days to allow it to stabilize before the oxygen carrier was evaluated experimentally. Based on the change in mass, the conversion was 92% complete after seven days of baking.

In the coat-then-bake (CTB) method, copper was first deposited on the fresh β-SiC spheres by impregnation with rotary evaporation with multiple impregnation cycles as described above. After all CuO additions were complete, the material was placed in a muffle furnace in air at 980 °C for 7 days allowing the β-SiC to convert to SiO_2. Slight sintering was observed, so after baking, the solid material was broken apart and sieved to a size range of 105 to 150 μm.

In the bake-then-coat (BTC) method, the β-SiC material was first baked in air at 980 °C for 7 days. The resulting SiO_2 was then impregnated with CuO by rotary evaporation with multiple impregnation cycles as described above. After CuO impregnation,

Table 2. Summary of Si-Based Oxygen Carriers Produced in This Study

code	support	CuO addition technique	preparation method	no. of CuO impregnation cycles	CuO (wt%)	
					target	measd
WI-20	SiC powder	wet impregnation	--	1, 2, 4, 8	20	19
RV-20	SiC powder	rotary evaporator	--	1, 2, 4, 8	20	19
RV-BTC-20	SICAT spheres	rotary evaporator	bake-then-coat	6	20	19
RV-CTB-15	SICAT spheres	rotary evaporator	coat-then-bake	6	16	15
RV-CTB-40	SICAT spheres	rotary evaporator	coat-then-bake	10	42	40
RV-CTB-60	SICAT spheres	rotary evaporator	coat-then-bake	10	64	61

the material was left overnight at 200 °C in air. The final material was sieved between 105 and 150 μm.

Considerations would have to be made to adapt these methods to a commercial scale. Such considerations could include altering the CuO impregnation method and reducing the baking time. It is possible that the baking time could be decreased considerably, but the effects of baking time were not studied in this work.

2.1.4. Summary of Carriers. All of the carriers that were produced in this study are summarized in Table 2. Carriers prepared using SiC powder were prepared by WI and RV (each of which includes carriers prepared by 1, 2, 4, and 8 impregnation cycles) and are represented by two groups. The actual CuO content for carrier RV-CTB-40 was determined quantitatively by iodometric titration repeated three times. Approximately 1 g of RV-CTB-40 was placed in HCl to dissolve the CuO completely. The solution was diluted with water, ammonia, and acetic acid to form a buffer of pH 4–5. Potassium iodide (2 g) was added to the solution and was then titrated with the thiosulfate solution. The titration was completed in the presence of thiocyanate using starch as the indicator. Because the measured CuO content determined quantitatively was consistent with the value calculated based on the mass of oxygen uptake/loss in TGA tests, all other measured CuO content values reported are based on TGA data. The measured CuO content is lower than the target value because during the impregnation of CuO, some CuO can stick to the flask instead of the support material. The amount of Cu stuck to the flask is small (usually less than 5%) and can be recovered.

2.2. Thermogravimetric Analysis. Each oxygen carrier was analyzed by either a TA Instruments Q500 or Q600 thermogravimetric analyzer (TGA) to determine its reactivity without fuel in multicycle tests. The TGA experiments cannot predict oxygen carrier performance under CLOU conditions when fuel is present but were used to observe complete oxidation and reduction reactions over multiple cycles. For each experiment, the mass of the sample was between 25 and 35 mg. The experiments were performed isothermally at a given temperature (between 850 and 950 °C). The samples were oxidized in 100 mL/min of air. The spontaneous decomposition (reduction) of the samples was promoted in 100 mL/min of nitrogen. To ensure complete oxidation and decomposition reactions, the respective gas conditions were maintained for 30 min. To analyze the TGA data, the conversion of the oxygen carriers for each oxidation and reduction reaction was determined using the following equations:

$$X_{ox} = \frac{m_t - m_{red}}{m_{ox} - m_{red}} \quad (2)$$

$$X_{red} = \frac{m_{ox} - m_t}{m_{ox} - m_{red}} \quad (3)$$

X_{ox} and X_{red} represent fractional conversion for the oxidation and reduction reactions, m_t is the sample mass at a given time, m_{red} is the mass of fully reduced sample with all copper as Cu_2O, and m_{ox} is the mass of fully oxidized sample with all copper as CuO.

The rates of the reduction portions of the experiments were determined by treating the conversion data with a linear model. The data were trimmed from 1 to 90% to capture the linear portion, and the calculated regression slope of the line approximates the rate constant in units of percent-conversion/second. The conversion data

for the oxidation portions of the experiments were treated by a pseudo-first-order model which best fit the data:

$$X_{ox} = X_f - (X_f - X_i)e^{-k(t - t_0)} \quad (4)$$

Each rate constant was calculated by trimming the first 5% completion to capture the portion of data that best fit the pseudo-first-order model, where X_f is the value the completion approaches at the end of the reaction, X_i is the initial completion value (around 5%), t_0 is the time at which the reaction reaches 5% completion, and k is the calculated rate constant.

2.3. Particle Characterization. The surface area and pore volume of the support materials were determined by the Brunauer–Emmett–Teller (BET) method at 77 K by nitrogen adsorption/desorption. Oxygen carrier samples were imaged using a Hitachi S-300N scanning electron microscope (SEM). Energy dispersive X-ray spectroscopy (EDS) was carried out with an EDAX HIT S3000N 132-10 alongside the SEM images to confirm the appearance of and locate elemental silicon and copper. The crushing strengths of the oxygen carriers reported were determined by the force necessary to fracture a single particle. The values reported are the average values of 30 measurements using a Shimpo FGE-5X digital force gauge.

2.4. Fluidized Bed Testing. To determine the physical suitability of the oxygen carriers, as well as to further investigate reaction performance, the materials were subjected to fluidized-bed testing under CLOU conditions. The samples were oxidized in air and were allowed to decompose (reduce) under nitrogen. The physical durability (resistance to both attrition and agglomeration) of the material was evaluated at temperatures between 750 and 950 °C.

The fluidized bed reactor comprises a quartz tube housed within a Carbolite VST 12/600 Clamshell furnace with a temperature ceiling of 1200 °C. The quartz reactor (Figure 2) has four zones: (1) inlet, (2) sintered quartz distributor to support the particle bed, (3) freeboard expansion zone, and (4) outlet. Figure 3 is a schematic of the entire fluidized bed system. Gas flow was controlled by mass flow controllers and introduced to the reactor housed within the furnace. The product gas was filtered for fines capture, the water was condensed from the gas, and then the gas was analyzed using a 4-channel California Analytical Instruments ZRE analyzer. The analyzer measures the concentrations of CO, CO_2, and CH_4 by nondispersive infrared sensors and O_2 using a fuel cell sensor. The total volumetric flow rate of dry gas was tracked using a dry gas meter.

Tests in the fluidized bed system were conducted over multiple oxidation/reduction cycles. For each experiment, approximately 20 g of carrier sized between 105 and 150 μm was loaded into the bed, which was placed into the furnace and heated from room temperature to the target reaction temperature at a rate of 5 to 7 °C/min while fluidizing with air. For each reduction/oxidation cycle, nitrogen was fed to the bed at 1.0 to 1.5 standard liters per minute and maintained until the analyzer showed negligible oxygen concentration (30 to 60 min). The fluidizing gas was then switched to air to reoxidize the carrier, and air flow was maintained for 30 min. The ratio of actual superficial velocity (U) to the minimum fluidization velocity (U_{mf}) or U/U_{mf} was calculated to be between 10 and 24 for the various carriers and conditions studied.[20]
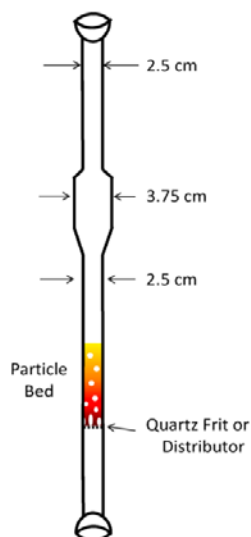
Figure 2. Schematic of quartz reactor used for fluidized bed studies. The particle bed is held, and the reactant gas is distributed by a sintered quartz frit. The particle bed is 2.5 cm in diameter.
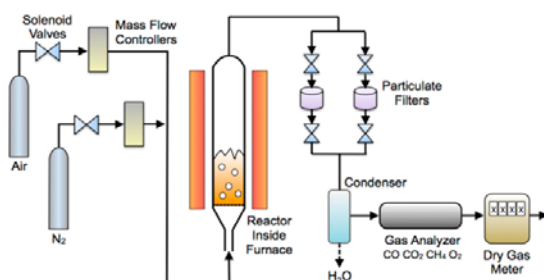

Figure 3. Schematic of fluidized bed test system.

Figure 4. SEM images of WI-20 prepared by wet impregnation using (a) 1 addition, (b) 2 additions, (c) 4 additions, and (d) 8 additions.

Figure 5. SEM images of RV-20 prepared by rotary evaporation using (a) 1 addition, (b) 4 additions, and (c and d) 8 additions. The arrow in c indicates the darker area which is identified as SiC by EDS.

3. RESULTS AND DISCUSSION

3.1. Comparison of Preparation Techniques. *3.1.1. Wet Impregnation versus Rotary Evaporation.* The WI-20 and RV-20 carriers were prepared identically using SiC powder, with the exception that the WI-20 was made using the conventional incipient wetness technique and the RV-20 was prepared using the rotary evaporation technique. Figure 4 shows SEM images of samples prepared by wet impregnation. EDS imaging did confirm that the portion that is darker is the SiC and the lighter portion is CuO. SEM images show that the majority of the CuO clumped together and did not deposit uniformly onto the SiC surface. The quality of CuO deposition was not improved by multiple additions for all the wet impregnation samples.

Figure 5 shows SEM images of the RV-20 carrier prepared by rotary evaporation. Looking at images Figure 5a and b, it is apparent that about half of the SiC surface is coated. SEM images of the 8 addition sample (Figure 5c and d) show a very uniform coating all across the SiC surface. Multiple additions using the rotary evaporator improved the evenness of CuO coating. Figure 5c shows a portion where the CuO coating must have chipped away or fallen off the SiC surface giving a
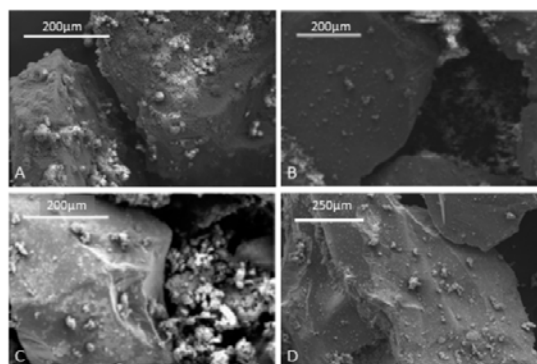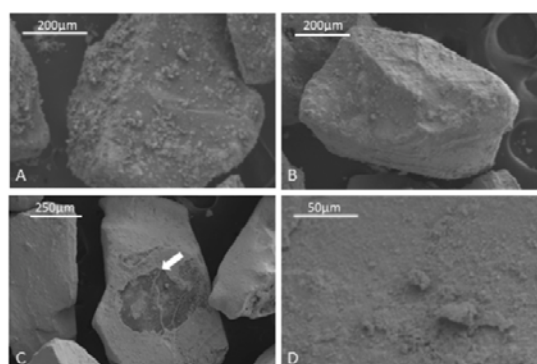
visualization of how thick the CuO coating was coated on the rest of the SiC surface.

To compare the reactivity of the oxygen carriers produced by wet impregnation and those prepared by rotary evaporation, oxidation and reduction rates were measured on 25−35 mg samples using the Q600 TGA at 935 °C. All samples had 20 wt % CuO, and carriers produced using 1, 2, 4, and 8 copper addition cycles were tested. For each TGA experiment, five oxidation/reduction cycles were conducted. For each of the five cycles between CuO and Cu_2O, a rate constant was calculated for the spontaneous decomposition step and for the oxidation step in the manner described earlier. A large difference was observed between the rate constants calculated for the first cycle when compared to the other four cycles, so the first cycles were omitted in the calculations used to obtain the average rate constants reported in Table 3.

As can be seen from Table 3, the carriers prepared by rotary evaporation have a much faster average rate of reaction than those prepared by the wet impregnation method for both the oxidation and spontaneous reduction reactions. There is no statistical trend in the observed reaction rates relating to the number of CuO additions for either method. Figure 6 and Figure 7 show a comparison of all reaction rates constants measured for the WI and RV carriers. The individual rate

Energy & Fuels

Table 3. Average Rate Constants during Oxidation and Reduction at 935 °C for 20 wt % CuO Oxygen Carriers Prepared with SiC Powder

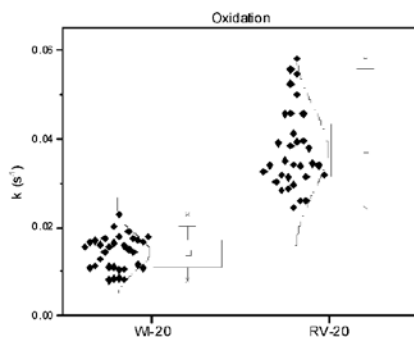| method of preparation	no. of Cu additions to achieve 20 wt % CuO			
	1	2	4	8
	oxidation rate constant $(s^{-1}) \times 1000$			
wet impregnation	14	17	11	15
rotary evaporation	43	28	44	35
	reduction rate constant $(s^{-1}) \times 1000$			
wet impregnation	7.2	6.0	4.6	6.4
rotary evaporation	15	14	13	9.0

Figure 6. Comparison of oxidation rates at 935 °C for carriers prepared by wet impregnation (WI-20) and rotary evaporation (RV-20) methods.
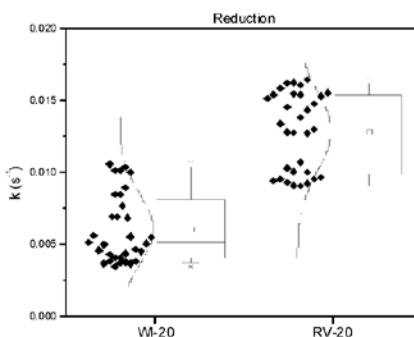

Figure 7. Comparison of reduction rates at 935 °C for carriers prepared by wet impregnation (WI-20) and rotary evaporation (RV-20) methods.

constants for each oxidation and reduction cycle that went into calculating the average values reported in Table 3 are present in the figures. It is apparent that there is a statistical difference in rates between the preparation methods. While there is some overlap in the data between preparation methods, statistical analysis confirms that the RV carriers average rate values are significantly greater than those of WI carriers.

Based on SEM imaging and the measured reaction rates, oxygen carriers prepared using the rotary evaporation method are superior to those prepared by wet impregnation. The addition of CuO to the SiC powder was more evenly distributed on the surface, thus leading to superior reaction rates. All subsequent oxygen carriers were prepared by impregnation by rotary evaporation using multiple additions.

3.1.2. Bake-then-Coat versus Coat-then-Bake. The RV-BTC-20 and RV-CTB-15 carriers were prepared identically, except that BTC was produced using the bake-then-coat method and CTB was prepared using the coat-then-bake method described previously. The same ratio of copper(II) nitrate to support material was used for each. The lower copper content of the CTB material (Table 2) is due to the increase in mass of the support material as it oxidized during baking step. In initial TGA experiments, the BTC carrier displayed better reaction rates for both oxidation and reduction reactions (Table 4) which were calculated for the fourth oxidation/reduction

Table 4. Rate Constant Values from TGA Experiments for BTC and CTB Carriers at 935 °C

oxygen carrier	oxidation rate constant (s^{-1}) $\times 1000$	reduction rate constant (s^{-1}) $\times 1000$
RV-BTC-20[a]	15	11
RV-CTB-15[a]	3.8	4.0
RV-CTB-40[a]	4.4	4.3
RV-CTB-40[b]	48	9.1

[a]Freshly prepared carrier. [b]After 20 h of fluidized bed experiments.

cycle using fresh oxygen carrier material. However, as will be shown later, the BTC carrier demonstrated poor performance in the fluidized bed, with the carrier agglomerating at temperatures lower than those targeted for chemical looping combustion processes, while the CTB carrier performed well. Consequently, subsequent carriers were all prepared using the coat-then-bake method. For the CTB carriers, the CuO is impregnated into a support material with a high pore volume. After baking and sintering the support material, the pore volume is decreased greatly, and the CuO gets secured inside the particles. It is reasonable to conclude that the CuO content allowable by the CTB method of preparation could be increased by varying the physical characteristics of the raw support material, such as increasing the pore volume or changing the size or shape of the particles; however, further work is needed to determine what effects changing the properties of the support material would have on carrier performance.

3.2. Physical Characteristics of Carrier Particles. SEM and corresponding EDS images (Figure 8) were taken of the RV-CTB-15 carrier at three stages in the preparation process: after the impregnation of CuO was complete, after baking was complete, and after fluidized bed testing. The images taken of the oxygen carrier before baking confirm (Figure 8a) that the predominant element on the external surface is Cu while Si is less apparent. Images of oxygen carrier after baking and after fluidized bed experiments (Figure 8b and c, respectively) show that Si becomes more apparent while Cu becomes less apparent. These results are favorable because, as de Diego et al. have reported, the CuO deposited on the external surface of support particles is likely to be lost during fluidization.[15] The coat-then-bake method allows for the CuO to be buried inside the SiO_2 which reduces the amount of CuO likely to be lost in fluidized bed environments and contribute to agglomeration.

The SEM images also show that multiple spheres can fuse together during the sintering of the β-SiC. The fused spheres are mostly broken apart after being crushed and sieved, but some remained fused together. The amount of fused spheres in images taken of the oxygen carriers before and after fluidized bed experiments were not significantly different, so it is believed
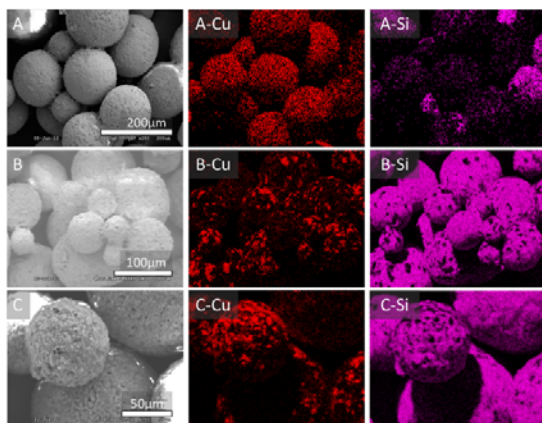
Energy & Fuels   Article

Figure 8. SEM and corresponding EDS images for elemental Cu and Si of RV-CTB-15 (a) before baking, (b) after baking, and (c) after fluidization.

that fusions of spheres occur during the baking step and are not formed in fluidized bed experiments.

3.3. Oxygen Carrying Capacity. The ability of the carriers to maintain oxygen carrying capacity over many oxidation/reduction cycles was evaluated in the TGA by cycling the gas between air and nitrogen. Results for 20 cycles of the RV-CTB-40 carrier at 900 °C are shown in Figure 9. The oxygen carrying capacities, represented by the weight difference between cycles, as well as reactivity as observed by the time to fully oxidized or reduce the carrier, remained constant throughout the 20 cycles. Similar oxygen carrying capacity was observed for RV-CTB-40 before and after being processed in the fluidized bed for more than 20 h. The change in mass of the samples before and after fluidized bed experiments remained consistent with the CuO load of 40 wt %. All of the CuO remained active and able to react without interference from the support material.

3.4. Rates of Oxidation and Spontaneous Reduction. TGA experiments were performed on the RV-CTB-40 carrier, and the rates of reaction are reported in Table 4. Initial TGA experiments using freshly made carriers were insufficient to determine the true reaction rates and evaluate the carriers prepared by the CTB method due to the great difference observed in reaction rates for both oxidation and reduction
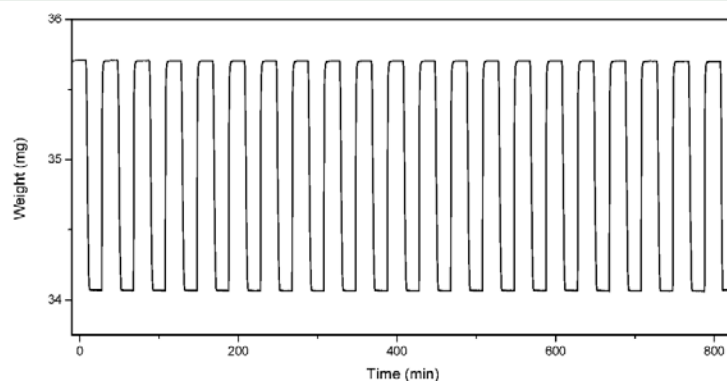
reactions between samples tested after seven days of baking at 980 °C and samples taken after 20 h' worth of fluidized bed experiments. This behavior suggests that as the conversion of β-SiC to SiO_2 becomes more complete, the rates of oxidation and reduction improve.

Conversion of the oxidation of RV-CTB-40 versus time at each temperature is presented in Figure 10. For all temper-
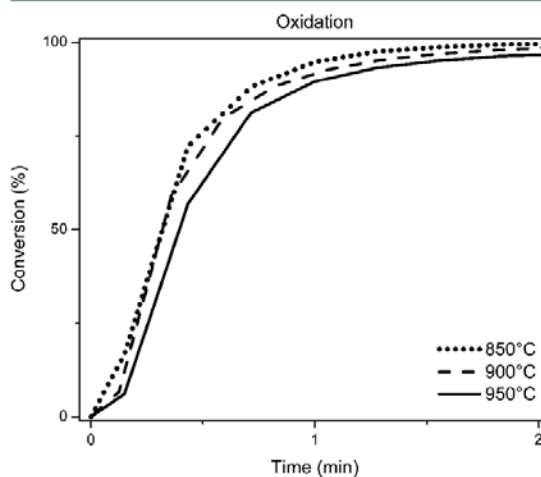

Figure 10. Oxidation of Cu_2O to CuO for RV-CTB-40 measured in the TGA at 850, 900, and 950 °C.

atures tested, 90% conversion was achieved in about a minute. The rate of oxidation slowed somewhat as temperature increased, which is consistent with observations from other studies[14,16,21] at this temperature range and is a result of lower oxygen driving force as the equilibrium partial pressure of oxygen increases with temperature.

The conversion profile of spontaneous reduction (release of O_2) for the RV-CTB-40 carrier is shown in Figure 11. At the highest temperature (950 °C), reduction was complete in about 1.5 min. At lower temperatures, the rate of reduction was correspondingly lower, such that completion at 900 °C required about 4 min and 850 °C required about 12 min. The rates of the reactions were used to determine the activation energy of the reaction. The observed activation energy is 220
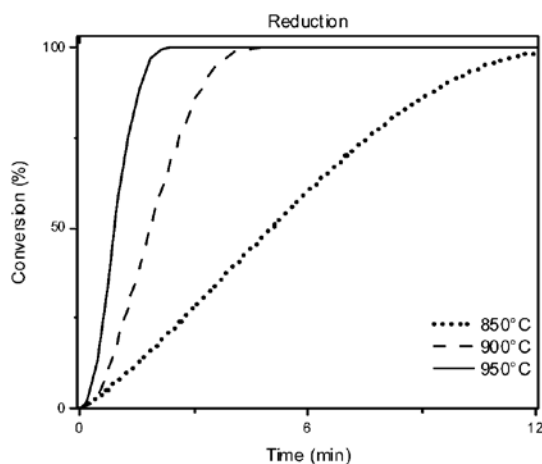

Figure 9. TGA trace of RV-CTB-40 for 20 oxidation/reduction cycles at 900 °C.

Figure 11. Reduction of CuO to Cu_2O for RV-CTB-40 measured in the TGA at 850, 900, and 950 °C.

Table 5. Measured Agglomeration Temperature in the Fluidized Bed

oxygen carrier	CuO loading (wt%)	agglomeration temp (°C)
RV-BTC-20	19	850
RV-CTB-15	15	>1000
RV-CTB-40	40	>1000
RV-CTB-60	61	950

kJ/mol, (Figure 12) which is comparable to what has been reported for reduction of other copper-based carriers operating in the CLOU regime.[6,22]
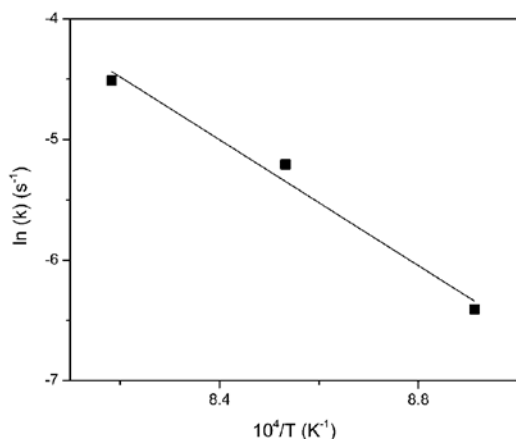

Figure 12. Arrhenius plot for spontaneous reduction of oxygen carrier RV-CTB-40.

3.5. Fluidized Bed Performance. To test suitability of use in fluidized bed systems, the RV-CTB carriers with 15, 40, and 60 wt % CuO were fluidized in the lab-scale reactor as the temperature was steadily increased to 1000 °C. The RV-CTB-15 and RV-CTB-40 materials remained fluidized to a temperature of 1000 °C and showed no agglomeration. The RV-CTB-60 material showed no agglomeration in tests up to 900 °C, but agglomerated at about 950 °C, suggesting that the maximum CuO content for practical use in fluidized bed systems, using β-SiC as the support material and using the coat-then-bake method, is somewhere between 40 and 60 wt % CuO. Results of agglomeration tests are summarized in Table 5.

The RV-CTB-40 carrier underwent a total of 10 oxidation and reduction cycles that were carried out at 850, 900, and 950 °C. The total time spent in the fluidization experiments was

approximately 20 h. The crushing strengths of the RV-CTB-40 and RV-CTB-60 carriers after fluidized bed experiments were determined to be 4.1 ± 0.2 N and 4.5 ± 0.2 N, respectively. A rule of thumb is that carriers with crushing strengths less than 1.0 N are not suitable for fluidized bed testing. The high crushing strength observed for these carriers is supported in SEM images after fluidized bed experiments (Figure 8c), as the particles retained their spherical shape throughout all experiments. A subsequent study evaluated attrition and associated loss of fines by measuring the mass of material captured on filters downstream of the reactor, shown in Figure 3. Each hour the gas flow was switched from one filter to another so that the progression of fines generation could be measured on an hourly basis. For both the RV-CTB-40 and RV-CTB-60 materials, steady-state loss of bed material averaged roughly 0.002 wt % per hour, confirming the physical resiliency of the particles in a fluidized bed environment.

Fluidized bed tests performed with the bake-then-coat oxygen carrier (RV-BTC-15) resulted in agglomeration at roughly 850 °C. As noted earlier, this performance is unacceptable, so the BTC method was not investigated further. Overall, the fluidized bed tests indicate that the ability of the CTB materials to resist agglomeration was due to the method used to prepare the oxygen carriers and not just the result of the raw materials used.

Fluidized bed experiments were carried out in inert conditions. Experiments involving coal are needed to further understand the characteristics of oxygen carriers. As is the case in conventional Cu-based CLC, the volatiles will react directly with the oxygen carriers; however, the spontaneous reduction of the oxygen carriers will be required to complete combustion of the fuel.

4. CONCLUSIONS

Oxygen carriers prepared by copper impregnation using silicon carbide as an initial support material, then calcining the carrier in air to oxidize the β-SiC to SiO_2, are promising for chemical looping with oxygen uncoupling processes. Carrier performance is improved by (1) using a rotary evaporation technique to evaporate the copper nitrate solvent, (2) using the coat-then-bake method in which copper is loaded onto the β-SiC particles before they are calcined to SiO_2 and (3) loading the copper through multiple additions. The commercially available β-SiC catalyst support is strong, and the CTB method of preparing oxygen carriers provides protection from CuO being worn off and lost as fines or agglomerating in the reactor while allowing for oxygen carrier to remain reactive. CuO loadings of as much as 60 wt % were achieved, and oxygen carriers with a CuO load of up to 40 wt % were reactive in TGA and fluidized bed experiments and showed no signs of agglomeration and insignificant attrition during extended fluidized bed testing at temperatures up to 1000 °C.

Energy & Fuels

■ AUTHOR INFORMATION

Corresponding Author

*E-mail: sean.b.peterson@utah.edu.

Notes

The authors declare no competing financial interest.

■ ABBREVIATIONS

BET = Brunauer−Emmett−Teller
BTC = bake-then-coat
CLOU = chemical looping with oxygen uncoupling
CTB = coat-then-bake
EDS = energy dispersive X-ray spectroscopy
RV = rotary evaporator
SEM = scanning electron microscopy
TGA = thermogravimetric analyzer
WI = wet impregnation

■ REFERENCES

(1) Lyngfelt, A.; Leckner, B.; Mattisson, T. A fluidized-bed combustion process with inherent CO_2 separation; application of chemical-looping combustion. *Chem. Eng. Sci.* **2001**, *56* (10), 3101−3113.

(2) Ekstroem, C.; Schwendig, F.; Biede, O.; Franco, F.; Haupt, G.; de Koeijer, G.; Papapavlou, C.; Rokke, P. E. Techno-economic evaluations and benchmarking of pre-combustion CO_2 capture and oxy-fuel processes developed in the European ENCAP project. *Energy Procedia* **2009**, *1* (1), 4233−4240.

(3) Mattisson, T.; Lyngfelt, A.; Leion, H. Chemical-looping with oxygen uncoupling for combustion of solid fuels. *Int. J. Greenhouse Gas Control* **2009**, *3* (1), 11−19.

(4) Azad, A.-M.; Hedayati, A.; Ryden, M.; Leion, H.; Mattisson, T. Examining the Cu-Mn-O spinel system as an oxygen carrier in chemical looping combustion. *Energy Technol. (Weinheim, Ger.)* **2013**, *1* (1), 59−69.

(5) Azimi, G.; Ryden, M.; Leion, H.; Mattisson, T.; Lyngfelt, A. Iron manganese oxide combined oxides as oxygen carrier for chemical-looping with oxygen uncoupling. *AIChE J.* **2013**, *59* (2), 582−588.

(6) Mattisson, T. Materials for chemical-looping with oxygen uncoupling. *ISRN Chem. Eng.* **2013**, 526375−19 pp.

(7) Baraki, R.; Konya, G.; Eyring, E. M. *Investigation of the Reaction Kinetics of Oxygen Carriers in Chemical Looping Combustion*, Twenty-Sixth Annual International Pittsburgh Coal Conference, Pittsburgh, PA, 2009.

(8) Arjmand, M.; Azad, A.-M.; Leion, H.; Lyngfelt, A.; Mattisson, T. Prospects of Al_2O_3 and $MgAl_2O_4$-supported CuO oxygen carriers in chemical-looping combustion (CLC) and chemical-looping with oxygen uncoupling (CLOU). *Energy Fuels* **2011**, *25* (11), 5493−5502.

(9) Wang, S.; Luo, M.; Wang, G.; Wang, L.; Lv, M. Analysis of reactivity of a CuO-based oxygen carrier for chemical looping combustion of coal. *Energy Fuels* **2012**, *26*, 3275−3283.

(10) Mattisson, T.; Leion, H.; Lyngfelt, A. Chemical-looping with oxygen uncoupling using CuO/ZrO_2 with petroleum coke. *Fuel* **2009**, *88* (4), 683−690.

(11) Johansson, M.; Mattisson, T.; Lyngfelt, A. Investigation of Mn_3O_4 with stabilized ZrO_2 for chemical-looping combustion. *Chem. Eng. Res. Des.* **2006**, *84* (A9), 807−818.

(12) Adanez-Rubio, I.; Gayan, P.; Garcia-Labiano, F.; de Diego, L. F.; Adanez, J.; Abad, A. Development of CuO-based oxygen-carrier materials suitable for chemical-looping with oxygen uncoupling (CLOU) process. *Energy Procedia* **2011**, *4*, 417−424.

(13) Adanez-Rubio, I.; Arjmand, M.; Leion, H.; Gayan, P.; Abad, A.; Mattisson, T. P.; Lyngfelt, A. Investigation of combined supports for Cu-based oxygen carriers for chemical-looping with oxygen uncoupling (CLOU). *Energy Fuels* **2013**, *27*, 3918−3927.

(14) Eyring, E. M.; Konya, G.; Lighty, J. S.; Sahir, A. H.; Sarofim, A. F.; Whitty, K. Chemical looping with copper oxide as carrier and coal as fuel. *Oil Gas Sci. Technol.* **2011**, *66* (2), 209−221.

(15) de Diego, L. F.; Garcia-Labiano, F.; Gayan, P.; Celaya, J.; Palacios, J. M.; Adanez, J. Operation of a 10 kWth chemical-looping combustor during 200 h with a $CuO-Al_2O_3$ oxygen carrier. *Fuel* **2007**, *86* (7−8), 1036−1045.

(16) Gayan, P.; Adanez-Rubio, I.; Abad, A.; de Diego, L. F.; Garcia-Labiano, F.; Adanez, J. Development of Cu-based oxygen carriers for Chemical-Looping with Oxygen Uncoupling (CLOU) process. *Fuel* **2012**, *96*, 226−238.

(17) Adanez-Rubio, I.; Gayan, P.; Abad, A.; de Diego, L. F.; Garcia-Labiano, F.; Adanez, J. Evaluation of a spray-dried $CuO/MgAl_2O_4$ oxygen carrier for the chemical looping with oxygen uncoupling process. *Energy Fuels* **2012**, *26* (5), 3069−3081.

(18) Moene, R.; Makkee, M.; Moulijn, J. A. High surface area silicon carbide as catalyst support. Characterization and stability. *Appl. Catal., A* **1998**, *167* (2), 321−330.

(19) Ledoux, M. J.; Pham-Huu, C. Silicon carbide: A novel catalyst support for heterogeneous catalysis. *CATTECH* **2001**, *5* (4), 226−246.

(20) Kunii, D.; Levenspiel, O. *Fluidization Engineering*, 2nd ed.; Butterworth-Heinemann: Newton, MA, USA, 1991.

(21) Zhu, Y.; Mimura, K.; Isshiki, M. Oxidation mechanism of Cu_2O to CuO at 600−1050°C. *Oxid. Met.* **2004**, 207−222.

(22) Sahir, A. H.; Sohn, H. Y.; Leion, H.; Lighty, J. S. Rate analysis of chemical-looping with oxygen uncoupling (CLOU) for solid fuels. *Energy Fuels* **2012**, *26* (7), 4395−4404.

APPENDIX D

ILMENITE AS AN INERT SUPPORT FOR COPPER-BASED

OXYGEN CARRIER MATERIAL FOR USE IN CLOU

D.1 Abstract

Among the critical aspects needing investigation for the implementation of chemical-looping into an industrial-scale reactor, oxygen carrier development remains at the forefront. A successful oxygen carrier will have a high carrying capacity, high redox rates and an optimal relationship between cost and physical durability. Both iron and copper have displayed desirable characteristics for a chemical-looping reactor. The high reactivity, oxygen carrying capacity and CLOU capabilities make copper a potentially suitable oxygen carrying material. When coupled with the superior physical durability of iron, a copper/iron bimetallic carrier proves very effective as an oxygen carrier material. Ilmenite is a low-cost iron-ore that has been proven an effective and inexpensive oxygen carrier material. The performance of ilmenite/copper bimetallic carrier in both TGA and fluidized-bed has been investigated in this work. To test the reactivity with solid fuels, the char of a bituminous coal (Illinois #6) has been tested along with the $Cu\text{-}FeTiO_2$ carrier in a fluidized-bed.

D.2 Introduction

Chemical-looping with oxygen uncoupling (CLOU) is an energy generation technology suitable for use with solid fuels such as coal, petroleum coke and biomass, that offers inherent separation of CO_2 with comparatively little energy penalty. CLOU involves cycling metal-based solid "oxygen carrier" particles between two fluidized-bed reactors. In the air reactor, the metal is oxidized by oxygen, resulting in an O_2-depleted effluent stream. The oxidized carrier is transported to a fuel reactor fluidized by steam and/or CO_2, where the thermodynamics of CLOU carriers are such that gaseous oxygen is

favored. The released O_2 combusts the fuel, resulting in a product gas of mostly CO_2 and steam. Condensation of the steam results in a nearly pure stream of CO_2 suitable for sequestration with little additional processing required. CLOU is recognized as one of the most promising CO_2 capture-ready technologies for energy production from coal, and research in this area has accelerated rapidly in recent years.

A key consideration of CLOU technology is the oxygen carrier material. Several pure and mixed metals have been identified as having suitable thermodynamics for oxygen release in the fuel reactor [1,2,3,4]. Many investigations have focused on copper, cycling between oxidized cupric (CuO) and cuprous (Cu_2O) oxide:

$$Cu_2O(s) \ + \ \tfrac{1}{2}\,O_2(g) \ \leftrightarrow \ 2\,CuO(s) \hspace{3em} (22)$$
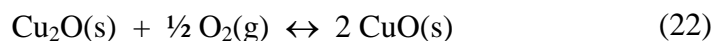
In thermogravimetric (TGA) experiments, CuO/Cu_2O powder, on its own, can be oxidized to CuO in an air environment and reduced to Cu_2O in an inert environment over many cycles [100]. However, in fluidized-bed conditions similar to those that would be used in a commercial CLOU system, pure CuO agglomerates, which makes it unsuitable for use in a fluidized system. Support materials, such as alumina, titania, zirconia, ceria and sepiolite, have been investigated to act as inert binders that allow the use of CuO in the fluidized conditions required for CLOU [1, 4, 6-11]. While the main concern that justifies the need of a support material is agglomeration, the support material also improves the kinetics of the oxidation and reduction reactions of the copper oxides [7].

A simple method for introducing CuO to a support material to prepare oxygen carriers for CLOU experiments is incipient wetness impregnation [8]. The incipient wetness method has provided supported CuO that performed well in TGA experiments.

However, de Diego et al. has reported that CuO on the external surface of the support material can be worn off in a fluidized environment, contributing to agglomeration of the material. This means that the CuO content is limited by the pore size of the support material for oxygen carriers prepared by incipient wetness. Compounds that are stable in both oxidizing and reducing environments at temperatures up to 1000°C and have a significant pore size are not readily available. Other methods for preparing supported copper particles, such as mechanical mixing [12], spray drying [13] and freeze granulation [1] have shown promise. But in some cases these methods have produced materials that lack the mechanical strength needed to be viable candidates for use in CLOU [12, 13].

A few studies have been performed which look into bimetallic oxygen carriers. A bimetallic carrier presents the developer with the opportunity to customize an oxygen carrier based upon the strengths of the individual components. For example, by creating an oxygen carrier based upon iron and copper, a material may be engineered with the structural integrity of iron while maintaining the CLOU capabilities of copper. Siriwardane et al. reported that the bimetallic combination of iron and copper as an oxygen carrier performed well while using a synthesis gas for reduction up to 900 °C [14].

D.3 Experimental

D.3.1 Preparation and Characterization of Oxygen Carriers

D.3.1.1 Ilmenite

Natural ilmenite powder (Atlantic Equipment Engineers) was sieved to a range of 150–250 microns and used as a support for the CuO. Adánez et al. [15] observed an increase in the rates of both oxidation and reduction of ilmenite after multiple cycles of oxidation in air and reduction in gas mixtures containing H_2, CO or CH_4. They observed that the increase in reaction rates occurs in only a few cycles, and referred to this phenomenon as an "activation period." Although the oxidation and reduction rates increased, a decrease in oxygen carrying capacity from 4 wt% to 2 wt% was observed after approximately 100 cycles. It is not clear, however, what mechanism(s) may be responsible for these changes. It is possible that during the first few cycles as the reaction rates increase that the redox conditions may be increasing a transport resistance by, for example, altering the micropore volume. Because the properties of ilmenite change during activation, it is important to investigate the deposition of CuO on both activated and nonactivated ilmenite. Some of the ilmenite material was thus activated by processing the raw material in a lab-scale fluidized-bed at 900°C while cycling between air (oxidation) and 5% CH_4 in N_2 (reduction) for 30 minutes each, for five complete cycles.

D.3.1.2 Preparation Technique

CuO was loaded onto the ilmenite by impregnation via rotary evaporation. A copper nitrate solution of about 2 M was prepared by dissolving copper(II) nitrate tri-

hydrate (Sigma-Aldrich) in acetone. The ilmenite powder and copper nitrate solution were mixed in a flask using a rotary evaporator. The materials were mixed and the acetone evaporated at an external temperature of approximately 50 °C to promote the quick evaporation of the solvent while avoiding bumping. Once the acetone had evaporated, a heating mantle was used to increase the temperature at a rate of approximately 25°C/min to a final external temperature of about 375°C. Once all of the material in the flask had turned black and the decomposition of copper(II) nitrate to CuO was complete, the flask was removed and allowed to cool. After the flask had cooled, the next addition of CuO took place. For each sample, copper(II) nitrate was added to the ilmenite in multiple additions to reach the target CuO content. A summary of the oxygen carriers produced in this study is reported in Table 15.

D.3.1.3 Thermogravimetric Analysis

Each oxygen carrier material was analyzed in a thermogravimetric analyzer (TGA) to determine its reactivity in multicycle tests. The TGA experiments were conducted using a TA Q500 instrument. For each experiment, the sample with a mass between 30-40 mg was heated to the target temperature in 100 mL/min of air. Nitrogen gas, at a rate of 100 mL/min, was then used to promote spontaneous reduction of the sample. The cycle was then completed as the sample was re-oxidized in air. Fractional completion, X, describes reaction progression. Fractional completion is defined in terms of mass at a given time (m_t), mass of the reduced (Cu_2O) sample (m_{red}) and mass of fully oxidized (CuO) material (m_{ox}). Fractional completion for oxidation, X_{ox}, and reduction, $X_{red,}$ are defined as follows:

Table 15. Summary of oxygen carrier materials prepared. The name indicates if the ilmenite was activated prior to CuO deposition (ACT) or if nonactivated ilmenite was used (NA) and the number indicated the % CuO by weight of the material.

Code	CuO Loading (wt%)	Number of CuO Additions	BET Surface Area (m2/g)	Particle Size (µm)
ACT-20	20	6	0.299	150 – 250
NA-20	20	6	4.2	150 – 250
NA-30	30	9	2.3	150 – 250

1 All agglomeration was soft – particles were easily separated with mild physical agitation.

$$X_{ox} = \frac{m_t - m_{red}}{m_{ox} - m_{red}} \tag{23}$$

$$X_{red} = \frac{m_t - m_{ox}}{m_{red} - m_{ox}} \tag{24}$$

D.3.2 Fluidized-Bed Performance

Performance of the carriers in a fluidized-bed environment was evaluated in a lab-scale fluidized-bed system (FZB, Figure 38), which is modeled on a system developed at Chalmers University. The reactor is made of quartz and is housed within a Carbolite VST 12/600 Clamshell furnace with a maximum operating temperature of 1200°C. The reactor has four zones (Figure 39): (1) inlet, (2) sintered quartz distributor supporting the particle bed, (3) freeboard expansion zone and (4) outlet. The ID of the reaction tube is 2.5 cm. In order to maintain a well-fluidized system, the typical resting bed height was about 2.5 cm (or 1 diameter tall). Gas flow is controlled by a series of mass flow controllers and is introduced to the reactor housed within the furnace. The exit gas is filtered to remove fines and water is condensed from the gas before it is sent to a 4-channel California Analytical Instruments ZRE NDIR/fuel call analyzer. The analyzer
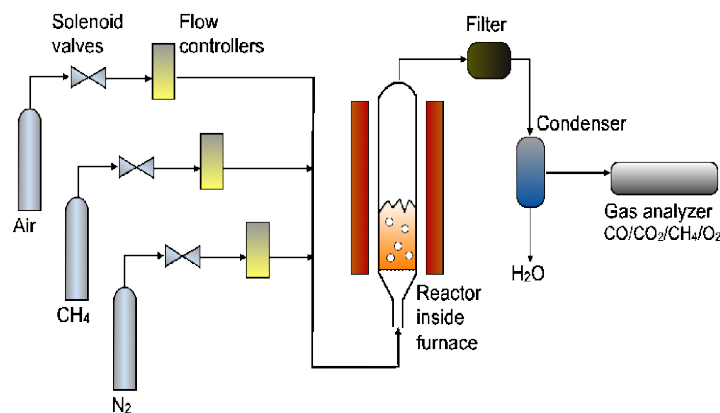
Figure 38: Schematic of the bench-scale fluidized-bed reactor system used at the University of Utah.

measures the volume percents of CO, CO_2, CH_4 and O_2. A dry gas meter measures the total volume of gas fed through the system.

For typical operation, the reactor was charged with 20-30 g of oxygen carrier particles and heated at 7 °C/min to 850°C. During heating, the bed was fluidized with nitrogen to mitigate agglomeration. Upon reaching 850°C, the fluidizing gas was cycled between nitrogen and air for 2 hours to encourage thermally driven migration of the copper oxide below the surface of the carrier. During cycling, each gas was fed for 30 minutes before switching to the other. The reactor was then heated further to 900°C and gases cycled again for 2 hours. Finally, the reactor temperature was raised to 950°C and 3 air/nitrogen cycles were performed.

Performance of the CuO/ilmenite carrier during CLOU combustion of coal was tested by introducing small batches of coal into the reactor. After the carrier underwent the initial cycling at progressively higher temperatures as described above, the temperature was adjusted to that for the coal experiments. The carrier was oxidized in air, after which excess air was removed by passing a very small flow of nitrogen (1 ml/min)
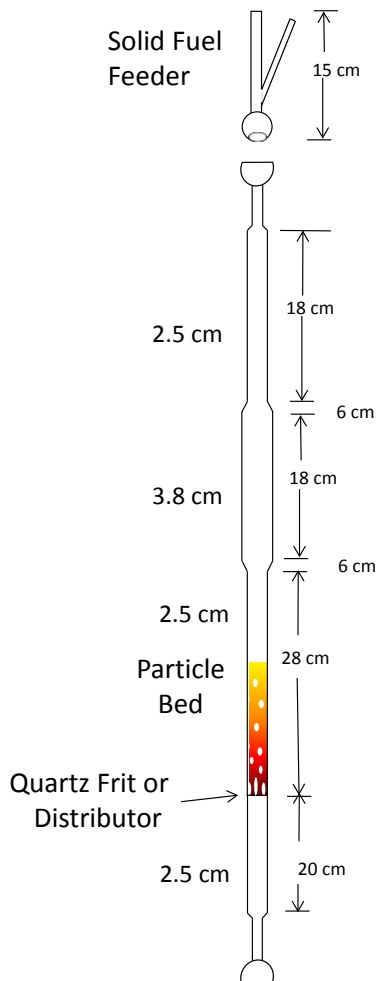
Figure 39: Schematic of quartz fluidized-bed reactor. The particle bed sets upon a porous quartz distributor with a nominal maximum pore size of 16 - 140 microns.

through the reactor for approximately 2 minutes. The gas flow was then shut off to

reduce blow-out of the fuel while it was added from the top of the reactor (Figure 39).

After the addition of the solid fuels the flow of nitrogen was increased to the standard

flow of 1 SLPM and the coal was allowed to react with oxygen released from the carrier

particles. The evolution of gases was monitored by the analyzer and gas meter. The fuel

was allowed to burn out evidenced by the increase in oxygen partial pressure and

decrease in CO_2 partial pressure. Upon completion, the reacting gas was switched back to air to regenerate the carrier. Coal processing was performed at two temperatures, 900 and 950°C.

The fuel used for testing was char made from Illinois #6, an eastern U.S. bituminous coal. The ultimate and proximate analyses of the coal are provided in Table 16. The coal was dried at 125°C for 3 hours to remove the moisture and then heated to 1000°C under nitrogen for 8 hours for devolatilization. The fuel was sieved to a particle size range of 150–250 microns. The amount of fuel used in the tests was calculated so that the carbon in the fuel could be completely oxidized by the theoretical amount of oxygen released from the oxygen carrier sample in the reactor, while allowing for 10% excess oxygen. Conversion of the fuel is calculated based on the conversion of carbon to carbonaceous gases – assuming the char has been stripped of all volatile matter.

For the combustion of solid fuels, it is requisite to perform a carbon balance analysis to evaluate conversion of the fuel and to understand effective combustion rates. The carbon balance is performed using the flow rate of the purge gas as a baseline. It is assumed that the gases recorded by the analyzer, along with the inert purge, combine to make the majority of the gases evolved from fuel combustion. By assuming that any other species evolved from the combustion are in quantities small enough to have a negligible effect on the total flow rate of the effluent gases, the molar flow rate of the analyzed species may be determined.

The total volumetric flow rate may be determined by calculating the volume fraction of the inert purge gas (ϕ_{purge}), assuming that is the difference between one and the sum the volume fractions (ϕ_i) of CO_2, CO, CH_4 and O_2.

Table 16: Illinois #6 coal proximate, ultimate and heating value analysis.

Proximate Analysis

Moisture (wt% as received fuel)	2.54
Ash (wt% Dry)	12.33
Volatile matter (wt% dry)	39.40
Fixed carbon (wt% dry)	48.28

Ultimate Analysis (wt% dry ash-free)

Carbon	78.91
Hydrogen	5.50
Nitrogen	1.38
Sulfur	4.00
Oxygen	10.09
Chlorine	0.11

Heating Value

HHV, dry (Btu/lb)	12,233

$$\phi_{\text{purge}} = 1 - \sum \phi_i ; \quad i = CO_2, CO, CH_4, O_2 \qquad (25)$$

The volume fraction of the purge gas (N_2) is then used to calculate the total

effluent volumetric flow rate of gases (Q_{tot}).

$$Q_{\text{tot}} = \frac{\phi_{N_2}}{Q_{N_2}} \qquad (26)$$

The total volumetric flow rate multiplied by the individual specie volume

fractions gives the volumetric flow rate of each of the individual gaseous species. The

ideal gas equation is then employed to determine the molar flow rate of each component

(equation 28).

$$Q_i = \phi_i \times Q_{tot}; \quad i = CO_2, CO, CH_4, O_2 \qquad (27)$$

$$n_i = \frac{Q_i P}{RT} \qquad (28)$$

The carbon balance is then performed by adding the total number of moles of

carbonaceous gases and then multiplying by the molecular weight of carbon - 12 g/mole.

The resulting mass of carbon is compared to the mass of the sample introduced to the

reactor generating a conversion profile based on the conversion of carbon.

D.4 Results and Discussion

D.4.1 Characteristics of the Oxygen Carrier Particles

D.4.1.1 Microscopic Imaging

The investigated materials were imaged by a Hitachi S-300N scanning electron microscope (SEM) to permit visualization of the surface on the scale of 10 μm to 1 mm. Energy dispersive X-ray spectroscopy (EDS) was carried out with an EDAX HIT S3000N 132-10 alongside the SEM images to confirm the appearance of and locate elemental titanium, iron, and copper. SEM images of ilmenite in both the fresh and activated states are included. Carrier NA-20 was observed by SEM immediately after being produced and after undergoing five oxidation and reduction cycles in TGA experiments. As seen in Figure 40, the surface of the nonactivated ilmenite is smooth while the surface of the activated ilmenite has acquired a rough surface. The surface roughness may be a consequence of carbon deposition during the reducing phase of the activation process, since methane may have been catalytically cracked by the ilmenite. EDS elemental mapping was used to identify the distribution of copper on the samples and to determine how TGA experiments affected carrier structure. Figure 40 images C and D show that the TGA experiments with air/N_2 cycling change the makeup of the particles. After TGA experiments, the EDS shows that little Cu is present on the surface in contrast to those particles which had not been used in TGA experiments. The particles that were exposed to several redox cycles in TGA experiments display a sponge-like surface. This could be the result of CuO migration due to the multiple reduction and oxidation cycles, but the EDS maps suggest that that is not the case; instead, the shown that activation of the ilmenite can alter the surface properties of ilmenite, it is possible
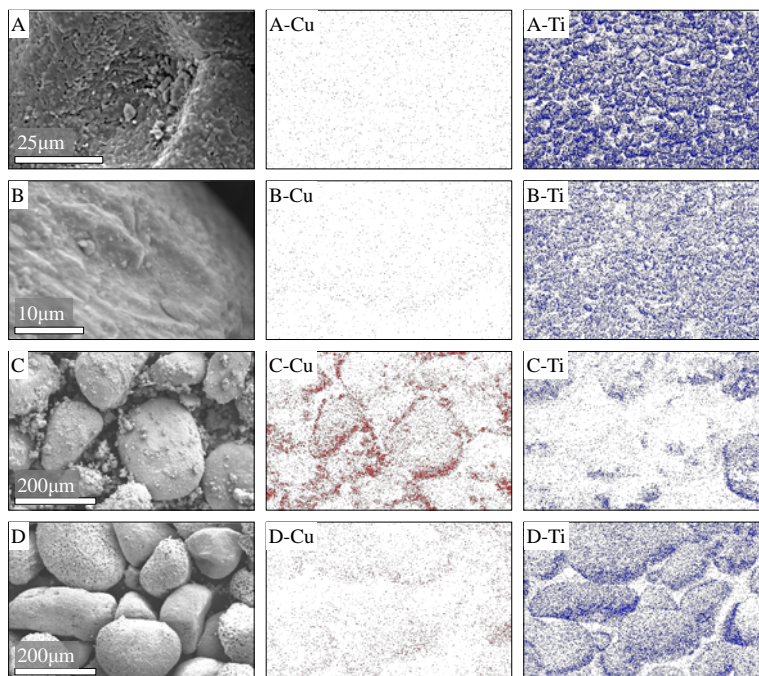
Figure 40: SEM images of A) activated ilmenite, B) nonactivated ilmenite, C) ACT20 before TGA experiment, and D) ACT20 after TGA experiment. C and D include EDS elemental mapping for elemental Cu and Ti.

that the addition of CuO and the multiple oxidation and reduction cycle have caused the surface of the ilmenite to be altered and engulf the CuO. The sponge-like surface could be the channels through which the oxygen travels to and from the particle.

D.4.1.2 Distribution of Cu, Fe and Ti Within Single Particles

Freshly prepared carriers NA-20 and ACT-20 were analyzed by laser ablation ICP-MS to determine composition across a cross-section of the material. Particles were fixed in an epoxy and allowed to set. The epoxy was then sliced and polished to expose cross-sections of the particles. As the 15μm wide laser scanned in a line across the material, the material was vaporized and the gas was analyzed by mass spectroscopy. The analytical technique allows determination of what elements are present to

within15μm.

For carrier ACT-20, Cu was present only very near the surface of the particle (Figure 41). In the inside of the particle, essentially no Cu was detected. In contrast, the results for carrier NA-20 (Figure 42) show a distribution of Cu much less concentrated at the particle surface and appears to have penetrated to the center of the particle, albeit at low concentrations. This indicates that the activation of the ilmenite with the procedure used in this study does not improve penetration or evenness of copper distribution in the particle. Thus, preprocessing of the ilmenite can affect final carrier properties. Further investigation would be needed to determine the ideal method of preparation of the oxygen carrier material and the ideal particle size to maximize the amount of CuO present and the reactivity of the material.
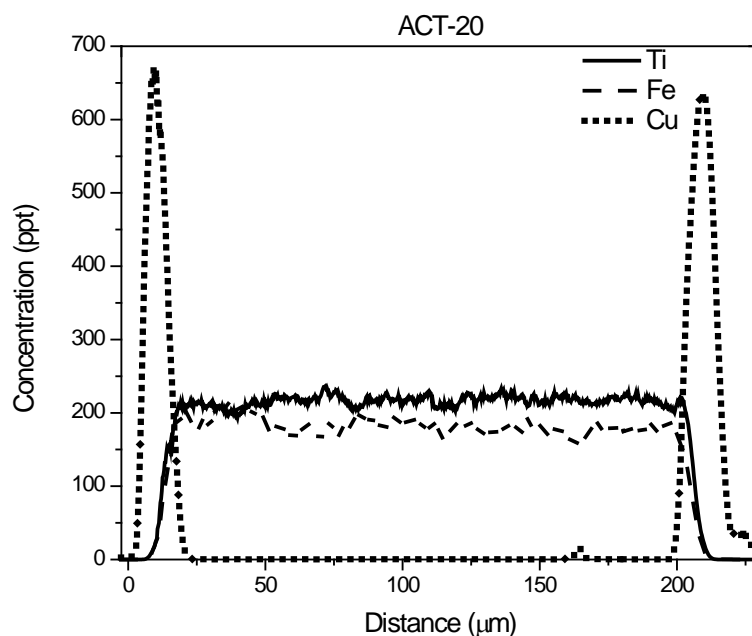
Figure 41: Laser ablation results for carrier ACT-20, produced using activated ilmenite. The elemental concentrations are shown in parts per thousand (ppt).
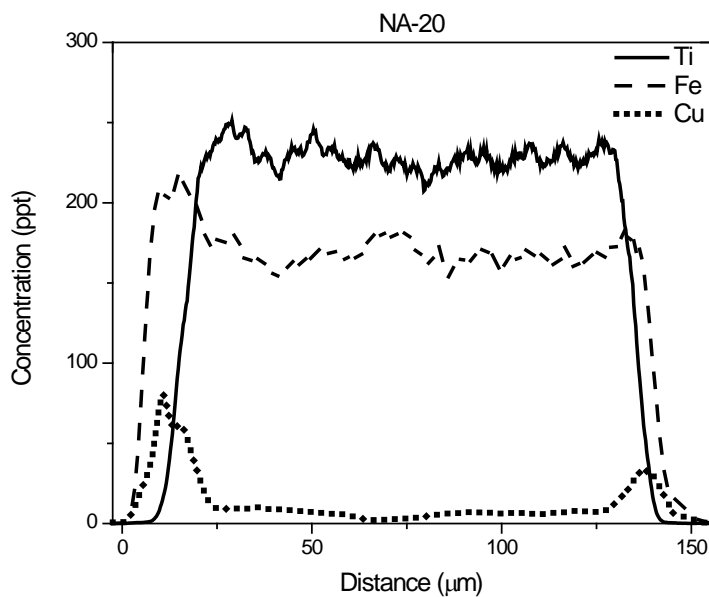
Figure 42: Laser ablation results for carrier NA-20. The elemental concentrations are shown in parts per thousand (ppt).

D.4.1.3 Oxygen Carrying Capacity

Multicycle TGA experiments were performed in which the oxygen carriers were cycled between the reduced and oxidized forms for over 10 cycles (Figure 43). The measured mass increase during oxidation indicated that the copper loading was very close to the target loading. No significant change in mass between cycles was observed, indicating that oxygen carrying capacity of the copper could be sustained, and that no interaction between the ilmenite and copper reduced carrying capacity. It was observed that completion of the reduction cycle slowed somewhat after several cycles, such that complete reduction was not achieved (as evidenced by a slight downwards slope of the mass curve) even after 30 minutes.
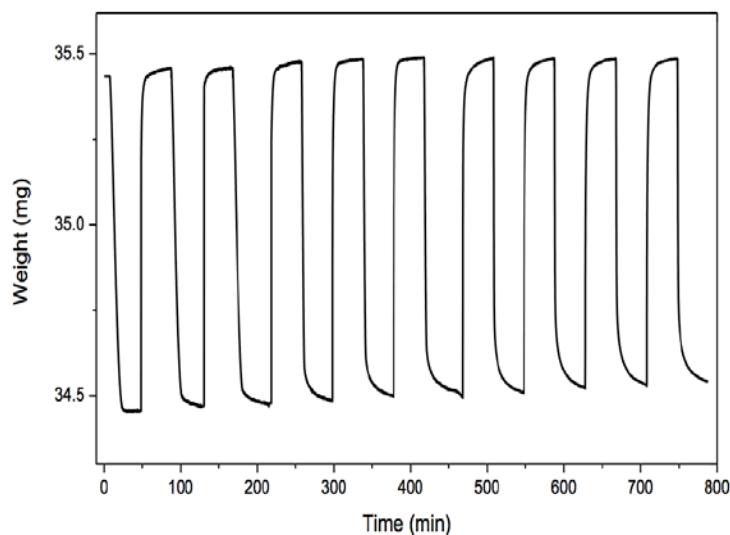
Figure 43: Mass of carrier NA-30 over 10 oxidation/reduction cycles in the TGA.

D.4.1.4 Rates of Reduction and Oxidation

Figure 44 shows the rates of carrier reduction (O_2 release) in nitrogen at 850, 900 and 950°C. At 900 and 950°C, more than 75% conversion was achieved in less than 2 minutes, but the rate slowed significantly after that, so that 90% conversion was not achieved until approximately 10 minutes. This may be a result of difficulty accessing copper in the core of the particle (Figure 42). The rate at 50% conversion was determined from the slope of the mass loss curve and the activation energy for reduction was calculated to be 240 kJ/mol (Figure 45).

The time required for oxidation in the TGA experiments was found to decrease as the temperature was increased from 850 to 950°C (Figure 46). This is consistent with what has been observed in other studies of oxidation of Cu_2O to CuO, and is due primarily to a decrease in driving force of the oxidation reaction as the equilibrium O_2 partial pressure approaches the partial pressure of the fed gas environment at higher
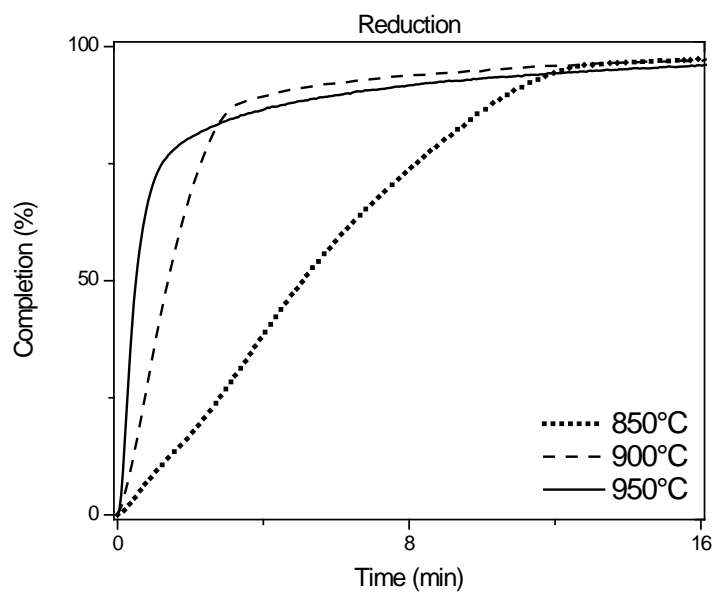
Figure 44: Reduction in TGA of NA-30 measured at 850, 900 and 950°C.
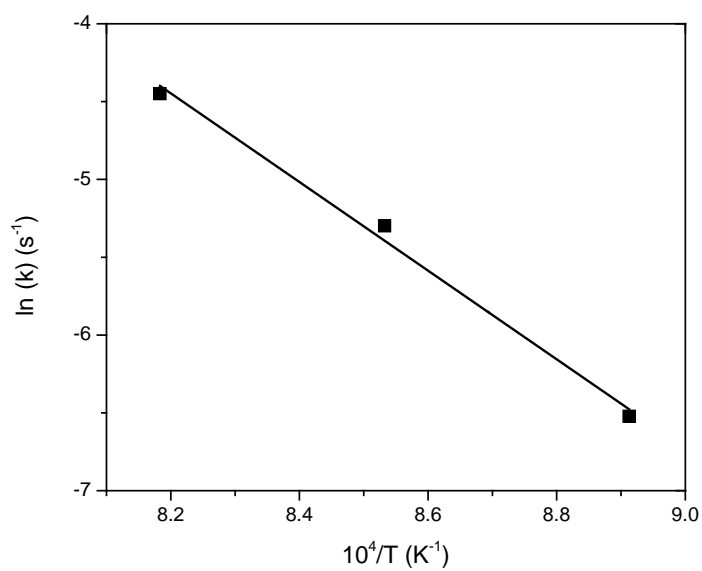copper-based CLOU carriers have found.

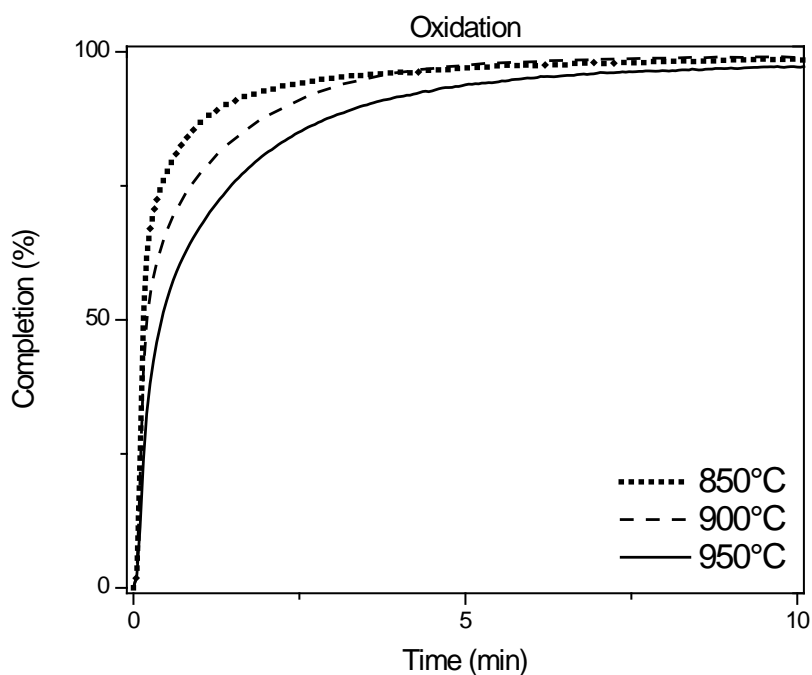

Figure 45: Arrhenius plot for reduction of NA-30 carrier.

Figure 46: Oxidation in TGA of NA-30 measured at 850, 900, and 950°C.

temperatures.

D.4.2 Fluidized-bed Performance

D.4.2.1 Cycling Between Air and N$_2$

Each of the materials was cycled between air and nitrogen at temperatures from 850 to 950°C. The clamshell design of the furnace housing allowed observation of the bed, so agglomeration could be observed visually. The carriers were able to be successfully heated to 850°C without significant agglomeration. At temperatures above 850°C, the materials began to show signs of agglomeration. At temperatures above 950°C, catastrophic agglomeration was observed.

In order to mitigate agglomeration, the temperature ramp during heating was

slowed from 10°C per minute to 5°C per minute. This change raised the agglomeration temperature above 850°C, suggesting that more gentle heating allows the material to stabilize, possibly avoiding high concentrations of agglomeration-prone copper at the particle surface. During heating, it was also observed that the bed must be maintained under full fluidization conditions or agglomeration may begin to occur.

Regions with limited gas flow are most prone to agglomeration in fluidized-bed systems. While good fluidization was maintained throughout testing, it was observed that stagnant zones would begin to collect defluidized particles. These zones included the sloped region of the free board expansion zone as well as zones near the wall at the base of the particle bed closest to the gas distributor plate. The particles were not strongly stuck together; simple agitation of the particle bed would be enough to break it free.

Expected operating temperatures of a copper-based chemical-looping system are between 900 and 1000°C, so it is important to test oxygen carrier materials above 900 °C. Because of the agglomeration propensity observed at temperatures above 850°C, testing of the CuO-ilmenite carriers above that temperature was conducted carefully, with slow heating and periodic redox cycling. The material was heated slowly to 850 °C and then cycled between CuO and Cu_2O under alternating atmospheres of air and nitrogen for 1 hour each cycle for 4 cycles. After the 4 cycles were completed, the temperature was increased another 50°C and the cycling was repeated. The temperature was then set to the desired operating temperature. This process allowed the agglomeration temperature for the NA-30 material to be increased from 850°C to greater than 950°C. This increase in agglomeration temperature may be explained using the laser ablation ICP findings displayed in Figure 41. For the materials that were exposed to elevated temperatures, the

copper oxide on the particle surface began to migrate from the surface toward the inside of the particles. A similar technique is used within the semiconductor industry, where thermally driven diffusion of impregnating dopants is performed regularly in order to alter the conductive properties of the silicon.

This thermal treatment of the material was most effective during gas cycling. To verify this, a sample of the NA-30 material was subjected to baking at 950°C under air for 36 hours in a muffle furnace without being subjected to fluidization conditions. After baking, the material was agglomerated, but was easily broken apart by simple agitation, which indicates sintering was not significant and that fluidization conditions may keep the particles from agglomerating. This product did not perform any better than nonbaked material under fluidization and agglomerated in the fluidized-bed before reaching 950°C. Therefore, it is believed that cycling between oxidizing and inert conditions may provide a better means for the thermally driven diffusion of the copper oxide molecules.

D.4.2.2 With Solid Fuel Addition

The evolution of gases during the combustion of the char prepared from the coal represented in Table 16 is presented in Figure 47. The figure shows three regions for the reaction: initially, air is used to oxidize the oxygen carrier. The gas is switched to nitrogen at about 50 seconds and after a period of about 50 more seconds, the oxygen is depleted and levels off around 2% by volume, which corresponds to the equilibrium concentration at the reactor temperature. Once the oxygen vol% levels off, the purge gas is turned off and the fuel is introduced, which may be seen in Figure 47 as the spike in the carbonaceous gases and the drop in the oxygen level. Interestingly, the oxygen does not
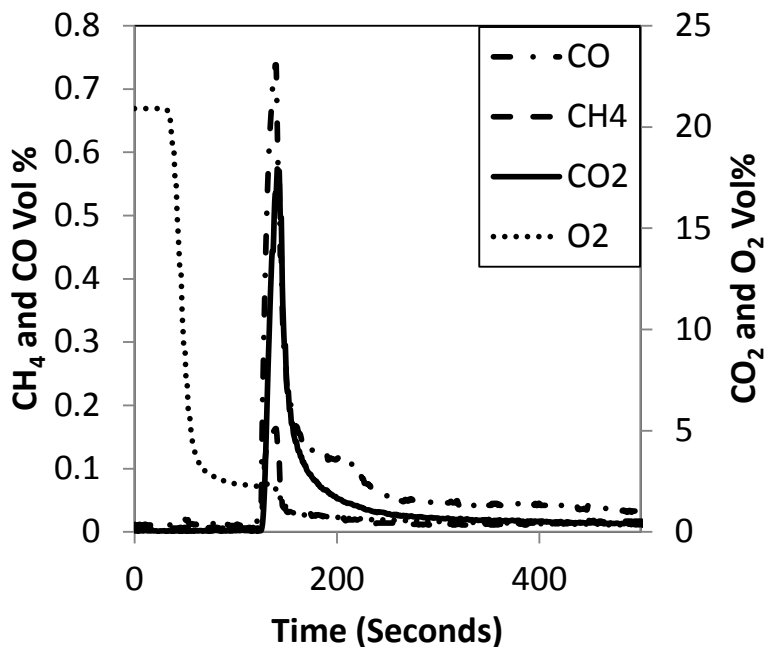
Figure 47: Evolution of effluent gases during combustion of Illinois #6 Char using the NA30 material at 900 °C.

drop to zero and continues to evolve from the surface of the oxygen carrier particles faster than it can be consumed.

Figure 48 and Figure 49 display the conversion of the fuel versus time. As may be seen in Figure 49, the rate of consumption of the fuel is much faster at 950°C than it is at 900°C, and the conversion of the solid fuel would be attained in approximately 1 hour. This, however, is unlikely. Due to the operating temperature, the decomposition of the CuO should occur in less than a few minutes.

It is quickly seen that the oxygen carrier has completely released all of its oxygen from Figure 49. The rate of conversion of the fuel changes drastically around 30 seconds. Initially, the fuel burns quickly, but seems to slow around 30 seconds. This is most likely due to the particles being completely converted from CuO to Cu_2O long
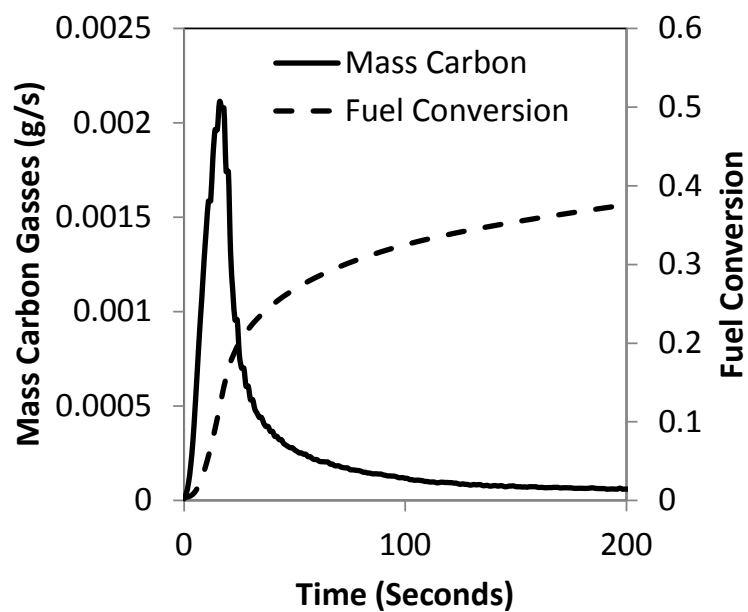
Figure 48: Conversion of the fuel vs. time with the evolution of carbon (as gas) from the combustion of Illinois #6 Char at 900 °C.
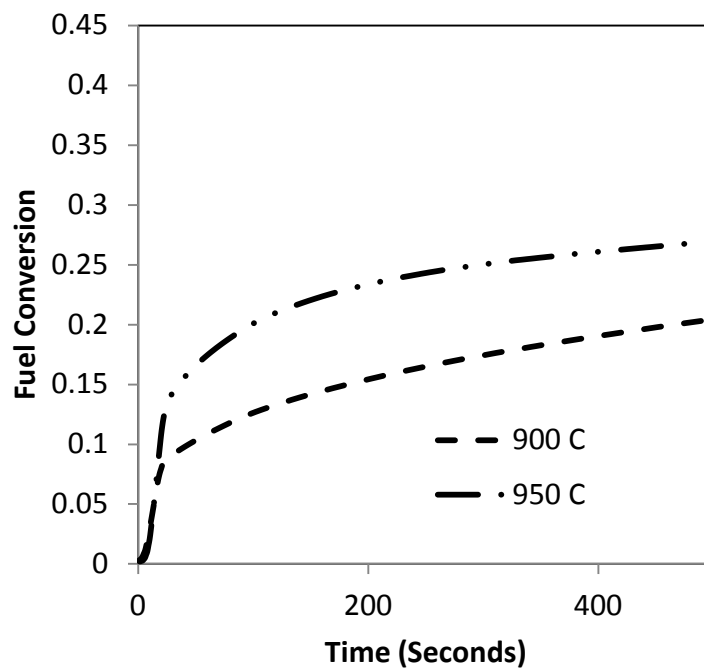

Figure 49: Conversion of Illinois #6 char at two temperatures using NA30 material under CLOU conditions.

before the fuel is converted. This may be caused from poor mixing in the fluidized-bed between the oxygen carriers and the fuel particles or simply the fuel not being very highly reactive.

This may be accounted for by using a more reactive fuel, decreasing fuel particle size, increasing mixing from fluidization or even increasing the oxygen carrier reactor charge (thereby increasing the bed depth). By increasing the bed depth, the release of oxygen from the particles in the bottom of the bed essentially inhibits the decomposition of the particles downstream by decreasing the oxygen partial pressure driving force. This inhibition would slow the release of oxygen allowing for a slower burning fuel.

In Figure 50, it may be seen that the production ratio CO_2/CO is roughly twice as large at 950°C than at 900°C. The largest difference between these two temperatures is seen around 25 seconds and is possibly an effect of residual volatiles not removed during the charring process. The char is produced at relatively low heating rates; therefore, the volatile compounds evolve from the fuel. Therefore, the volatiles are better consumed at the higher temperatures likely due to the increased equilibrium partial pressure of oxygen at the higher temperatures which increases the rate at which the oxygen is liberated (Figure 44). The faster CuO decomposition rate provides more oxygen in the chamber to react with the low residence time volatiles.

D.5 Conclusions

The development of a novel oxygen carrier by the mixture of ilmenite and copper oxide is presented. The performance of the oxygen carrier in both a fluidized-bed and TGA is also presented. The bimetallic Cu-Fe carrier made from ilmenite and copper
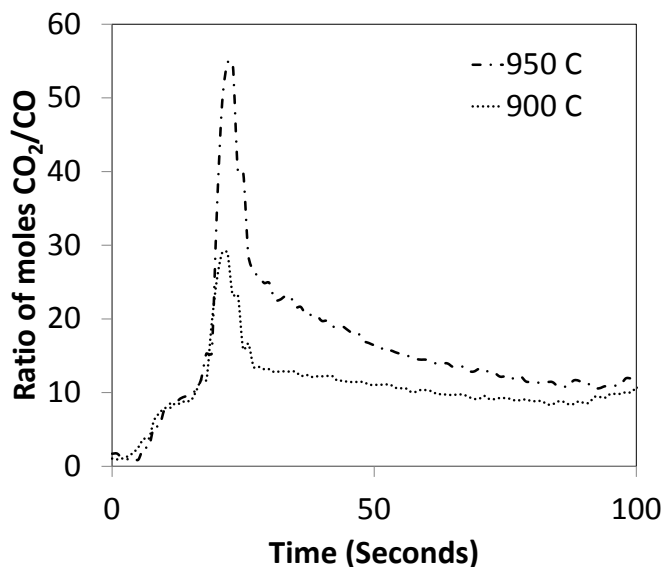
Figure 50: Ratio of moles of CO_2 to moles of CO evolved during the combustion of Illinois #6 char at two temperatures using NA30 material as oxygen carrier.

nitrate trihydrate performed well a nitrogen atmosphere within TGA and while using a char made from the devolatilization of a bituminous coal. The increase in temperature from 900 °C to 950 °C significantly increased the ratio of CO_2/CO production during combustion of the char. The material developed successfully operated at 950 °C without significant agglomeration using the described preparation method.

D.7 References

[1]   Mattisson, T., Lyngfelt, A., Leion, H. Chemical-looping with oxygen uncoupling for combustion of solid fuels. Int J Greenh Gas Con. 2009, 3 (1): 11-19.

[2]   Azimi, G., Rydén, M., Leion, H., Mattisson, T., Lyngfelt, A. $(Mn_z Fe_{1-z})_y O_x$ combined oxides as oxygen carrier for chemical-looping with oxygen uncoupling. AIChE J. 2013, 59(2): 582–588. doi:10.1002/aic.13847.

[3]   Arjmand, M., Hedayati, A., Azad, A.-M., Leion, H., Rydén, M., & Mattisson, T. $Ca_{(x)}La_{(1-x)}Mn_{(1-y)}M_{(y)}O_{(3-\delta)}$ (M=Mg, Ti, Fe, or Cu) as Oxygen Carriers for Chemical-Looping with Oxygen Uncoupling (CLOU). Energ & Fuel. 2013, 27 (8): 4907 – 4107. doi:10.1021/ef3020102

[4]   Mattisson, T. Materials for Chemical-Looping with Oxygen Uncoupling. ISRN Chem Eng. 2013(1): 1–19. doi:10.1155/2013/526375

[5]   Baraki, R., Konya, G., Eyring, E. M. Investigation of the Reaction Kinetics of Oxygen Carriers in Chemical Looping Combustion. Twenty-Sixth Annual International Pittsburgh Coal Conference, Pittsburgh, PA, 2009.

[6]   Arjmand, M., Azad, A.-M., Leion, H., Lyngfelt, A., Mattisson, T. Prospects of Al2O3 and MgAl2O4-Supported CuO Oxygen Carriers in Chemical-Looping Combustion (CLC) and Chemical-Looping with Oxygen Uncoupling (CLOU). Energ Fuel. 2011, 25 (11): 5493-5502.

[7]   Wang, S., Luo, M., Wang, G., Wang, L., Lv, M. Analysis of Reactivity of a CuO-Based Oxygen Carrier for Chemical Looping Combustion of Coal. Energ Fuel. 2012, (26): 3275-3283.

[8]   de Diego, L. F.; Garcia-Labiano, F.; Gayan, P.; Celaya, J.; Palacios, J. M.; Adanez, Operation of a 10-kW Chemical-Looping Combustor during 200 h with a CuO-Al2O3 Oxygen carrier. Fuel. 2007, 86 (7-8): 1036-1045.

[9]   Johansson, M.; Mattisson, T.; Lyngfelt, A. Investigation of Mn3O4 With Stabilized ZrO2 for Chemical-Looping Combustion. Chem Eng Res Des. 2006, 84 (9): 807-818.

[10] Adanez-Rubio, I.; Gayan, P.; Garcia-Labiano, F.; de Diego, L. F.; Adanez, J.; Abad, A. Development of CuO-based oxygen-carrier materials suitable for Chemical-Looping with Oxygen Uncoupling (CLOU). Energ Proc. 2011, (4): 417-424.

[11] Adanez-Rubio, I., Arjmand, M., Leion, H., Gayan, P., Abad, A., Mattisson, T. P., & Lyngfelt, A. (2013). Investigation of Combined Supports for Cu-based Oxygen Carriers for Chemical-Looping with Oxygen Uncoupling (CLOU). Energ Fuel. 2013, 27 (7): 3918 – 3927. doi:10.1021/ef401161s.

[12] Gayan, P.; Adanez-Rubio, I.; Abad, A.; de Diego, L. F.; Garcia-Labiano, F.;

Adanez, J. Fuel 2012, 96, 226-238.

[13] Adanez-Rubio, I.; Gayan, P.; Abad, A.; de Diego, L. F.; Garcia-Labiano, F.; Adanez, J. Energy Fuels 2012, 26 (5), 3069-3081.

[14] Siriwardane, R. V., Ksepko, E., Tian, H., Poston, J., Simonyi, T., Sciazko, M. Interaction of Iron-Copper Mixed Metal Oxide Oxygen Carriers with Simulated Synthesis Gas Derived from Steam Gasification of Coal. Applied Energy, 2013, 107 (C): 111-123.

[15] Adánez, J., Cuadrat, A., Abad, A., Gayán, P., de Diego, L. F., Garcia-Labiano, F. Ilmenite during Consecutive Redox Cycles in Chemical-Looping Combustion. , 2010 , 24 (2): 1402-1413.